AD NUMBER

AD483258

NEW LIMITATION CHANGE

TO

Approved for public release, distribution unlimited

FROM

Distribution authorized to U.S. Gov't. agencies and their contractors; Administrative/operational Use; Nov 1965. Other requests shall be referred to Air Force Flight Dynamics Labs, Research and Technology Div., Wright-Patterson AFB, OH 45433.

AUTHORITY

Air Force Wright Aeronautical Labs ltr dtd 24 Apr 1980

AD483258

SPECTRAL AND EXCEEDANCE PROBABILITY MODELS OF ATMOSPHERIC TURBULENCE FOR USE IN AIRCRAFT DESIGN AND OPERATION

FRANCIS E. PRITCHARD
CALVIN C. EASTERBROOK
GEORGE E. McVEHIL

CORNELL AERONAUTICAL LABORATORY, INC.

TECHNICAL REPORT AFFDL-TR-65-122

NOVEMBER 1965

AIR FORCE FLIGHT DYNAMICS LABORATORY
RESEARCH AND TECHNOLOGY DIVISION
AIR FORCE SYSTEMS COMMAND
WRIGHT-PATTERSON AIR FORCE BASE, OHIO

AFFDL-TR-65-122

NOTICES

When Government drawings, specifications, or other data are used for any purpose other than in connection with a definitely related Government procurement operation, the United States Government thereby incurs no responsibility nor any obligation whatsoever; and the fact that the Government may have formulated, furnished, or in any way supplied the said drawings, specifications, or other data, is not to be regarded by implication or otherwise as in any manner licensing the holder or any other person or corporation, or conveying any rights or permission to manufacture, use, or sell any patented invention that may in any way be related thereto.

Qualified users may obtain copies of this report from Defense Documentation Center.

Foreign announcement and dissemination of this report is not authorized.

DDC release to OTS is not authorized. The distribution of this report is limited because the report contains technology identifiable with items on the strategic embargo lists excluded from export or re-export under U.S. Export Control Act of 1949 (63 Stat. 7) as amended (50 U.S.C. App 2020.2031) as implemented by AFR 400-10.

AFFDL-TR-65-122

SPECTRAL AND EXCEEDANCE PROBABILITY MODELS OF ATMOSPHERIC TURBULENCE FOR USE IN AIRCRAFT DESIGN AND OPERATION

FRANCIS E. PRITCHARD
CALVIN C. EASTERBROCK
GEORGE E. McVEHIL

FOREWORD

This final report was prepared by the Cornell Aeronautical Laboratory, Inc., Buffalo, New York, in partial fulfillment of USAF Contract Number AF 33(615)-1883. The contract was initiated under Project Number 1367, "Structural Design Criteria", Task Number 136702, "Aerospace Vehicle Structural Loads Criteria". The work was administered under the direction of the Air Force Flight Dynamics Laboratory, Research and Technology Division, Air Force Systems Command, Wright-Patterson Air Force Base, Ohio, Mr. Paul L. Hasty (FDTR), Project Engineer.

The work reported in this study was conducted by the Flight Research and Applied Physics Departments of Cornell Aeronautical Laboratory, Mr. F.E. Pritchard, CAL Project Engineer, and covers the period from June 1964 to May 1965. The manuscript was released by the authors in May 1965 for publication as an RTD Technical Report.

As well as the authors of this report, the following scientific and engineering personnel contributed to the work: R.L. Peace and G.D. Hess of the Applied Physics Department, C.B. Notess of the Transportation Research Department, and W.H. Shed of the Flight Research Department. Professor H.A. Panofsky of the Pennsylvania State University was a consultant to CAL for the project. The project was directly supervised by J.M. Schuler, head of the Flight Dynamics Section of the Flight Research Department and by Mr. R.J. Pilie, acting head of the Atmospheric Physics Section and assistant head of the Applied Physics Department. Mr. W.O. Breuhaus, head of the Flight Research Department provided the over-all supervision.

The authors are grateful for the assistance furnished by the NASA Langley Research Center and the Boeing Company, Airplane Division, Wichita Branch.

The Contractor's report number is VC-1954-F-1.

This technical report has been reviewed and is approved.

RICHARD F. HOENER
Acting Chief
Structures Division

ABSTRACT

Atmospheric turbulence data in many forms, from many sources, have been combined in both spectral and exceedance probability models of the vertical component of atmospheric turbulence. These models will be useful in aircraft structural design procedures as well as in other analytical procedures involving aircraft operations.

For the spectral probability models, a simple analytical form for the spectrum is chosen which yields a good fit to the available measured spectra. The parameters of the spectrum are related to physical and meteorological factors in tabular and graphical form, and probability distributions of the pertinent meteorological parameters have been obtained from climatological data. The resulting probability distributions of the spectral parameters have been computed.

A normalized exceedance model is developed that represents the overall cumulative probability distribution of the vertical turbulence velocity for the special probability density function of the rms vertical gust velocity recommended in NACA TN 4332. The basic model involves one parameter, namely altitude, but may be modified by using correction factors that have also developed. The correction factors account for varying terrain types, season, and time of day.

These models of the vertical component of atmospheric turbulence represent what should be an improvement over previous models because of the significant amount of data which has become in recent years. Nevertheless, the lack of sufficiently reliable data remains a substantial problem.

AFFDL-TR-65-122

TABLE OF CONTENTS

LIST OF FIGURES

LIST OF FIGURES (Cont.)

LIST OF TABLES

LIST OF SYMBOLS

a_i Inverse slope parameter for U_{de} or n_z cumulative frequency distributions

A Turbulence scale factor

A_x $= \sigma_x / \sigma_w$ Ratio of rms response of x to rms vertical velocity, units of x /ft sec^{-1}

b_i Inverse slope parameters used in functional representation of turbulence, ft sec^{-1}

$\bar{c}$ Mean or reference value of wing chord, ft

c_p Specific heat of air at constant pressure

C $= \dfrac{K_g \, \rho_0 \, S V_e \, C_{L_\alpha}}{2W}$, Gust response factor, g /ft sec^{-1} EAS

C_{L_α} Airplane lift-curve slope, rad^{-1}

f Frequency, cyc sec^{-1}

F $= f\bar{c}/V$, Reduced frequency

g Acceleration of gravity, 32.2 ft sec^{-2}

h Pressure altitude, ft

H Vertical flux of heat by turbulence

i An index (subscript); $\sqrt{-1}$

k $= 1/\lambda$, wave number, ft^{-1}

K_g Gust alleviation factor of Reference 47

K_ϕ Gust alleviation factor of Reference 24

k $= 0.40$, von Karman's constant

ℓ A length parameter, ft

L Scale of turbulence, ft

m Correction factor (used with a subscript)

LIST OF SYMBOLS   (Cont.)

$M(x)$ — Average number of exceedances with positive slope of the level x per unit time or distance in flight operations

n_3 — Incremental normal acceleration of airplane (positive in direction of airplane z axis), g

$N(x)$ — Average number of exceedances with positive slope of the level x per unit time or distance for a single Gaussian process

N_o — Average number of exceedances (or crossings) with positive slope of the zero level per unit time or distance

$p(\xi)$ — Probability density function of ξ

$p(\xi|\eta)$ — Probability density of ξ conditioned on η

$P(\xi)$ — Cumulative probability distribution of ξ

P_i — Proportion of flight time spent in given type of turbulence

R_r — Terrain factor

S — Reference (wing) area of airplane, ft^2

t — Time, sec

T — Absolute temperature

u_* — $= (\tau/\rho)^{1/2}$, friction velocity, ft sec^{-1}

U_{de} — Derived equivalent gust velocity, ft sec^{-1}

U_{dt} — $= U_{de}\sqrt{\rho_0/\rho}$, Derived true gust velocity, ft sec^{-1}

$\bar{V}$ — Mean horizontal wind speed, ft sec^{-1}

V_e — Equivalent airspeed, ft sec^{-1}

V_T — Airplane true speed, ft sec^{-1}

w — Vertical gust velocity (positive in direction of airplane z axis), ft sec^{-1}

W — Weight of airplane, lb

x — Unspecified airplane response quantity

Z — Altitude above the terrain, ft

ix

LIST OF SYMBOLS (Cont.)

γ $= \partial T / \partial z$, Temperature lapse rate

Γ $= (u_*^3 c_p \rho T)/(gKH)$, An atmospheric stability parameter with dimensions of length

ζ Airplane short period damping ratio

λ Gust wavelength, ft

μ_g $= \dfrac{2W}{C_{L_\alpha} \rho \bar{c} g S}$, Airplane mass ratio

ρ Air density, slug ft^{-3}

ρ_0 Sea level value of air density, slug ft^{-3}

σ_x rms value of response x, units of x

σ_w rms value of vertical gust velocity component, ft sec^{-1}

τ Surface stress, lb ft^{-2}

ϕ_x Spectral density of response x, (units of x)^2/units of argument of ϕ_x

ϕ_w Spectral density of vertical gust velocity component, (ft/sec)^2/units of argument of ϕ_w

ω $= 2\pi f$, Frequency, rad sec^{-1}

ω_n Airplane short period natural (undamped) frequency, rad sec^{-1}

Ω $= \omega/V_T = 2\pi/\lambda = 2\pi k$, Spatial frequency (longitudinal), rad ft^{-1}

SECTION 1

INTRODUCTION

One of the primary problem areas in the design of airplane structures is the atmospheric turbulence environment. Turbulence may be the critical structural design problem through either the small repetitive gusts or the large, infrequent, but sometimes disastrous gusts. Moreover, for some airplanes, particularly transport airplanes, both the large and the small gusts can lead to critical design problems. The large gusts determine the basic structural static strength, and the small gusts determine the fatigue life of the structure. To design properly the airplane structure to withstand the rigors of the atmospheric turbulence environment within acceptable reliability limits, a model of the turbulence environment must be available in a form amenable to the modern techniques of structural load calculation. The statistical methods now in use appear to be the most logical approach in view of the statistical nature of the turbulence. What is needed, then, is an adequate and reliable model of atmospheric turbulence that is amenable to the statistical methods for load calculation.

The work covered in this report represents an effort to update and improve the models of the vertical turbulence velocity now in use by including new and more recent data as well as by trying new analytical methods.

A significant quantity of new spectral and VGH-type data has become available since publication of the NACA (NASA) TN 4332 in 1958 (Reference 27) and MIL-A-8866(ASG) in 1960 (Reference 53), the latter being based strongly on the results of the former. Relatively large quantities of spectral and VGH data for altitudes below 1000 feet above the terrain have become available recently.

Furthermore, a large percentage of the spectral and some of the VGH data were presented with enough accompanying meteorological and physical data to permit a more sophisticated model of turbulence in the atmospheric boundary layer. Through recent sampling programs employing the U-2 airplane, a large quantity of VGH peak count data has become available for altitudes approaching 75,000 feet. These data are especially concentrated in the altitude band from 50,000 to 70,000 feet where other aircraft have not been able to operate satisfactorily for sampling purposes. On the other hand, except for spectra measured during thunderstorm and cumulus cloud penetrations, there are no spectral data available for altitudes above some very few thousand feet.

1

The turbulence modeling problem has been approached from two essentially different directions:

1. An analytical form for the spectrum is chosen so that the relations between the spectral parameters, scale and mean-square intensity, and the meteorological parameters, primarily stability, mean wind speed and height above the terrain, can be identified and determined. Then probability density functions for the meteorological parameters are determined from climatological data.

2. Based on the assumption of a spectral function including the scale, but not the mean square intensity, measured peak count and exceedance statistics from normal acceleration data recorded during routine commercial and military flight operations are converted into both the probability density and the cumulative probability of the root-mean-square intensity of turbulence.

Both approaches have been designed and carried out to provide models of the actual atmospheric turbulence environment, models that are presumed to be independent of any given airplane, airplane operations, geographical locations, and other sources of unwanted bias. The two approaches were employed simply because of the basic theories relating measured data on the one hand and the parameters with which the measured data vary on the other. The spectral data are most easily related to meteorological parameters. The peak count or exceedance data are most easily related to those parameters associated with airplane operations, especially altitude. In the range of altitudes near the ground where both spectral and peak count or exceedance data abound, it should be possible to obtain good agreement between the results of both approaches, at least within a restricted set of conditions that would in theory permit agreement.

SECTION 2

SUMMARY

As discussed in the Introduction, the atmospheric turbulence model is developed in this report along two essentially different approaches, one involving the turbulence spectra directly and the other involving peak count and exceedance statistics in which the spectra play an important but indirect role. The different approaches were employed because of the nature of the basic data and because of the analysis procedures that were employed to develop the turbulence model. The model was developed only for the vertical component of the turbulence velocity.

Section 3 deals with the turbulence power spectra and their relationship to the physical and meteorological parameters:

1. surface roughness and terrain type,
2. height above the surface,
3. wind conditions (both velocity and shear), and
4. atmospheric stability.

An analytical form for the spectrum, that proposed by Lappe and Davidson (Reference 1) and later used by Lappe in his analysis of B-66 low-level gust data, was chosen. It appears to fit all the available measured spectra within limits, yet is simple enough to facilitate straightforward analysis. This spectral form fits not only the B-66 low-level data, but also the available tower spectra, low-level spectra measured by aircraft in England and Africa, and thunderstorm penetration spectra.

The relationships found between the spectral parameters and the physical and meteorological factors are presented in tabular and graphical form suitable for design and prediction purposes. The distributions of the pertinent meteorological parameters have been obtained through a climatological study, and the resulting expected distributions of the spectral parameters computed using the proposed interrelationships.

Thunderstorm spectra are analyzed separately in Section 4 because, unfortunately, there are little if any supplementary data to accompany the measured spectra. It was found difficult to correlate measured spectra with any physical or meteorological parameters. The B-66 storm penetration spectra were, however, fitted with the previously-mentioned spectral function, and it was found that a possibly useful correlation apparently exists between the mean-square intensity (variance) and the scale length. The scale length increases with increasing mean-square intensity.

3

Section 5 is devoted to a brief summary of the existing knowledge of clear air turbulence and related physical and meteorological parameters at the higher altitudes, for which at present there are little data of any statistical significance.

Through the efforts of NASA and various military groups in the USA, England and Canada, a considerable quantity of VGH-type statistical data has become available in the past few years. Fortunately these more recent data have been mostly well documented and well supported by the necessary supplementary information needed to permit accurate analysis of the data and to make reliable estimates of any statistical bias. The VGH data, along with certain spectral data that existed in statistically significant quantities, were developed into an exceedance probability model of turbulence. The particular graphical form of the model is the form recommended by Houbolt, Steiner and Pratt (Reference 24), that is, the results are presented as "generalized prediction curves".

In particular, the exceedance model consists of parameters defining both the probability of encountering turbulence of a given type and the intensity of the given type of turbulence. These parameters are presented primarily as a function of height above the terrain. Correction factors are given, when possible, to account for the variation of turbulence with physical parameters other than height such as terrain roughness, season and time of day. The correction factors are presented generally only for low altitudes above the terrain since it is only at the low altitudes where sufficiently reliable data exist.

The exceedance model is presented for all altitudes from ground level to 100,000 feet, but above approximately 70,000 feet, reasonable extrapolations were made because no directly applicable data exist.

Generally, the exceedance model presented in this report may be compared with the earlier NASA (NACA) model in Reference 27. The comparison will show that for small vertical gust velocities the model of this report is more severe (i.e., has a greater number of exceedances), whereas for the larger gust velocities the present model is considerably less severe.

Although the spectral and exceedance models of the vertical gust velocity presented in this report are considered to be improvements over and extensions of previous models, the resulting models clearly show the effects of the lack of sufficient data. Obtaining meaningful and useful atmospheric turbulence data at all altitudes of interest remains the area in which the greatest efforts should be directed.

4

SECTION 3

THE LOW-LEVEL TURBULENCE MODEL

This section deals with turbulence in the layer of atmosphere extending from the surface to about 1000 feet. The boundary layer occupies approximately the first 300 feet of this depth with the remainder being part of a gradual transition to the geostrophic region above. It is in this 1000-foot layer that most of the turbulence spectrum measurements have been obtained and, hence, the greatest potential exists for fruitful analysis.

The data used for the low-level spectral analysis were obtained both from fixed tower measurements and from aircraft measurements. The tower data came mainly from two sources, Round Hill (Reference 2), and Brookhaven (Reference 3). The aircraft spectra were taken from the Douglas B-66 program (Reference 4) and from an R.A.E. low-level study (Reference 5). If both types of measurements are correct, the data must necessarily fit together in a fairly orderly fashion to produce a continuous and logical model over the 1000-foot layer.

The results of the analysis do indeed show that the tower and aircraft data are compatible. Since the tower data have much more detail in the accompanying meteorological measurements, they have proven valuable in determining the meteorological factors affecting the higher level aircraft data where reliable stability measurements do not exist.

3.1 THE FORM OF THE SPECTRUM

Monin (Reference 6) has shown, using similarity theory, that the spectrum near the ground can be expressed as

$$f \, \phi(f) = \sigma_w^2 \, q \, (F, z/\Gamma) \tag{1}$$

where $q(F, z/\Gamma)$ is a universal function and $f \, \phi_w(f)$ is the logarithmic spectrum, i.e., the product of frequency and the spectral density. The Monin-Obukhov stability length Γ is defined by $(u_*^3 c_p \rho T)/(g K H)$ where $u_* (\tau/\rho)^{1/2}$, τ is the surface stress, c_p is the specific heat of air at constant pressure, $K = 0.40$ is von Karman's constant, and H is the vertical turbulent heat flux. Equation 1 states that the shape and magnitude of the spectrum is determined completely by σ_w, f, and z/Γ. The similarity theory can be expected to apply only at relatively low levels (below 100 meters, perhaps) and over relatively smooth, homogeneous terrain. However, the same spectral shape appears valid for a much broader range of heights and conditions. Since the

boundary layer case must eventually fit within any over-all turbulence model, it is not unreasonable to begin by generalizing the dimensional argument presented in Equation 1 to

$$f \Phi_w(f) = \sigma_w^2 g\left(F', z/r\right) \tag{2}$$

where $F' = \dfrac{f\ell}{V}$. The new length parameter ℓ replaces z . We would expect ℓ to be equal to z near the ground over smooth terrain, but to possibly depart from this behavior in other conditions. There is some inconsistency in replacing z by ℓ in F, but not in z/r ; however, at this point we carry the z/r dependence only as a reminder that the spectrum is a function of stability.

From a general review of the literature, we are led to consider two possible analytical expressions for $f \Phi_w(f)$. From Panofsky and McCormick (Reference 7)

$$f \Phi_w(f) = \frac{\sigma_w^2 \, 4F}{(1 + 4F)^2} \tag{3}$$

and from Lappe (Reference 1)

$$f \Phi_w(f) = \frac{\sigma_w^2 \, 2\pi \frac{\mathscr{L}}{V} f}{\left(1 + 2\pi \frac{\mathscr{L}}{V} f\right)^2} \tag{4}$$

Both of these models have proven capable of fitting observed spectra. The former has been applied mainly to data from fixed towers; the latter to aircraft observations. It is readily seen that these two expressions yield the same spectral shape. However, neither includes the effect of stability, and the Lappe equation does not explicitly include any influence of height, although $\mathscr{L}$ turns out to be a function of height when Equation 4 is applied to observations.

To relate the variables in the two forms so that a single, consistent model can be applied to both kinds of data, and to bring both models into agreement with similarity theory, we generalize the Panofsky-McCormick model by writing

$$f \Phi_w(f) = \frac{\sigma^2 A(z/r) F'}{\left[1 + (A(z/r)F']^2} \tag{5}$$

We have introduced a function of stability $A(z/r)$ in place of the constant 4, and we have replaced F by F'. We now have

$$g(F', z/r) = \frac{A(z/r)F'}{\left[1 + A(z/r)F'\right]^2} \tag{6}$$

6

in accord with similarity theory. It follows that, for the Lappe model to be consistent, we must have

$$2\pi\mathscr{L} = A(z/\Gamma)\ell$$

or

$$\mathscr{L} = \frac{A\ell}{2\pi} \tag{7}$$

We now have an analytical expression for the spectral density which we may write in terms of the longitudinal wave number k as

$$\Phi_w(k) = \frac{\sigma_w^2 A\ell}{(1+A\ell k)^2} \tag{8}$$

where A is a function of stability and $\ell \approx z$ for low levels. [1]

The analytical expression of Equation 8 has been checked for fit against 33 spectra computed from tower wind measurements and over 100 spectra computed from low-level gust data taken by aircraft. The method used to fit the curves was simply to solve Equation 8 for σ_w^2 and $A\ell$ using two points on the measured spectra. The two points are chosen near the upper and lower frequency limits of each spectrum, but far enough from the ends to insure that the data are free of errors inherent in the measurement technique. In every case, a very close fit can be obtained by suitable choice of these points.

---

[1] Transformation of spectral parameters is made in the following way:

$$\sigma_w^2 = \int_{f_1=0}^{f_2=\infty} \Phi_w(f)\,df = \int_{f_1=0}^{f_2=\infty} \Phi_w[f(k)]\,df(k) = \int_{k_1}^{k_2} \Phi_w[f(k)]\,\frac{df}{dk}\,dk$$

By notation

$$\Phi_w = \left[f(k)\right]\frac{df}{dk} \equiv \Phi(k)$$

so that

$$\sigma_w^2 = \int_0^\infty \Phi_w(f)\,df = \int_{k_1}^{k_2} \Phi_w(k)\,dk$$

Now for the particular transformation from Equation 5 to Equation 8, we use Taylor's hypothesis, $f = k\bar{V}$, so

$$\Phi(k) = \bar{V}\Phi(f); \qquad k_1 = 0, \; k_2 = \infty$$

If we differentiate $\mathbf{k}\,\Phi_w(\mathbf{k})$ with respect to $\mathbf{k}$, we get:

$$\frac{d\left[\mathbf{k}\,\Phi_w(\mathbf{k})\right]}{d\mathbf{k}} = \sigma_w^2 \left[\frac{A\ell}{(1+A\ell\,\mathbf{k})^2} - \frac{2\mathbf{k}\,(A\ell)^2}{(1+A\ell\,\mathbf{k})^3}\right]$$

Equating this expression to zero, we find the logarithmic spectrum has a maximum when

$$A\ell = \frac{1}{\mathbf{k}_m} \tag{9}$$

and $\mathbf{k}_m$ is the wave number at the maximum point. Thus, we see that corresponds to the wavelength of maximum energy in the spectrum. Using Equations 8 and 9, it is possible to determine $A\ell$ and σ_w^2 from a single point (the point of maximum energy) on the logarithmic spectrum.

3.2   THE FIT TO THE TOWER SPECTRA

The results of the Round Hill experiments include both the logarithmic spectra and the spectral density curves. At these lower levels, the lower frequency limit of the measurements is well below the peak of the $\mathbf{k}\,\Phi_w(\mathbf{k})$ spectra and the peak, in most cases, is well defined. These data afforded an excellent opportunity for checking the $A\ell$ value predicted by the two-point solution of Equation 8. The two-point solution was obtained using the spectral density curves and the value of $A\ell$ obtained from this solution was compared with the value determined by Equation 9 and direct observation of $\mathbf{k}_m$ on the $\mathbf{k}\,\Phi_w(\mathbf{k})$ spectra. The agreement is very good, indicating that the shape of the spectrum near the ground, even at the long wavelengths, is closely represented by the proposed analytical model. Figure 1 shows some representative comparisons of measured spectra and those computed by a two-point fit of the associated spectral density data to the proposed analytical equation.

3.3   THE FIT TO AIRCRAFT SPECTRA

In general, the aircraft data do not cover low enough frequencies to be able to measure $\mathbf{k}_m$. However, there has been one set of aircraft measurements made (Reference 8) that covers a range of wavelengths from 10 ft to 60,000 ft. A composite spectrum from this work is shown in Figure 2. The superimposed dotted curve is the computed spectrum obtained by fitting Equation 8 to the points $\mathbf{k} = .0005$, and $\mathbf{k} = .05$. The agreement is exceptionally good over the whole wavelength range, including the low-frequency end.
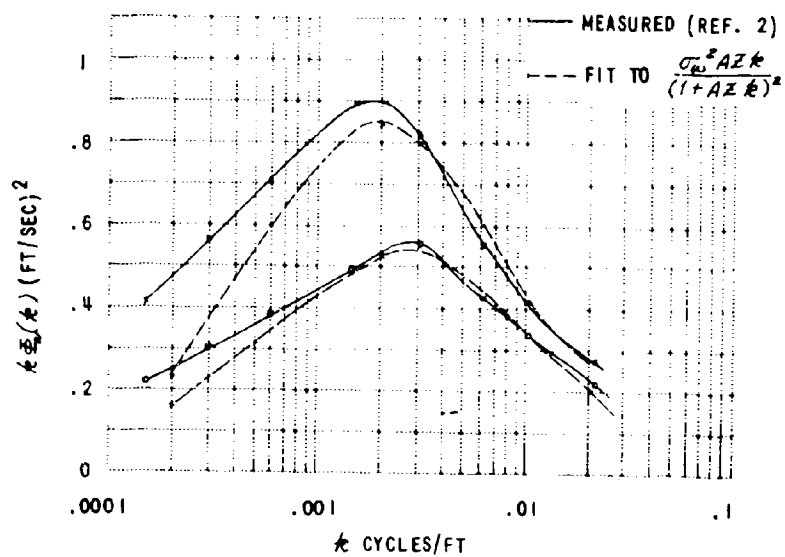
Figure 1. Comparison of Measured Tower Spectra with Analytical Form
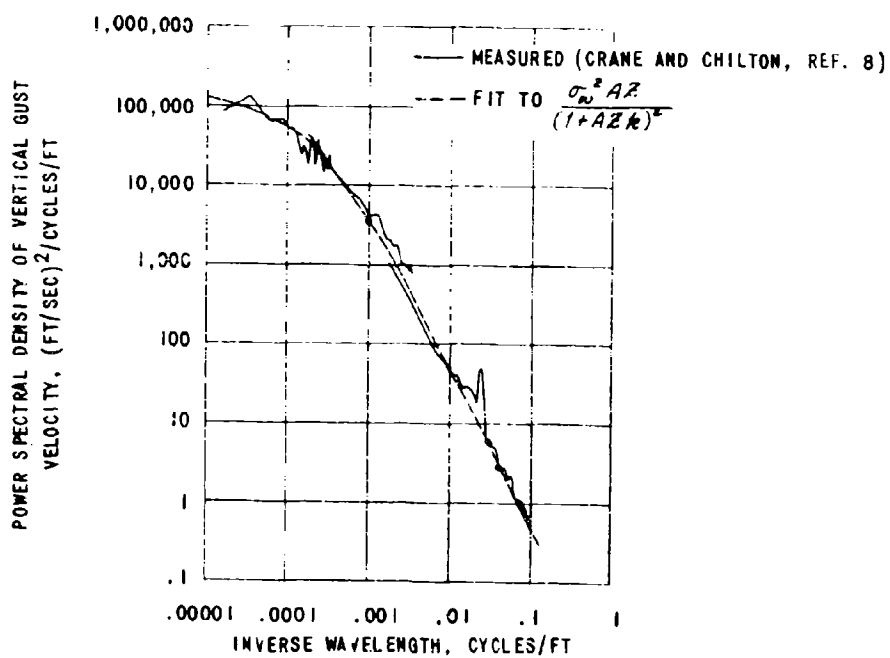

Figure 2. Comparison of Aircraft Spectrum with Analytical Form

Lappe has shown that the chosen analytical equation fits the B-66 spectra over the measured wavelength range and the work done at CAL with these spectra certainly confirms this. A very good fit has also been obtained to spectra published by the Royal Aircraft Establishment in England (Reference 5).

It has been well established, during work on this contract, that the spectral density Equation 8 provides a good fit to all the observed spectra over the measured range of wavelengths. From the tower spectra and from the spectrum measured by Crane and Chilton (Reference 8), it appears that this spectral form provides a realistic fit to the actual spectral density down to frequencies at least below the peak energy point.

3.4 TURBULENCE INTENSITY

The values of σ_w^2 computed from the many spectra cover a very wide range. We are then faced with the task of separating and identifying the factors responsible for this variation. If we consider all the possible sources of influence on the turbulence intensity at low levels, we are led to the following:

1. Surface roughness (terrain type)

2. Height above the surface

3. Wind conditions (both velocity and shear)

4. Atmospheric stability

The Douglas B-66 data provided the best means of getting at the effect of different terrain on low-level turbulence. These measurements were taken on specific flight tracks chosen to represent definite terrain classifications. The data taken over each terrain type cover a wide range of stability and wind conditions.

The computed σ_w values from all the available spectra were grouped into their respective terrain classification and mean values calculated for each height. A comparison of the means for each group shows a definite tendency for the rms gust velocity to increase with increasing surface roughness. There is also some evidence that the σ_w dependence on terrain roughness is a maximum in the 400 to 600 ft range and is slightly less at 200 and 1000 feet. The mean values of σ_w were then computed, using all the available data for each terrain type. Data for all heights within the terrain classifications were lumped together for this computation, since the small height dependence was thought to be too indefinite and insignificant to be considered. The mean values falling in each terrain classification are given in Table 1.

The ocean and water-land flight paths have a tendency to have less intense turbulence than the desert classification, even though the surface roughness is not likely to be significantly less. The difference here is probably due to stability, the air being more stable over water where the

10

water temperature is generally lower than the air temperature. It was decided to use the desert surface as the reference and to reduce all the σ_{w} values to this surface type by dividing by the ratio of the mean σ_{w} for the terrain being considered to the mean σ_{w} for the desert terrain. These ratios are included in Table 1. The ocean and water-land types are considered to be in the desert classification, as far as surface roughness is concerned, and hence the ratios for these are taken to be unity. All the σ_{w} values are reduced by the appropriate terrain factor R_{T} from Table 1 before the next step in the analysis. This first step essentially removes the effect of terrain on the σ_{w} values.

TABLE 1

TERRAIN FACTORS FOR SEVERAL TERRAIN CLASSIFICATIONS

	Ocean	Water-Land	Desert	Farm	Virgin Land	Low Mtns.	High Mtns.
$\overline{\sigma_{w}}$	1.58	2.32	2.8	3.05	3.20	3.70	4.0
R_{T}	1	1	1	1.1	1.15	1.3	1.4

According to the Monin-Obukhov similarity theory, the rms vertical gust velocity in the boundary layer for a given surface roughness is given by

$$\sigma_{w} = u_{*} G(R_{i}) = \overline{V} \, \psi(R_{i}, z) \tag{10}$$

where R_{i} is the Richardson number, $\overline{V}$ is the mean wind speed at the height where σ_{w} is measured and ψ and G are universal functions. The Richardson number is defined as

$$R_{i} = \frac{g}{\theta} \frac{\partial \theta}{\partial z} \left(\frac{\partial V}{\partial z} \right)^{-2} \tag{11}$$

where θ is the potential temperature. It can be shown that

$$\frac{\partial \theta}{\partial z} = \frac{\theta}{T} \left(\gamma_{a} + \frac{\partial T}{\partial z} \right) \tag{12}$$

where γ_{a} is the adiabatic lapse rate. Combining Equations 11 and 12, we have

$$R_{i} = \frac{g}{T} \left(\gamma_{a} + \frac{\partial T}{\partial z} \right) \left(\frac{\partial V}{\partial z} \right)^{-2}$$

Thus, Equation 10 becomes

$$\frac{\sigma_w}{\bar{V}} = \frac{1}{4}\left\{ \frac{g}{T}\left(\gamma_a + \frac{\partial T}{\partial z}\right)\left(\frac{\partial V}{\partial z}\right)^{-2} z \right\} \tag{13}$$

From Equation 13 we see that the quantity $\sigma_w/\bar{V}$ will be a function of height, lapse rate, and wind shear for a given terrain roughness. The wind shear term in Equation 13 is certainly undesirable since it is a parameter which is even more difficult to obtain than the lapse rate on a broad scale. However, the wind shear itself is a function of height and stability along with the surface roughness. This is substantiated by the tower data where a plot of $\sigma_w/\bar{V}$ as a function of $(\gamma_a + \gamma)$ and a plot of $\sigma_w/\bar{V}$ versus R_i show equally good correlation. From consideration of the tower data it appears then that Equation 13 may be rewritten in the functional form

$$\sigma_w/\bar{V} \approx H\left(\gamma_a + \frac{\partial T}{\partial z}, z\right) \tag{14}$$

for given surface roughness. If we now plot $\sigma_w/R_T\bar{V}$ as a function of height, assuming the correction factor R_T used to reduce all the data to a reference surface is sufficiently accurate, the spread of data points at a given height should be due only to stability. Figure 3 shows the resulting plot of all the available data including the tower data. First, we see that there is a large spread in the data at each height. We also see that this spread of points increases up to about 600 feet and then remains relatively constant. Finally we see that the majority of the data are concentrated in a band of near constant $\sigma_w/R_T\bar{V}$.

Atmospheric stability is a difficult quantity to measure and is certainly not easily assessed from flight-level temperature measurements and spot surface temperatures. The presence of cumuliform clouds indicates instability, but if the air is dry, a superadiabatic lapse rate can develop in the lower levels without cumulus forming. The lack of confidence in the stability estimates accompanying the measured spectra is a major problem source in analysis of the low-level turbulence spectra. The strong stability dependence is evident, but setting the quantitative stability boundaries without specific lapse rate measurements in the layer between the flight level and the surface is difficult. The final bounding of the stability regions in Figure 3 is based on the following considerations:

1. Considering all the meteorological data available, it appears that the majority of points will be in the region between neutral and slightly unstable lapse rates.

2. The curve drawn through the maximum $\sigma_w/\bar{V}$ points will closely represent the line of maximum possible instability (superadiabatic lapse rate).

3. For maximum stability conditions (inversions), the turbulence generated in the boundary layer should be quickly damped out with height.
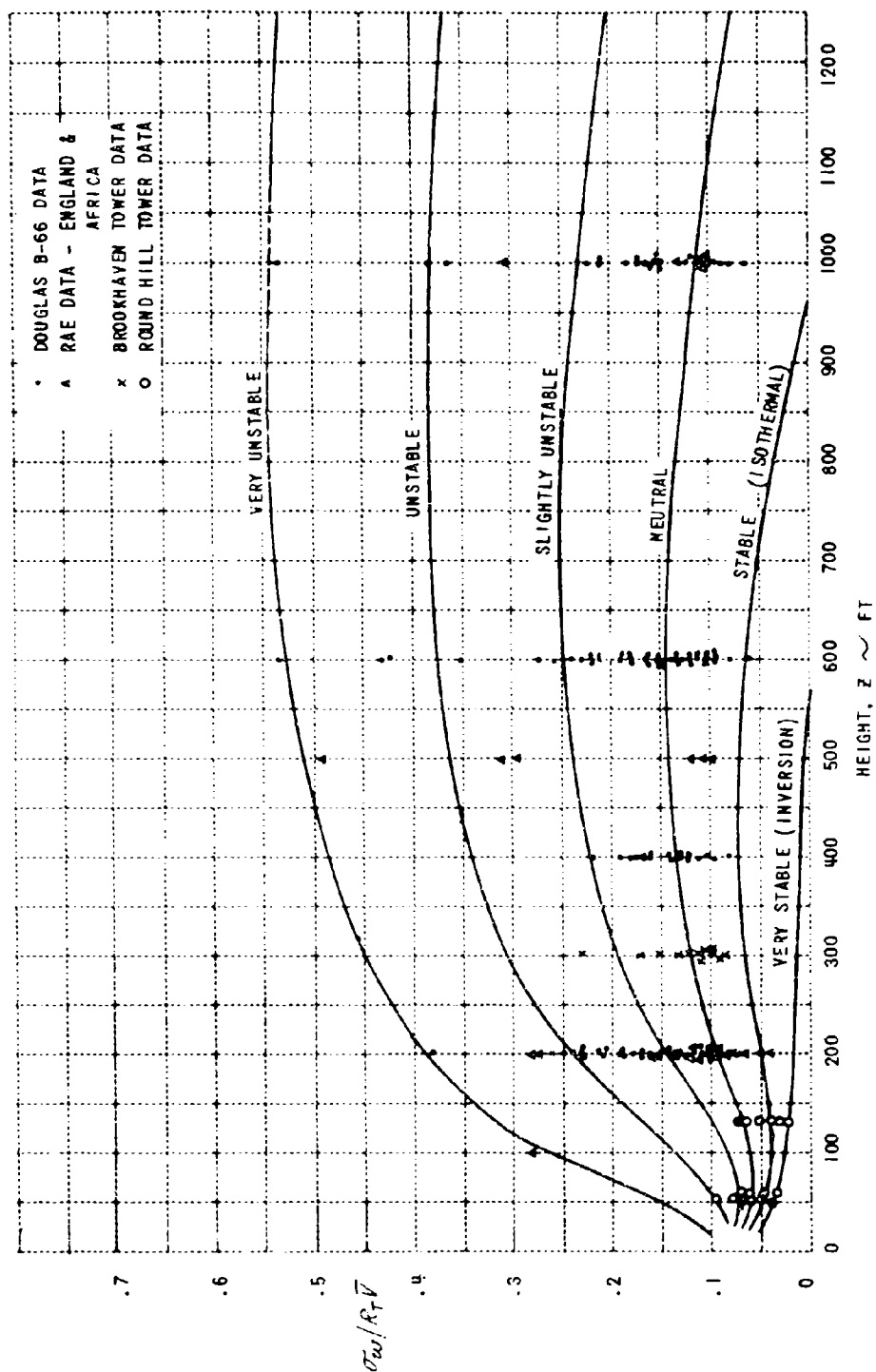
Figure 3. Terrain Normalized rms Vertical Gust Velocity Versus Height for Various Stabilities

13

4. The tower data should fit the over-all picture and act as a firm foundation to build upon.

5. The scale of turbulence is also a function of stability and should provide an independent means of checking the stability boundaries.

With the above items being carefully considered, the stability limits are set as in Figure 3. The tower data for 16, 40, and 91 meters proved to be very helpful in establishing the lapse rates for given $\sigma_w/\bar{V}$. The "slightly un-stable" line is drawn through points for the tower data with approximately dry adiabatic lapse rates. The approximate stability ranges represented on Figure 3 are: unstable, $\gamma \geq 3°C$ per thousand feet; neutral, $1.4 < \gamma < 3°C$ per thousand feet; and stable, $\gamma < 1.4°C$ per thousand feet.

The information indicated by Figure 3 relative to the rms gust velocity is summarized below,

1. $\sigma_w/\bar{V}$ increases with decreasing stability at all levels.

2. $\sigma_w/\bar{V}$ decreases with height under stable conditions.

3. $\sigma_w/\bar{V}$ remains relatively constant with height under neutral stability conditions.

4. Under unstable conditions, $\sigma_w/\bar{V}$ increases to a height of about 600 feet and then remains nearly constant.

5. At very low levels, $\sigma_w/\bar{V}$ decreases with height under all but the most severe instability conditions. This is due to the rapid increase in $\bar{V}$ in the first 50 to 100 feet from the surface (strong wind shear).

3.5 THE SCALE OF TURBULENCE

The term $A\ell$ of the spectral density equation, we have seen, represents the wavelength of maximum energy. For the low-level turbulence model (up to 1000 feet) ℓ is very nearly equal to the height z under certain conditions. If we force this relationship to be exact by letting $z = \ell$ for all conditions, then the scale of turbulence becomes Az where the scale factor A, according to the similarity theory, is a function only of stability and height. All the Az values computed from the spectra were divided by their respective measurement heights to get the value of the scale factor A. Comparison of the A values at each altitude shows no consistent relationship to the associated terrain type. However, there does appear to be a definite dependence of A on height. The A values were plotted against height only, ignoring the terrain classification (Figure 4). The existing spread in data points at any fixed height is then attributed to stability variations only. This result is substantiated by the tower data where detailed wind and temperature profiles were available. The difference between the actual lapse rate and the adiabatic lapse rate, $\gamma + \frac{\partial T}{\partial z}$, was computed for each A value. The correlation between
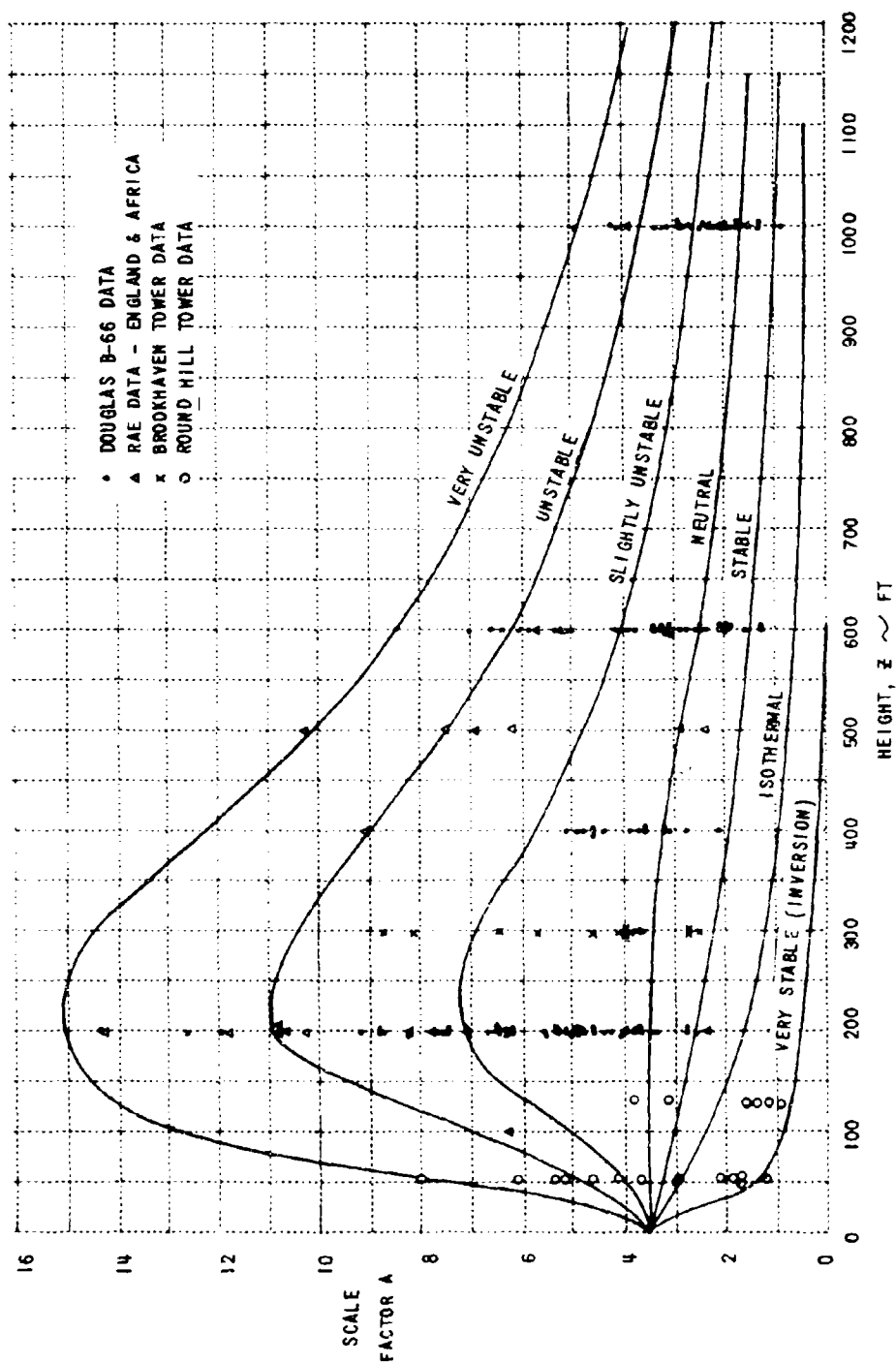
14

Figure 4. Scale Factor A Versus Height for Various Stability Conditions

the values and this stability parameter is reasonably good. The increase in scale parameter A is approximately linear with respect to the stability parameter $\left(\gamma + \frac{\partial T}{\partial z}\right)$. The stability curves drawn on Figure 4 were established using the stability information at the tower levels, and extended upward using the general distribution of the data points as a guide in the same manner (but independently) as for Figure 3.

Once these criteria had been applied independently to Figures 3 and 4, the stability limits were adjusted slightly to force consistency of the two figures. Since σ_w and $A\not z$ are computed from the same spectra, the stability lines should pass through the associated points on the two diagrams. The lines are adjusted on both plots in such a way as to provide the maximum correlation between the data and yet preserve most of the independent stability analysis.

The curves of Figure 4 convey the following information about the behavior of the scale of turbulence:

1. The scale of turbulence increases very rapidly with height under unstable conditions in the boundary layer, and continues to increase at a lower rate above this layer.

2. Under neutral conditions the scale factor A is nearly constant. Thus, the increase in the scale $A\not z$ is directly proportional to height.

3. Under very stable conditions the scale of turbulence is nearly constant with height.

4. The scale of turbulence increases with increasing instability at all levels.

5. The scale approaches a constant value in neutral and unstable conditions at a height well above 1000 feet.

3.6   LOW-LEVEL SPECTRUM PREDICTION

Figures 5 and 6 (spectrum prediction charts) are essentially the same as Figures 3 and 4 except for the reduction of the number of stability ranges included. For practical applications, three stability ranges, stable, neutral, and unstable, are considered adequate in view of the difficulty in estimating this parameter. The solid lines on these figures set the boundaries of the three ranges with the broken lines being used to represent each range. The stability limits used for these ranges are as follows:

1. Stable - lapse rate less than or equal to 1.4°C per 300 meters.

2. Neutral - lapse rate greater than 1.4°C per 300 meters but less than 3°C per 300 meters.

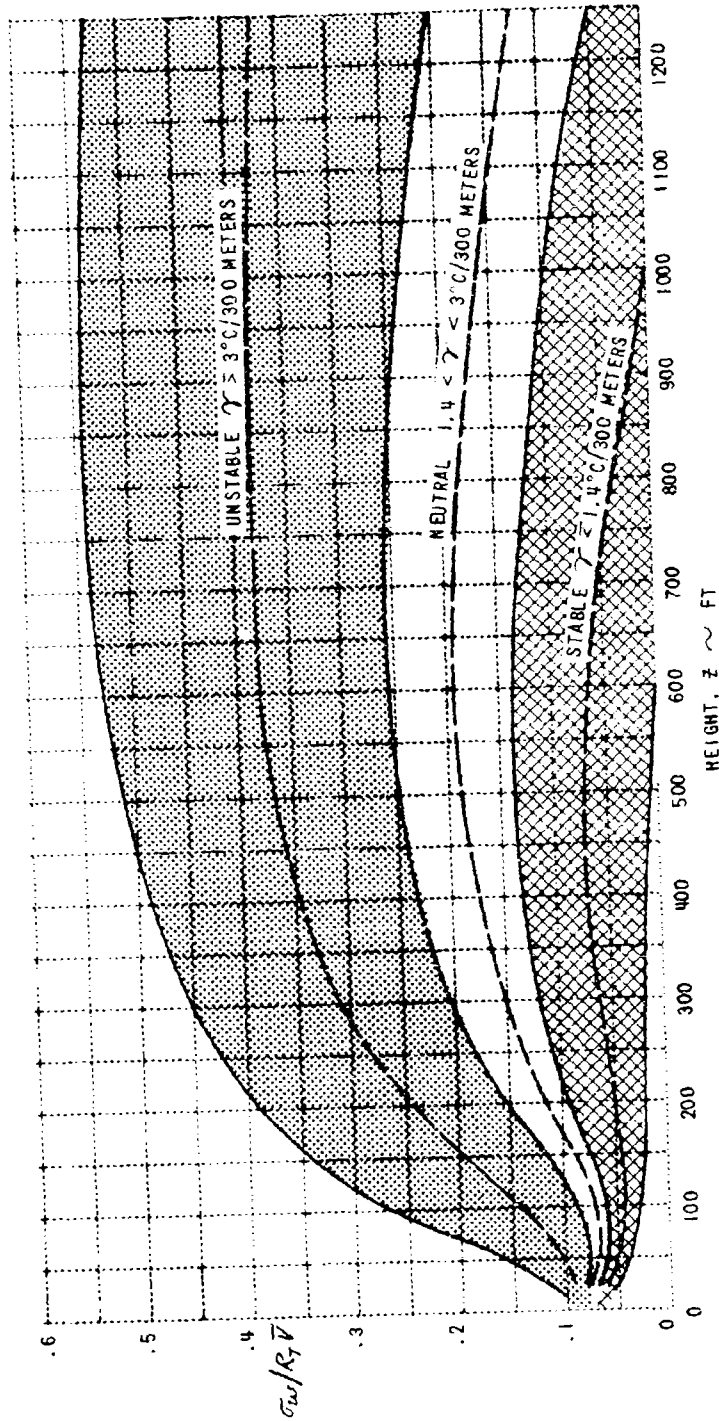| TERRAIN TYPE	OCEAN-DESERT	FARMLAND	FOREST & SWAMP	LOW MOUNTAINS	HIGH MOUNTAINS
TERRAIN FACTOR R_T	1	1.1	1.15	1.3	1.4

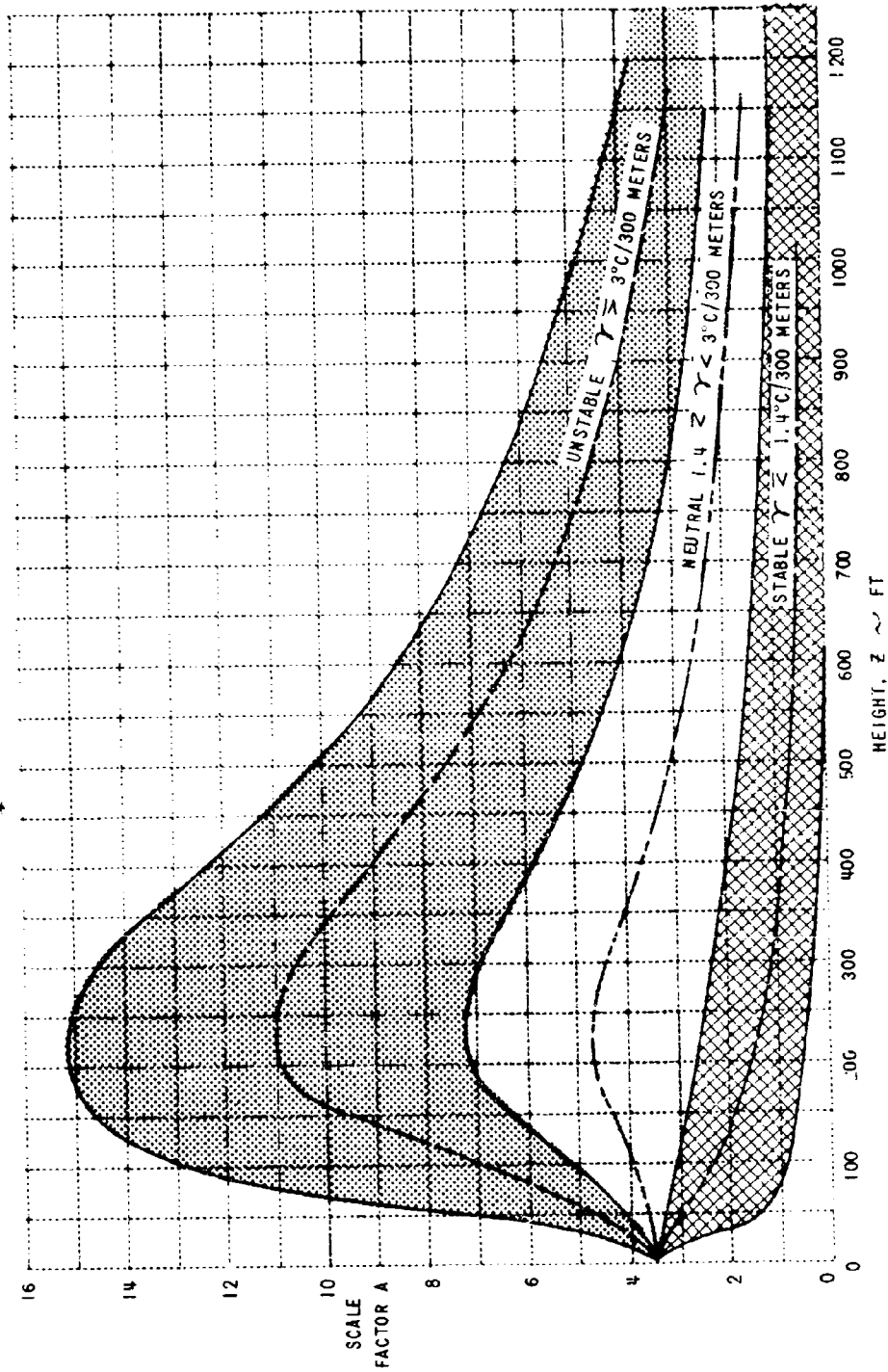Figure 5.   Spectrum Prediction Chart - rms Vertical Gust Velocity

17

Figure 6. Spectrum Prediction Chart - Scale Factor A

3. Unstable - lapse rate 3°C per 300 meters or greater.

Using the two charts (Figures 5 and 6) it is possible to estimate, with reasonable accuracy, an expected turbulence spectrum knowing a few basic flight parameters, namely, altitude, terrain type (5 classifications), expected stability range, and the expected mean wind velocity at the flight level. The scale factor A is obtained from Figure 6 and multiplied by the height $\bar{Z}$ to get the turbulence scale $A\bar{Z}$. The factor $\sigma_w/R_T\bar{V} = \epsilon$ is obtained from Figure 5. Thus, $\sigma_w^2 = (\epsilon R_T \bar{V})^2$ where R_T is the terrain factor and $\bar{V}$ is the predicted mean wind speed at height $\bar{Z}$.

3.7 GENERAL DISTRIBUTION OF TURBULENCE PARAMETERS

The final phase of the low-level turbulence model deals with the distributions of the wind velocity and atmospheric stability over a broad area and subsequently with the distributions of the dependent turbulence spectrum parameters. The area used for this investigation is the continental United States with 16 reporting stations being used as a source of meteorological data. It was decided that the small differences between the farmland, virgin land, and desert-ocean terrain types did not justify trying to classify reporting stations this carefully. Thus, these three categories were combined into a generally flat classification with a terrain factor of unity. The exposure ratios for the three remaining terrain types as represented by the continental United States are estimated to be: flat terrain 55%, low mountains 20%, and high mountains 25%. The reporting stations were then chosen to best represent the geographical and climatological areas of the United States, and, at the same time, maintain the above ratios between the number of stations in each of the three terrain categories.

The reporting stations selected are shown in Table 2.

TABLE 2

REPORTING STATIONS SELECTED FOR METEOROLOGICAL DATA

Flat $(R_T = 1)$	Low Mountains $(R_T = 1.3)$	High Mountains $(R_T = 1.4)$
Miami, Fla. Burrwood, La. Dodge City, Kansas Nantucket, Mass. Green Bay, Wisc. Midland, Texas Oakland, Calif. Bismarck, N. D. Omaha, Neb.	Greensboro, N. C. Seattle, Wash. Pittsburgh, Pa.	Albuquerque, N. M. Las Vegas, Nev. Lander, Wyo. Boise, Ida.

Two years of data covering the period July 1, 1957 through June 30, 1959 were processed in this analysis. All radiosonde and pilot balloon data for the above period were obtained for the above stations on punched cards from the National Weather Record Center in Asheville, North Carolina.

A computer program for the IBM 7044 was written to process this data as follows:

1. Compute the lapse rate in the layer from the surface to 300 meters for each observation.

2. Group the 150 and 300 meter wind velocities with their associated lapse rates.

3. Group the computed lapse rates and associated wind velocities into the three stability classes using the stability criteria discussed previously.

4. Compute the distribution of wind velocities at 150 and 300 meters associated with each of the three stability classifications for each of the four seasons, Spring, Summer, Winter and Autumn.

5. Compute the probability density $p(\sigma_w)$ for 150 and 300 meters using the wind distributions from 4 above and the equation $\sigma_w = \epsilon R_T \bar{V}$ from the previous section. The values for ϵ are obtained from Figure 5. The seasonal grouping is still maintained here.

6. Combine the data into an over-all $p(\sigma_w)$ distribution for all seasons for each of the stability ranges.

Since only the 150 meter and 300 meter winds were available on punch cards, the analysis is limited to these two heights (approximately 500 and 1000 feet).

The scale length A_Z, being independent of the wind velocity, has only a single value for each height and stability class used.

The final probability distributions $p(\sigma_w)$ are reproduced in Figures 7, 8, and 9. The distributions broken down into seasons showed little difference from the combined distributions, thus, only the latter are given. Figure 7 shows $p(\sigma_w)$ for flight levels of approximately 500 and 1000 feet above the surface for stable atmospheric conditions. The distribution for 1000 feet under this stability category is concentrated in the region σ_w less than 0.5 feet per second. Figure 8 presents the distributions for heights of 500 and 1000 feet under neutral conditions and Figure 9 shows the same for unstable conditions. A curious result is obtained for the $p(\sigma_w)$ distribution at 1000 feet under unstable conditions. The curve has a double peak, one peak centered at $\sigma_w = 4$ feet per second and the other at $\sigma_w = 7$ feet per second. The double peak in $p(\sigma_w)$ is a direct result of double maxima in the wind velocity distribution at 1000 feet.
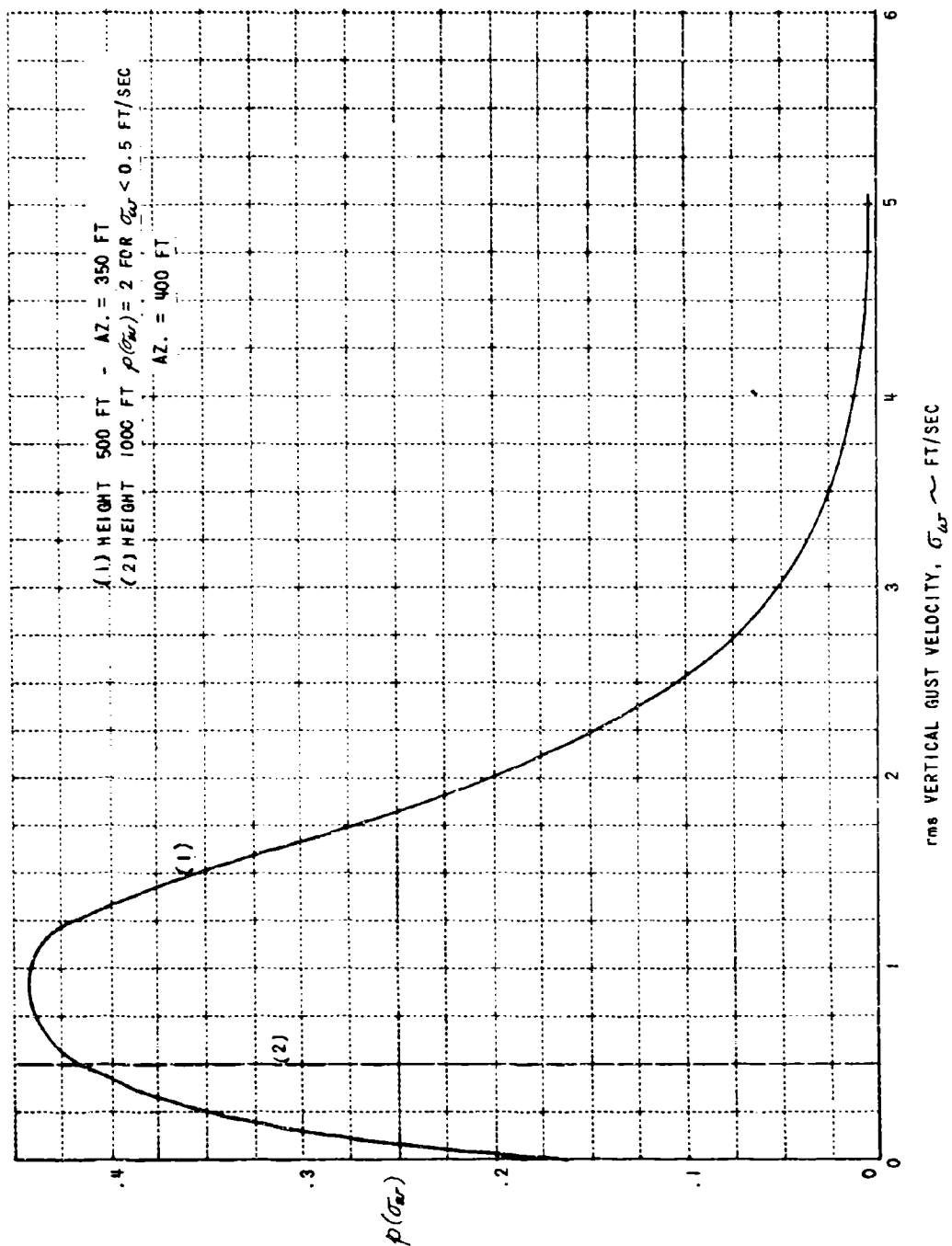
Figure 7. rms Vertical Gust Velocity Probability Density -- Stable Lapse Rate
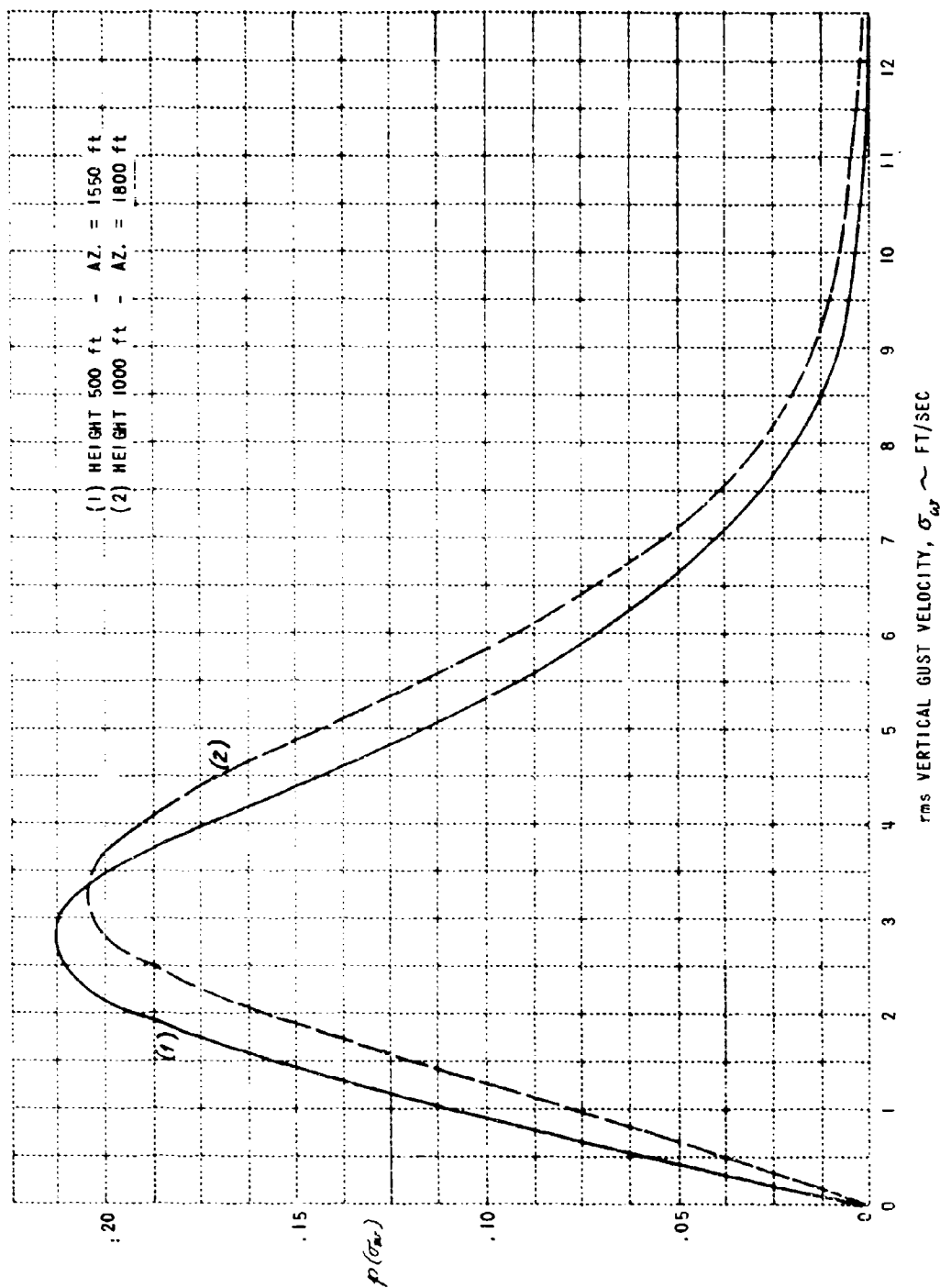
Figure 8. rms Vertical Gust Velocity Probability Density -- Neutral Lapse Rate
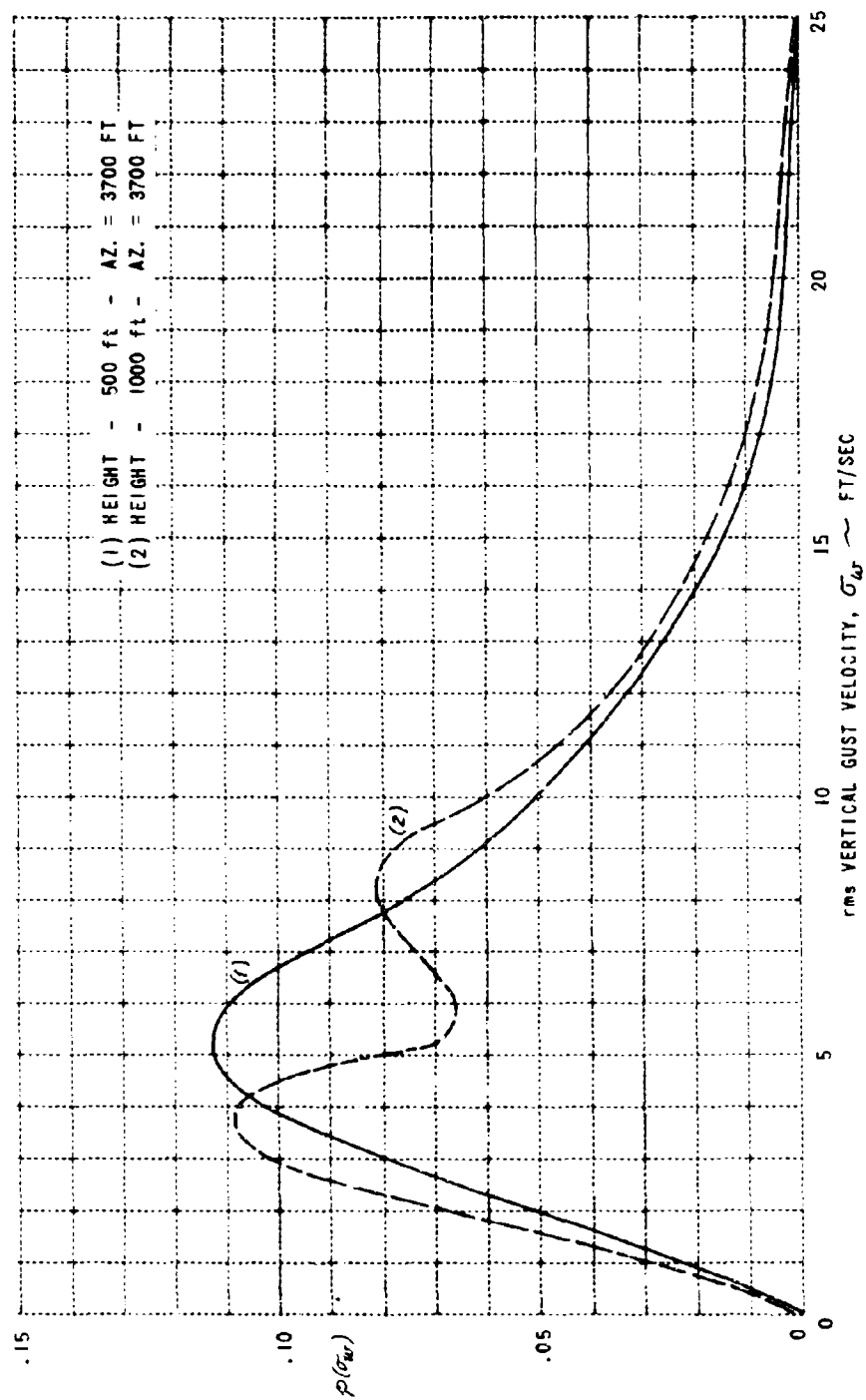
Figure 9.   rms Vertical Gust Velocity Probability Density -- Unstable Lapse Rate

The over-all σ_w-distribution curves shown in Figure 10 are the result of combining the stability categories with appropriate weighting factors. The ratio of the number of cases in each stability class as determined by the final computer output was, stable 43%, neutral 36%, and unstable 21%. It was thought, at first, that the radiosonde observation times would lead to a bias towards the stable and neutral categories. However, the three hour difference in local time across the country, together with the seasonal changes in sunrise and sunset apparently offset this bias. An independent estimate of the percentage of time each of the stability classes would apply in a 24-hour, year-round basis, came very close to the percentages above. Therefore, the composite distributions were derived using the computed ratios.

The curves in Figure 10, then, represent the expected distribution of σ_w for an aircraft sampling the whole of the United States on an annual, 24 hour basis.
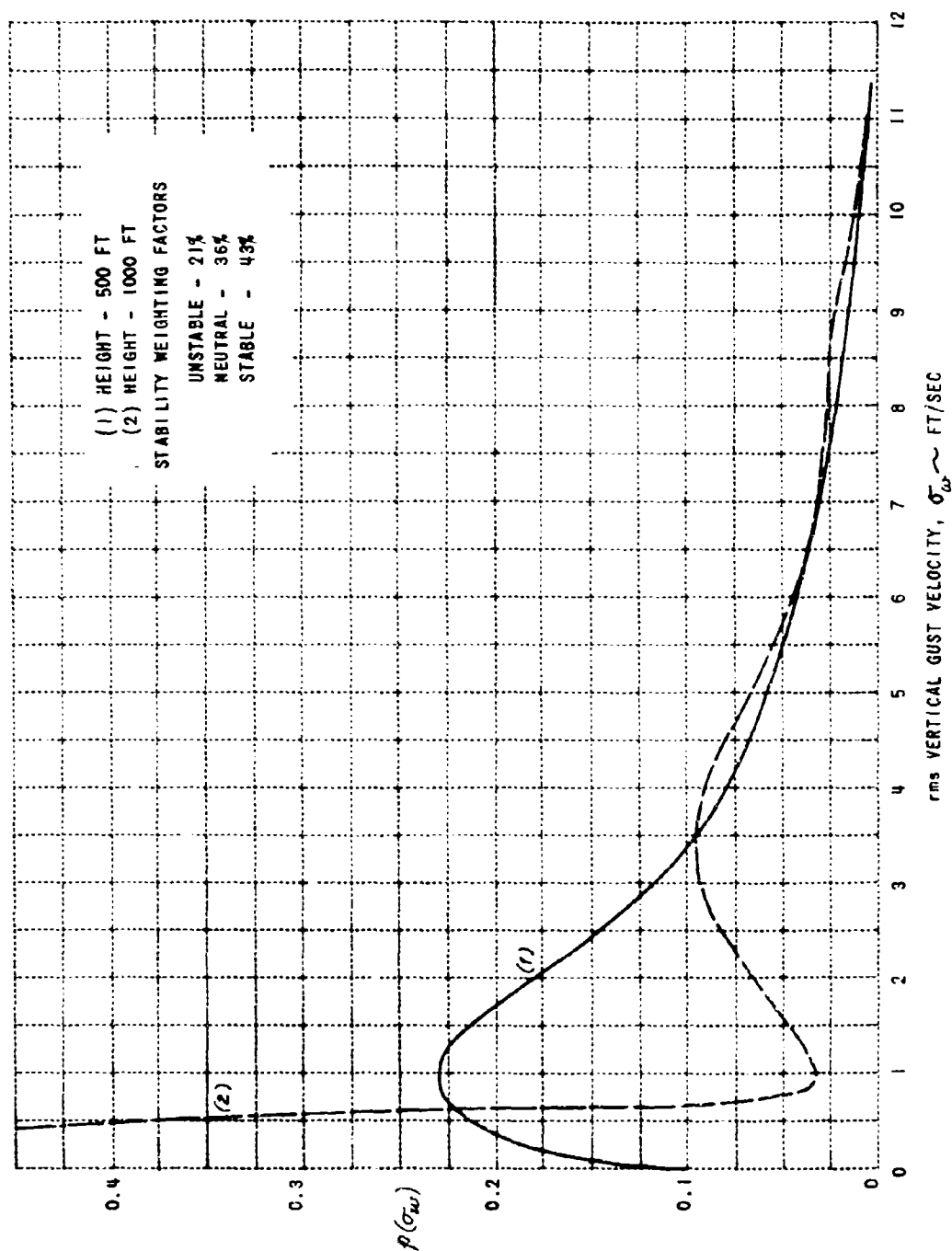
Figure 10. rms Vertical Gust Velocity Probability Density -- Combined Stability Conditions

SECTION 4

CONVECTIVE STORM TURBULENCE MODEL

The main group of spectra used in this analysis came from the Douglas B-66 turbulence program (Reference 9). The remainder of the spectra is taken from the storm penetration studies by NASA (Reference 10). There are 88 spectra in all, with the majority of penetrations being made through the upper levels in the range 25,000 to 40,000 feet. As in the previous low-level analysis, only the vertical gust spectra are considered.

The shapes of the storm spectra are essentially the same as those of the low-level spectra and appear to fit the same analytical form. There is no reason to suppose that height has any relationship to the scale of turbulence in the upper levels of convective storms, hence the $A\bar{Z}$ is replaced by L, and the storm spectral density equation becomes,

$$\phi_w(k) = \frac{\sigma_w^2 L}{(1 + kL)^2} \qquad (15)$$

Again, L is a measure of the scale of turbulence and represents the wave-length of maximum energy in the spectrum.

The two-point fitting technique was used once more to compute 88 pairs of values for σ_w^2 and L from the measured spectra. The results are plotted in Figure 11. Each point on the plot represents a pair of data points σ_{wi}, L_i corresponding to penetration i. Upon considering the data presented on Figure 11, it is immediately obvious that a certain correlation exists between rms gust velocity and scale size. In general, larger σ_w's are associated with larger scales. A closer examination of Figure 11 indicates that there may be two types of turbulence present in thunderstorms; a low intensity long wavelength form (represented by open symbols) and a more intense, shorter wavelength form (represented by solid symbols). The two regression lines shown in the diagram were computed using a least squares fit to the open and solid data points as indicated. The spread of data points about these two lines may well be explained by the inaccuracies in the measured spectra. However, the large difference in slope of the two regression equations is thought to be real. The unknown parameter which may be involved here is the position of the flight track relative to the main updrafts and downdrafts. It is not unreasonable to assume that the most intense, shorter scale, turbulence exists near the boundaries of the main drafts in areas of maximum shear. Penetrations made directly through or near the center of the main drafts would lead to short exposures to the shear areas and longer times spent in the long wavelength drafts, possibly accounting for regression line (1) in Figure 11. On the other hand, flight tracks along the edge of the drafts would prolong the exposure to the highly turbulent boundaries and thus lead to spectra character-ized by the regression line number (2). Unfortunately, this theory cannot be proven conclusively since no information is given regarding the position of the flight tracks relative to the active cells in the storms penetrated.
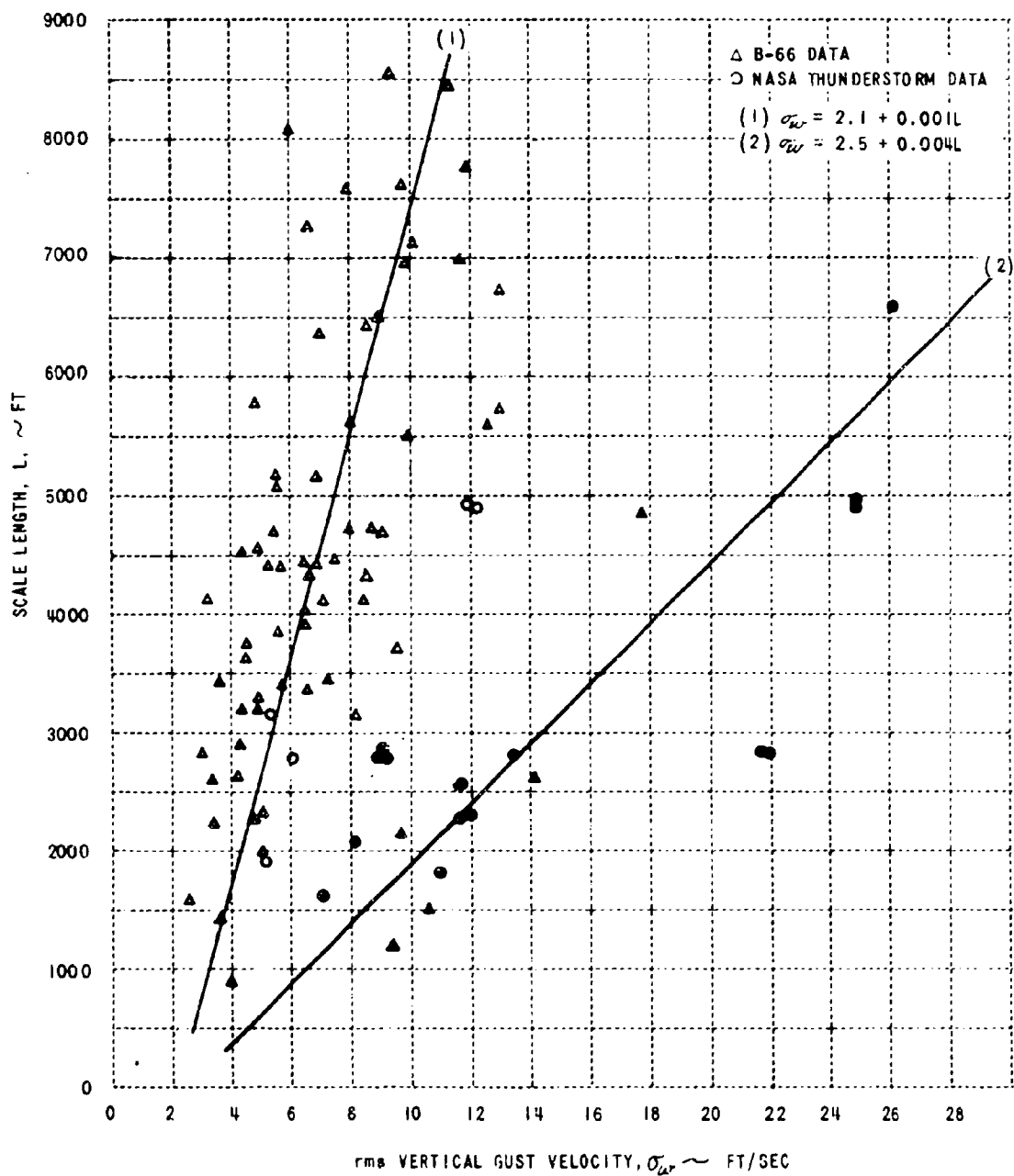
Figure 11· Distribution of Scale Length with rms Gust Velocity
For Thunderstorm Penetrations

27

We can, however, treat the data as a random sampling through thunderstorms, and thus consider the distribution of intensity and scale parameters to be the result of the entire sample. The probability density of the rms gust velocity is computed from the data using the expression,

$$p(\sigma_{w_i}) = \frac{N(\Delta \sigma_{w_i})}{N \Delta \sigma_{w}} \qquad (16)$$

where $p(\sigma_{w_i})$ is evaluated at the center of the interval $\Delta \sigma_{w_i}$

   $N(\Delta \sigma_{w_i})$ is the number of points falling in the interval $\Delta \sigma_{w_i}$

   N = total number of points

   $\Delta \sigma_{w}$ = 2 feet per second

The resulting distribution is shown in Figure 12. The peak occurs at a σ_{w} of about 5.5 feet per second but the long tail on the curve retains a finite probability of rms gust velocities exceeding 25 feet per second. This distribution is similar to the distribution given in the previous section for low-level turbulence under unstable conditions (Figure 9).

4.1 NUMBER OF GUSTS EXCEEDING GIVEN MAGNITUDE

It has been demonstrated by Press, Meadows, and Hadlock (Reference 11) that if turbulence is considered to be a stationary, Gaussian random process, results from random noise theory, as derived by S. O. Rice (Reference 12), may be applied to gain some useful information. The turbulence need only be locally Gaussian and stationary over a short time period (a single penetration through a convective storm). On this basis, an expression for the average number of positive (upward) gusts per unit distance may be written as follows:

$$N_0 = \left[\frac{\int_0^{\infty} k^2 \phi_w(k)\, dk}{\int_0^{\infty} \phi_w(k)\, dk} \right]^{\frac{1}{2}} \qquad (17)$$

Substituting Equation 8 for $\phi_w(k)$, N_0 can be integrated in closed form if the upper limit is finite. In practice, the aircraft which is sampling the turbulence assumes the role of a low pass filter with a cutoff wavelength which is of the order of magnitude of the wing chord distance. Thus, it appears practical to compute N_0 using an upper limit k_c in the range of a few feet to several tens of feet. Using Equations 8 and 17 we have

28
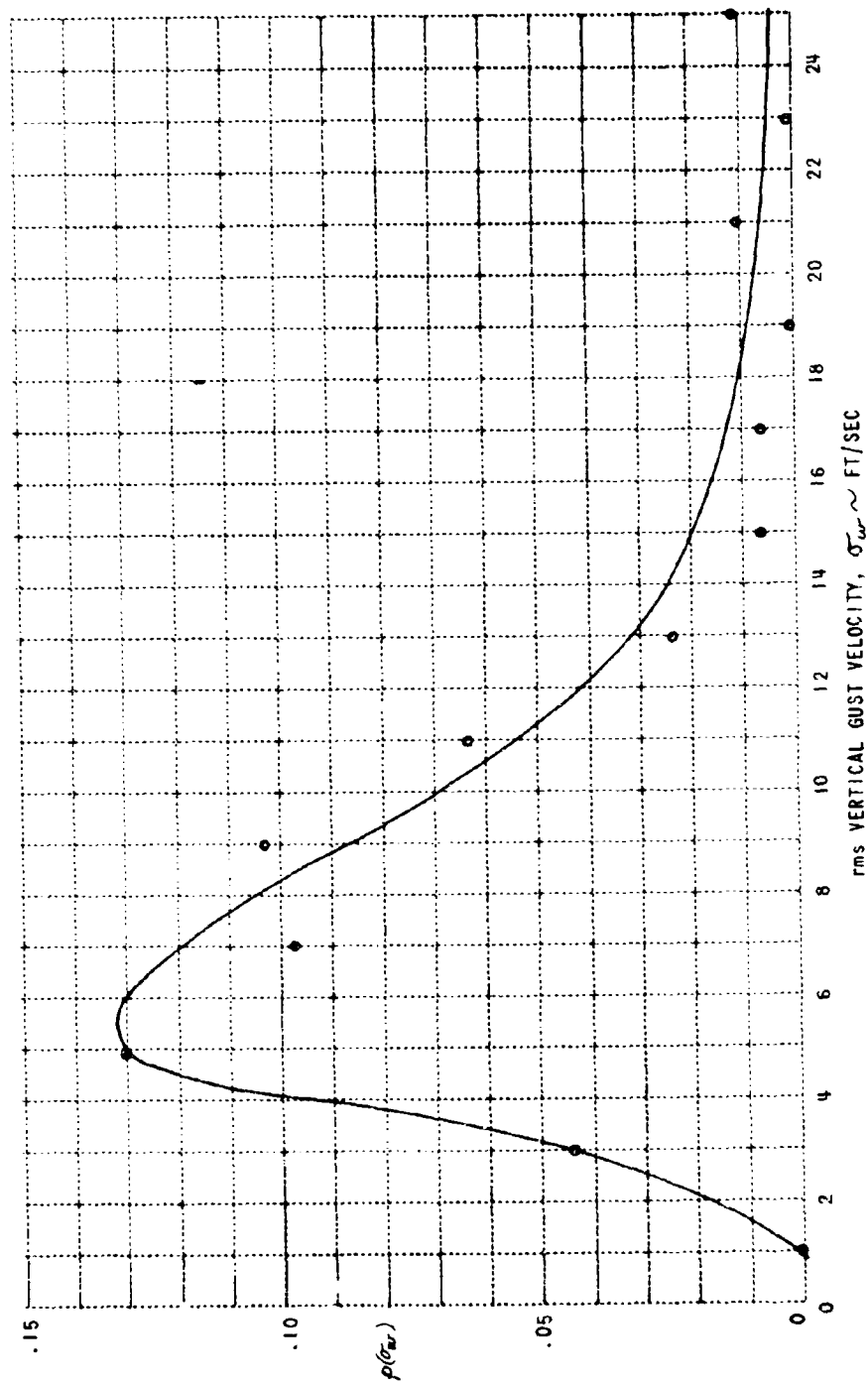
Figure 12. Probability Density of rms Vertical Gust Velocity in Thunderstorms

$$N_0 = \left[\frac{\int_0^{\hat{k}_c} \frac{\hat{k}^2 \sigma_w L}{(1+L\hat{k})^2} d\hat{k}}{\int_0^{\hat{k}_c} \frac{\sigma_w^2 L}{(1+L\hat{k})^2} d\hat{k}} \right]^{1/2} = \left[\frac{1}{L^2} \frac{\left[1 + L\hat{k} - 2\ell n(1+L\hat{k}) - \frac{1}{1+L\hat{k}} \right]_0^{\hat{k}_c}}{\left[-\frac{1}{1+L\hat{k}} \right]_0^{\hat{k}_c}} \right]^{1/2}$$

(18)

$$= \left[\frac{1}{L^2} \frac{1 + L\hat{k}_c - 2\ell n(1+L\hat{k}_c) - \frac{1}{1+L\hat{k}_c}}{1 - \frac{1}{1+L\hat{k}_c}} \right]^{1/2}$$

$$\approx \left(\frac{\hat{k}_c}{L} \right)^{1/2}, \quad L >> 1$$

(19)

For practical flight altitudes the L values will be large enough to make Equation 19 a very good approximation. Having computed the number of positive zero crossings, we can then go on to estimate the expected number of upward gusts per unit distance which exceed a given velocity w. This may be expressed as

$$N(w) = N_0 e^{-w^2/2\sigma_w^2}$$

(20)

The above is true for a single value of N_0 and σ_w (one particular turbulence spectrum). It has been shown in Reference 11 that if the distribution of σ_w is continuous, then Equation 20 can be replaced by

$$M(w) = N_0 \int_0^\infty p(\sigma_w) e^{-w^2/2\sigma_w^2} d\sigma_w$$

(21)

From the thunderstorm data of Figure 11, we see that L has a distribution as well as σ_w. Thus, $N_0 = (\hat{k}_c/L)^{1/2}$ will also have a distribution. We must then integrate over N_0 as well as σ_w. Equation 21 then becomes

$$M(w) = \int_0^\infty \int_0^{a_l} p(N_0 | \sigma_w) N_0 p(\sigma_w) e^{-w^2/2\sigma_w^2} d\sigma_w dN_0$$

(22)

where $p(\sigma_w)$ = probability density of σ_w

$p(N_0 | \sigma_w)$ = conditional probability density of N_0 for given σ_w

$N_0 = (\hat{k}_c/L)^{1/2}$, number of positive zero crossings per unit distance.

This double integral was evaluated by numerical methods using the distributions of L and σ_w given in Figures 11 and 12. In the computation the actual distribution of L is used up to $\sigma_w = 14$ ft/sec. Beyond this limit the data points are too sparse to compute a meaningful distribution and the number (2) regression line is used. $p(\sigma_w)$ is considered to be zero beyond $\sigma_w = 30$ ft/sec. The results of this computation are shown in Figure 13 for three different cutoff wavelengths. The curves are almost straight lines of the form

$$\log M(w) = \log M(0) - mw$$

where m is a constant and $M(0)$ depends on the cutoff wavelength. Curves for other cutoff wave numbers may be quickly calculated by simply multiplying the ordinate values for $k = 1$ foot^{-1} by the square root of the k_c value desired.
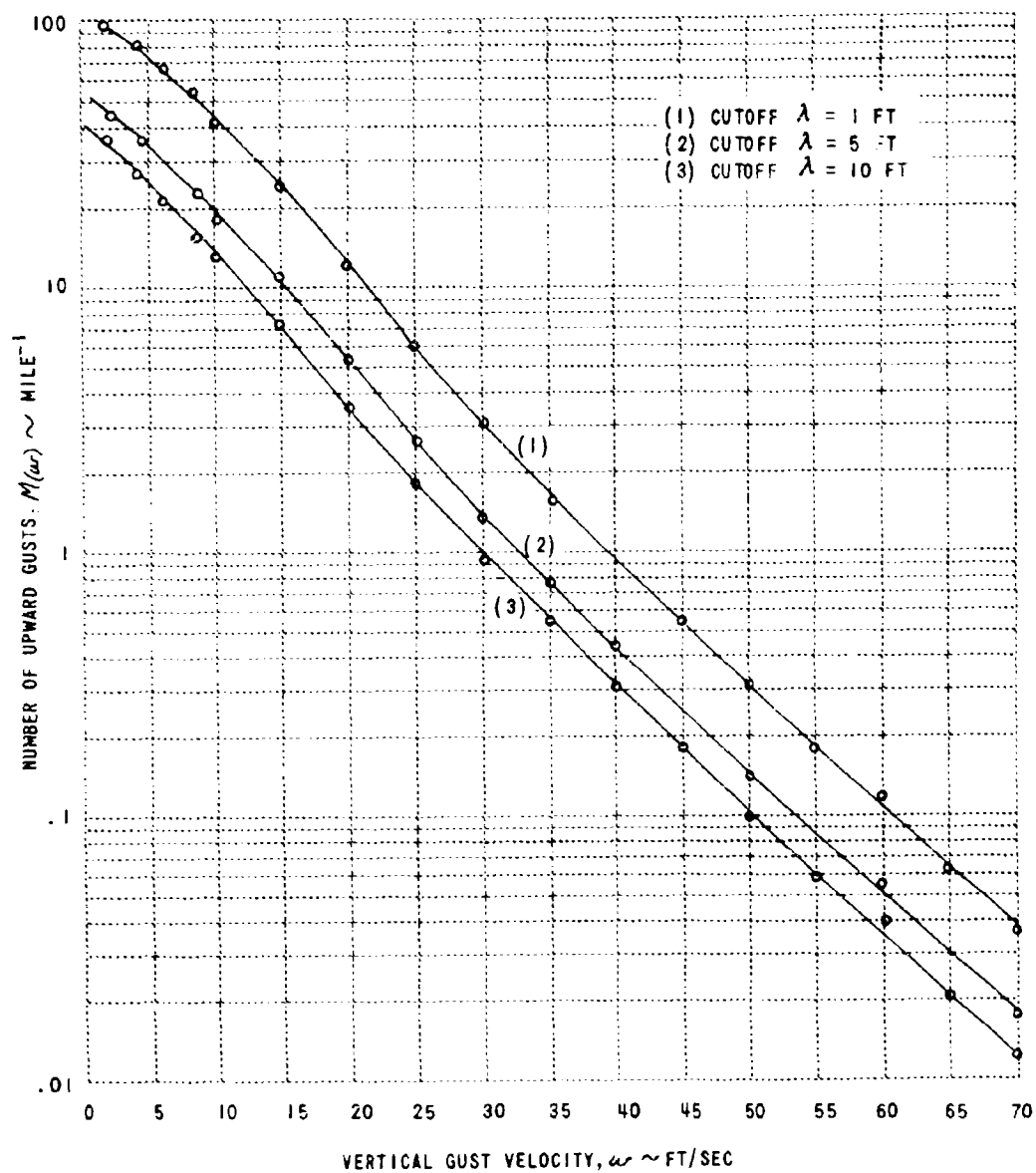
Figure 13. Expected Number of Upward Gusts per Mile of Flight Exceeding ω Ft/Sec for Thunderstorms

SECTION 5

TURBULENCE AT HIGH ALTITUDE

In the portion of the atmosphere above about 1000 feet, we can distinguish two classes of turbulence, normally referred to as storm and nonstorm turbulence. A more appropriate designation would be turbulence in cloud, referring to all turbulence in the troposphere that is found in or near clouds, and clear air turbulence (CAT), referring to turbulence in the stratosphere and in tropospheric regions without significant cloud formations. Tropospheric turbulence has been extensively sampled by VGH methods and, as illustrated by Section 6 of this report, a model for the probability of occurrence of specified gust intensities can be given with reasonable confidence for both storm and nonstorm turbulence. In addition, thunderstorm turbulence spectra are available from special observing programs with instrumented aircraft. A model for thunderstorm turbulence is given in Section 4.

It would be desirable to derive models for clear air turbulence and storm turbulence by the approach we have used in developing the low altitude model. The properties of the turbulence would first be related to meteorological factors, and then climatological data would be used to derive probability distributions for the turbulence variables. Unfortunately, there are virtually no spectral data available for either clear air turbulence or storm turbulence apart from thunderstorms. The Russian data of Shur (Reference 13) represent the only published spectra for CAT. Theory has not progressed far enough to predict the properties of the complete turbulence spectrum, or to definitely relate turbulence characteristics to meteorological variables. In view of this situation, it is clearly impossible to present any model for the turbulence spectrum and intensity distribution at high altitudes at this time.

In the remainder of this section, therefore, we restrict our discussion to a brief review of present knowledge of turbulence structure in the upper atmosphere, and discuss the limited evidence pertaining to spectral shape and the meteorological factors that lead to turbulence.

5.1 GENERAL STRUCTURE OF THE UPPER ATMOSPHERE

In that part of the atmosphere above about 25,000 feet, observed turbulence is almost exclusively the clear air type. Observations of air motion at these higher altitudes by many techniques (aircraft, balloons, and rockets) indicate that motions occur on three characteristic scales. At the largest scale there are the synoptic circulations depicted on weather maps. These have wavelengths in the range of one to several thousand kilometers. The next smaller class of important motions are mesoscale, with dimensions of the order of 100 km in the horizontal and 1 km in the vertical. Between the synoptic and mesoscales, the motion of the upper atmosphere is quite smooth, and few irregularities exist. The mesoscale motions have been detected only recently, but their occurrence appears to be quite common. Their horizontal

33

dimensions are large enough that they have limited direct effect on aircraft (except when executing rapid altitude changes) but they are of great interest as a possible source of actual clear air turbulence. Finally, on the smallest scale, there is CAT, the atmospheric motions with scales of a few hundred meters and smaller. CAT occurs less frequently than the mesoscale irregularities, though it is impossible with current data to accurately determine where and how often it does occur. Turbulence of light intensity is encountered fairly frequently by aircraft, but it has been estimated that moderate or severe CAT occurs in less than one percent of the upper troposphere and lower stratosphere (Panofsky, personal communication).

5.2   MODELS AND SPECTRA FOR HIGH ALTITUDE TURBULENCE

Numerous indices have been suggested as predictors of CAT. Since these all represent proposed relationships between CAT and mean meteorological quantities, they can be thought of as preliminary models. Unfortunately, none of the proposed relationships have been wholly successful, at least in part because of the lack of resolution in meteorological data available for testing them. Nearly all of the suggested predictors are derived from, or can be shown to be related to, theoretical considerations of the stability of waves or of the energy budget of turbulent flow. Wind shear and hydrostatic stability are nearly always included. A number of criteria for the prediction of CAT have been based on information available from a weather map or from routine aircraft observations, such as location with respect to the Jet Stream, curvature of the large scale flow, or magnitude of horizontal temperature gradients. The moderate success that has been obtained in relating some of these large scale features to CAT observations is almost certainly a result of the association of these features with strong wind shear and internal frontal zones. It is suggested that further improvement in models for relating turbulence to meteorological variables is unlikely to come from the introduction of additional meteorological parameters, but rather from a better knowledge of atmospheric fine-scale structure to which current theory can be applied.

At noted earlier, the only published spectra for clear air turbulence have been given by Shur (Reference 13). The main characteristics of these spectra are a high frequency portion that can be described by a -5/3 power law, and a lower frequency portion that shows a steeper slope represented by an exponent of -3. Shur explained the k^{-3} region as the result of energy dissipation by buoyancy. Since Shur's data appeared, Lumley (Reference 14) has presented a theoretical treatment of the turbulence spectrum for stably stratified flow that leads to the prediction of a k^{-3} range at low wave number, and to a $k^{-5/3}$ regime in the isotropic (inertial) sub-range. This substantiation of Shur's findings is encouraging, but many more data will be required before any definite conclusions can be drawn on the spectrum of clear air turbulence.

Spectral analyses of mesoscale motions by Kao and Woods (Reference 15) have shown energy decreasing with increasing wave number more rapidly than $k^{-5/3}$. However, this portion of the spectrum corresponds to wavelengths in the range 20-200 km, and is not representative of the region considered as CAT.

It is reasonable to expect from theory and from the limited data available that CAT spectra should obey a $k^{-5/3}$ law for high wave numbers. (For engineering application this region could probably be adequately approximated by a k^{-2} form, as used for the low altitude model.) At lower wave number, below perhaps 0.0015 m^{-1}, there is most likely a steeper region with slope exceeding $-5/3$, but the actual slope or extent of this portion cannot be determined until further data are available.

5.3 POSSIBLE PHYSICAL MECHANISMS FOR THE PRODUCTION OF CAT

The equation for the rate of change of turbulent energy in the atmosphere shows that turbulence may be generated either in regions of strong vertical shear of the horizontal wind, or in regions of unstable thermal stratification. The usual thermal stability of the stratosphere led originally to the notion that turbulence should be absent there; more recently the frequent observation of turbulence in the stratosphere led to the search for areas of unstable or adiabatic temperature distribution. Since such temperature distributions have been shown t be infrequent, it appears that CAT is most frequently produced by strong wind shear. Even where the thermal structure is hydrostatically stable, strong wind shear can produce turbulence despite the energy required to overcome the buoyancy forces. The Richardson number, which represents the ratio of turbulent energy dissipated in working against the stability to turbulent energy produced by shear, has been frequently used in attempting to relate CAT to wind and temperature. The failure to achieve high correlations between Richardson number and CAT occurrence is very probably a result of the lack of vertical resolution in upper air soundings. Computed Richardson numbers of necessity relate to mean conditions through an appreciable depth of atmosphere, and so may bear little relation to CAT produced in a thin internal region of sharp vertical gradients.

The existence of very narrow shear zones which represent internal boundaries between different air masses has been pointed out by Danielsen (Reference 16). These shear zones have been suggested by many authors to be a leading factor in the production of CAT. Internal fronts are characterized by strong wind shear and high stability. The Richardson number depends on the temperature gradient and inversely on the square of the wind shear; thus the narrower the frontal layer, the smaller is the Richardson number and the more likely is turbulence. Typical internal boundaries have vertical dimensions of the order of one thousand feet or less. Thus they are too narrow to be depicted in detail on regular upper air soundings, but because of their thinness, they are likely to lead to small values of Richardson number.

The preceding arguments are based on the hypothesis that CAT is produced directly through the growth of small disturbances in a favorable large scale atmospheric environment. An alternative explanation is that some CAT is produced indirectly by energy transfers from mesoscale disturbances. These mesoscale circulations have recently been studied by Hildreth (Reference 17), and observations of such circulations have been analyzed by Mantis (Reference 18) and Kao and Woods (Reference 15). It has been found that the mesoscale motions are definitely not isotropic; both velocities and

dimensions are considerably greater in the horizontal than the vertical direction. The exact nature of the motions has not been determined. They may be associated with gravity waves that result from perturbations introduced into regions of stable stratification and large wind shear. Or, alternatively, they may be more of the nature of turbulent eddies, with large vorticity.

There is adequate support in theory for the wide-spread occurrence of mesoscale motions, whether they are waves or eddies. In Reference 17, it is shown that certain expected combinations of wind and temperature structure will lead to the growth of waves from initial perturbations. A recent analysis by Pohle et al. (Reference 19) also indicates that horizontal wind shear on isentropic surfaces may produce mesoscale motions. It is interesting to note that similar conclusions have been reached for tropospheric motions by Peace (Reference 20).

Both the theory of turbulence (through the equation for turbulent energy) and classical wave theory show that with strong wind shear, eddies can exist and in certain circumstances waves will be unstable and will grow. These arguments pertain both to mesoscale motions and to small scale turbulence. Knowledge of upper atmosphere structure is adequate for us to be certain that favorable conditions for both mesoscale and small scale turbulence sometimes exist; there remains the question of which of these is ultimately responsible for observed CAT.

There are several reasons for believing that mesoscale motions, whether waves or vortices, could lead to CAT. If gravity waves continue to grow, they would eventually "break," thus leading to smaller scale turbulence. Eddies on the mesoscale could also result in eventual transfer of energy to higher wave numbers and into small-scale turbulence. It is clear from observations however, that CAT is much less common than the larger scale motions, so the problem remains of determining those precise conditions that lead to CAT, whether it is generated by mesoscale motions or directly.

In summary, it appears that CAT should be looked for in regions where unstable waves or mesoscale disturbances are likely to occur, and in narrow transition zones of large vertical wind shear. Such locations cannot be reliably located from current upper air data, so that future research into the causes of clear air turbulence should combine observations or turbulence with detailed probing of the atmospheric structure near the turbulent regions.

SECTION 6

THE EXCEEDANCE MODEL OF TURBULENCE

6.1   THE BASIC APPROACH

The presentation of the atmospheric turbulence data in this section is based on the theory developed by S. O. Rice (Reference 12) which enables one to calculate the number of times that a random variable, such as the vertical gust velocity w , exceeds a given level. Simple derivations of this theory for a stationary Gaussian (normal) process, the form which is generally considered applicable to the theory of the response of airplanes in random atmospheric turbulence, are given in Rice's classic paper as well as in References 21 and 22. The number of exceedances with positive slope of the level x per second for a single stationary Gaussian process of zero mean is

$$N(x) = N_{o,x} \, exp \left(- \frac{x^2}{2 \sigma_w{}^2} \right), \qquad sec^{-1} \qquad (23)$$

where $N_{o,x}$ is the number of zero crossings per second with positive slope, usually called the characteristic frequency, and σ_x is the rms value of x . The characteristic frequency may be calculated from the spectral density of x as follows, regardless of the probability density of x :

$$N_{o,x} = \frac{\sigma_{\dot{x}}}{2\pi \, \sigma_x} = \frac{1}{2\pi \sigma_x} \left[\int_o^\infty \omega^2 \phi_x (\omega) d\omega \right]^{1/2}, \qquad sec^{-1} \qquad (24)$$

Furthermore, σ_x , the rms value of x , can be calculated from the spectral density of x :

$$\sigma_x = \left[\int_o^\infty \phi_x (\omega) d\omega \right]^{1/2}, \qquad units \, of \, x \qquad (25)$$

Through the results of random process theory, one may also calculate $N_{o,x}$ and σ_x from either the autocorrelation function corresponding to $\phi_x (\omega)$ or the joint probability density function of x and $\dot{x}$. In the present work, however, it is more convenient to use the spectral density because of the frequency domain relationships between the spectrum of the vertical gust velocity and the spectra of the airplane responses.

The Applicability of Rice's Theory

It is useful at this point to discuss the applicability of Equations 21 and 22 to the problem of theoretically estimating the exceedance of an airplane response variable. Many studies, for example References 23 and 24, have shown that for short data runs on the order of 4 minutes, the probability density of the vertical gust velocity is closely Gaussian except for large values of w ($w \approx 3\sigma_w$) where the measured density is considerably larger than predicted by the Gaussian curve fitted to favor smaller values of w. Unfortunately, as a result of the general nonstationary character of atmospheric turbulence, it is impossible to obtain longer data runs so that a check of the probability density of w can be more reliably obtained. It is also quite common in other applications that fitted Gaussian density distributions underestimate the occurrence of large values of the random variable. For practical purposes, therefore, it is possible to regard the probability density of the vertical gust velocity as being Gaussian for short periods of time.

Furthermore, it is significant also that the vertical gust velocity has been shown to have an approximately Gaussian character for a large range of rms intensities including the intensities found in severe thunderstorms (Reference 10) (e.g., Figure 14).

Although the characteristic frequency $N_{o,x}$ may be evaluated either from measured data or theoretically, it is undoubtedly the weakest link in the chain of calculations required for the theoretical determination of $N(x)$. This is understandable in view of the large dependence of $N_{o,x}$ on frequency, due to the ω^2 factor in the integral of Equation 24. In fact, because none of the common mathematical forms for the vertical gust velocity spectrum approach zero rapidly enough with increasing high frequency, the integral for the characteristics frequency of the gust velocity does not converge. This undesirable feature of the common spectral forms may be overcome by making use of the concept of the "viscous subrange" wherein the spectrum theoretically approaches zero amplitude much more rapidly with frequency. Heisenberg's estimate of this asymptotic behavior is ω^{-7} (Reference 25). Theoretical calculations of $N_{o,x}$ for airplane response variables, although not troubled by convergence problems, require complex linear representations of the airplane transfer function, including consideration of unsteady aerodynamics and airplane flexibility, to achieve acceptable results.

In a practical sense, $N_{o,x}$ may be estimated from measured data in several ways. One approach suggested in Reference 11 makes use of short sample sections of the time history of the variable. Under the assumption that the variable is Gaussian (so that Equation 23 applies), one would determine, for instance, $N(2\sigma_x)$ and σ_x from a short sample section and solve for $N_{o,x}$ using Equation 23. Another approach involves numerical integrations of a measured gust or response spectrum. The integration, of course, cannot be carried to infinity because of the limited frequency range of the data, but the range of frequencies available is usually sufficient.
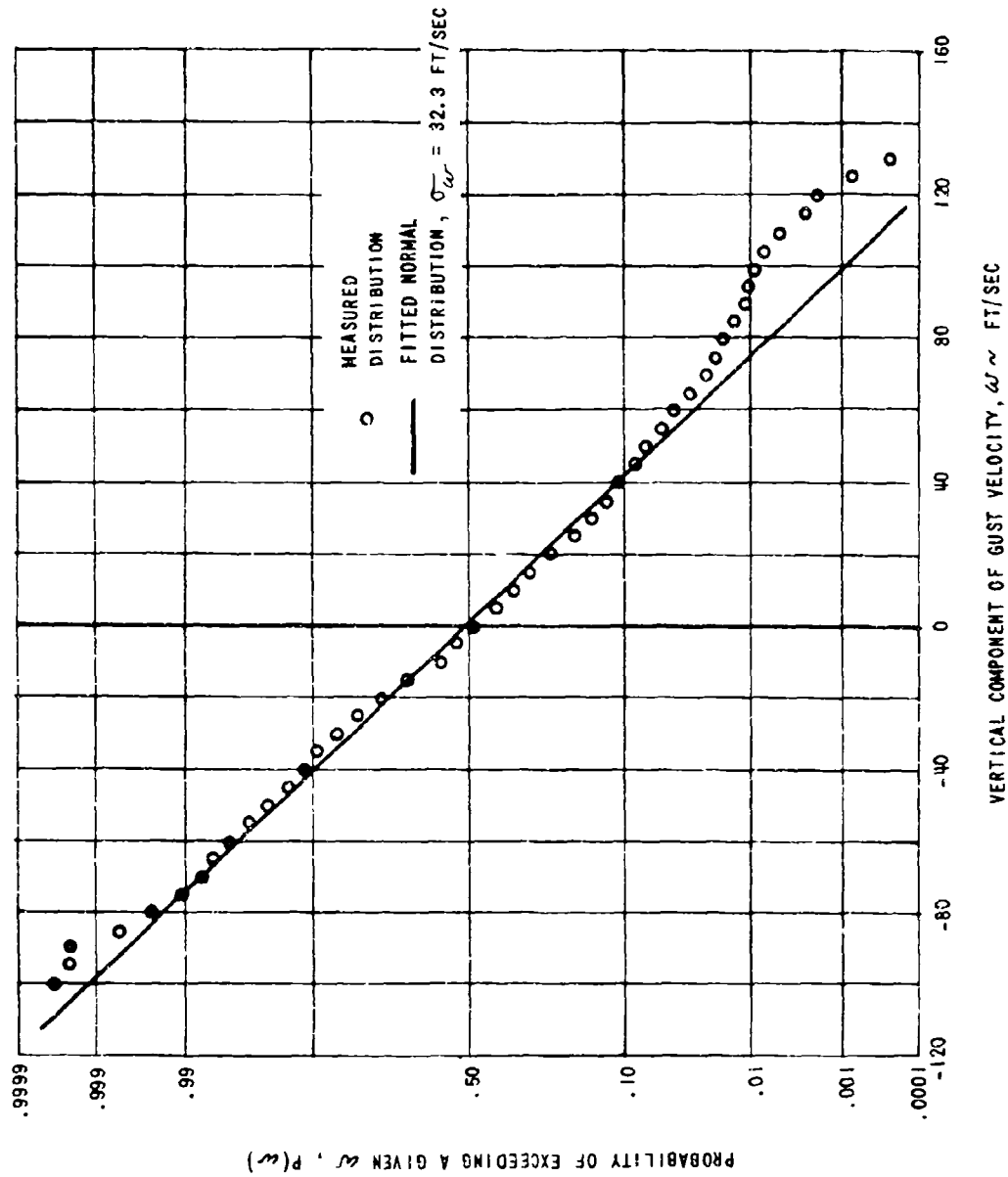
Figure 14. Cumulative Probability Distribution of the Vertical Gust Velocity for a Thunderstorm Penetration (from Ref. 10)

It may be assumed, therefore, that Equations 23 and 24 do in fact apply for purposes of calculating the assumed linear responses of airplanes to atmospheric turbulence.

The Extension to Cover Flight Operations

During the course of many hours or miles of flight operation, an airplane is subjected to various rms levels of the vertical gust velocity. As a result of this, the distribution of exceedances or peak counts is nearly always much different from a Gaussian distribution. In Reference 11, an analytical procedure was developed to cope with this situation based on the assumption that the airplane encounters turbulence of all intensities, that is, it is assumed that the airplane encounters continuous variations of the rms vertical gust velocity, σ_w. It is necessary, therefore, to specify a probability density function $p(\sigma_w)$, and when this is done, the over-all exceedance or peak count distribution is given by the integral

$$M(x) = N_{0,x} \int_0^\infty p(\sigma_w) \, exp\left(-\frac{1}{2}\frac{x^2}{\sigma_w^2 A_x^2}\right) d\sigma_w \tag{26}$$

where A_x and $N_{0,x}$ are independent of σ_w, and $\sigma_x^2 = \sigma_w^2 A_x^2$.

Since $p(\sigma_w) d\sigma_w$ represents the proportion of flight time that the airplane spends in turbulence of intensities from σ_w to $\sigma_w + d\sigma_w$, the integral may be thought of as a weighted average of Gaussian exceedance distributions (see Equation 23). The distribution $M(x)$ given by Equation 26 depends on flight condition through the parameters $N_{0,x}$ and A_x, which are functions of the scale of turbulence L and the airplane transfer function relating the response x to the gust velocity w.

Press, Meadows and Hadlock (Reference 11) also discuss three different probability density distributions which they assumed would be generally useful. However, in more recent work by NASA and others, only one of the three distributions has been used: it is Case a of Reference 11, which permits analytical integration of Equation 26. This probability density function is a Gaussian distribution that is restricted to positive values of the random variable, and therefore the amplitude has been appropriately multiplied by 2:

$$p(\sigma_w) = \frac{1}{b}\sqrt{\frac{2}{\pi}} \, exp\left(-\frac{1}{2}\frac{\sigma_w^2}{b^2}\right), \quad \sigma_w \geq 0 \tag{27}$$

Integration of Equation 26 with this probability density function yields

$$M(x) = N_{0,x} \, exp\left(-\frac{1}{b}\frac{|X|}{A_x}\right) \tag{28}$$

Furthermore, it has been assumed that there are at least two density functions $p_i(\sigma_w)$ to account for different types of turbulence. For example, the best known types of turbulence are those used by NASA (e.g., References 26 and 27), namely, the nonstorm and storm types having density functions $p_1(\sigma_w)$ and $p_2(\sigma_w)$ respectively. The density functions, both of the form of Equation 27, are combined according to the discrete probability of encountering either one:

$$p(\sigma_w) = P_1 p_1(\sigma_w) + P_2 p_2(\sigma_w) \tag{29}$$

The probabilities P_i, which can be considered the proportions of total flight time spent in the type of turbulence described by $p_i(\sigma_w)$, are constrained as follows.

$$P_0 + P_1 + P_2 = 1 \tag{30}$$

where P_0 is the probability of encountering smooth air conditions. Note that since $\sigma_w^2 \cong 0$ for smooth air, $p_0(\sigma_w) \neq 0$. Equations exactly analogous to 29 and 30 may be formed if more than two distinct types of turbulence are considered.

For several distributions $p_i(\sigma_w)$ with corresponding discrete probabilities P_i, Equation 28 may be written in the form

$$M(x) = N_{o,y} \sum_{i=1}^{n} P_i \, exp\left(-\frac{1}{b_i} \frac{|x|}{A_x}\right) \tag{31}$$

which, like Equation 28, is valid only for one scale of turbulence and one flight condition (aircraft transfer function). Equation 31, when n is 2 or 3, is the form used for the exceedance probability model in Section 6, except that the equation is put into a partly nondimensional form by dividing by $N_{o,x}$:

$$\frac{M(x)}{N_{o,x}} = P_1 \, exp\left(-\frac{1}{b_1} \frac{|x|}{A_x}\right) + P_2 \, exp\left(-\frac{1}{b_2} \frac{|x|}{A_x}\right) + P_3 \, exp\left(-\frac{1}{b_3} \frac{|x|}{A_x}\right) \tag{32}$$

The equation is only partly nondimensional when in this $M(x)/N_{o,x}$ vs. $|x|/A_x$ form because $|x|/A_x$ has the units of ft/sec.

41

Classification of the Types of Turbulence

For several reasons, two of which are listed below, rather nondescriptive names have been chosen for the major types of turbulence. These are:

P_1, ℓ_1 primary turbulence,

P_2, ℓ_2 secondary turbulence, and

P_3, ℓ_3 tertiary turbulence.

Primary and secondary turbulence may be associated with nonstorm and storm turbulence respectively, if desired, and the tertiary turbulence is the severe turbulence associated at low levels with certain terrain features such as described in Reference 46.

Airplane operations, particularly the operations of commercial airliners, have generally produced peak count or exceedance data showing two relatively distinct distributions. By a process of elimination based on circumstantial evidence, the two distributions have been named storm and nonstorm. The storm turbulence is identified first because the higher intensity distribution of the operational peak count data has an intensity closely matching the intensity measured specially in thunderstorms. The lower intensity distribution is then associated with nonstorm conditions. This breakdown of the operational data is based on the assumption that the rms turbulence velocities in thunderstorms are distributed according to Equation 27, whereas the actual distribution is more nearly like that shown in Figure 12. Although the differences between Equation 27 and the distribution of Figure 12 are large only for small rms intensities, the discrepancy tends to point out a need for more careful assessment of the situation.

Another example of the arbitrariness of breaking down the turbulence environment according to type of turbulence can be illustrated by considering the fact that the density distributions $p(\sigma_w)$ of Cases b and c of Reference 11 result in very good fits to measured data. Both of these distributions yield exceedance or peak count distributions exhibiting the same general characteristics as Equation 32. Ordinarily, the measured peak count and exceedance distributions curve upward at large gust velocities (or accelerations) more gently than allowed by the analytical form of Equation 32 with two or three terms. By analyzing the data available to them, Press, Meadows and Hadlock (Reference 11) decided that most peak count distributions were best fitted by the curves derived using Case b and c density distributions of σ_w . The data presented in Figure 8 of Reference 28 and Figure 6 of Reference 29, Vol. 1, for example, also show a more gradual upward curvature. One possible interpretation of these data is that, instead of being represented by a composite of 2 or 3 one-sided Gaussian distributions (like Equation 27), σ_w is represented by some non-Gaussian density distribution. It is evident that more research is necessary in this area to better define the basic approach.

The Approach to the Exceedance Model of Turbulence

The work described in this section deals with the problem of determining the parameters $P_1, \ell_1, P_2, \ell_2, P_3, \ell_3$ of Equation 32 as functions of the altitude above the terrain, Z. The exceedance probability model has, therefore, the functional form

$$\frac{M(x)}{N_{0,x}} = f\left(\frac{|x|}{A_x}, Z\right) \tag{33}$$

The P_i and ℓ_i parameters are presented graphically or in tabular form as functions of Z to define the basic model. Then to account for variation of the basic statistics due to terrain roughness, season, etc. correction factors for the P_i and ℓ_i parameters are developed.

Once the P_i and ℓ_i parameters have been defined, it is a simple matter to obtain the probability density $p(\sigma_w)$ and the cumulative probability distribution $P(\sigma_w)$ of the rms vertical gust velocity σ_w using Equations 29 and 27.

6.2 DETERMINATION OF THE P AND ℓ PARAMETERS

The exceedance probability model of this Section 6 was developed almost entirely from data obtained during routine airplane operations and during several special gust measurement programs. The analysis techniques varied widely according to the nature of the various data. Since all of the mathematical techniques employed to analyze these data require use of the vertical gust velocity spectrum, consideration was given to the various spectral forms that have been suggested, and a spectrum form was selected. The various methods used to determine the P and ℓ parameters have been described in numerous NASA reports, are not new, and are based largely on the properties of Equation 32.

Data Sources

Data used in the development of the exceedance probability model have been obtained from many different airplanes both military and civil; the airplanes range in size from small fighter airplanes to large turbojet bombers and transports. In terms of the sample time represented, by far the largest portion is VGH-type data; a very small percentage of the total data sample has come from direct gust measurement programs. The data come mostly from U.S. sources, but English and Canadian data are included. The data were collected using the airplanes listed in Table 3, which is separated according to the type of data obtained.

43

TABLE 3

DATA SOURCES FOR THE EXCEEDANCE MODEL

VGH-Type Data

Airplane	Reference	Origin
KC-135	30	U.S.A.
B-52 B-F	29	U.S.A.
Sabre Mk. V	31	Canada
DC-4M	32	Canada
Canberra B.6	33	England
A3D	34	U.S.A.
YRB-58A	35	U.S.A.
U-2	36, 37	U.S.A.
P-61	38	U.S.A.
F-27	39	U.S.A.
Viscount	40	U.S.A.
Britannia	41	Canada
Various Transport Airplanes	28	U.S.A.
Various Transport Airplanes	42	U.S.A.
Various Transport Airplanes	43	England

Direct Gust Data

Airplane	Reference	Origin
FH-1	44, 45	U.S.A.
NB-66B	9	U.S.A.
T-33	10	U.S.A.
F-86	10	U.S.A.
F-106A	46	U.S.A.
B-66B	4	U.S.A.
Canberra B.6	5	England

The Turbulence Spectrum Used for Exceedance Analysis

Until very recently, the most commonly used spectral form for the transverse components (w, v) of isotropic turbulence was the form attributed to Dryden:

$$\phi_w (\Omega, L) = \sigma_w^2 \frac{L}{\pi} \frac{1 + 3(L\Omega)^2}{\left[1 + (L\Omega)^2\right]^2} \quad , \quad \frac{(ft/sec)^2}{(rad/ft)} \tag{34}$$

which is here defined so that

$$\sigma_{w}^{2} = \int_{0}^{\infty} \phi_{w} \left(\Omega, L \right) d\Omega \, , \text{ (ft/sec)}^{2} \tag{35}$$

This spectrum is plotted in Figure 15 for a range of values of L . The longitudinal spectrum corresponding to Equation 34 is

$$\phi_{u} \left(\Omega, L \right) = \sigma_{u}^{2} \frac{2L}{\pi} \frac{1}{1 + (L\Omega)^{2}} \, . \tag{36}$$

Recently, a spectral form suggested originally by von Karman has been gaining wide approval both in the U. S. and England. The form exhibits an $\Omega^{-5/3}$ behavior for large Ω and is therefore consistent with theoretical results concerning the change of spectrum amplitude with frequency in the so-called "inertial subrange" (References 24 and 25). This spectrum, which is plotted for various L's in Figure 16, has the form

$$\phi_{w} \left(\Omega, L \right) = \sigma_{w}^{2} \frac{L}{\pi} \frac{1 + \frac{8}{3} \left(1.339 \, L \, \Omega \right)^{2}}{\left[1 + \left(1.339 \, L \, \Omega \right)^{2} \right]^{11/16}} \, . \tag{37}$$

for which Equation 35 holds. The corresponding longitudinal spectrum is

$$\phi_{u} \left(\Omega, L \right) = \sigma_{u}^{2} \frac{2L}{\pi} \frac{1}{\left[1 + \left(1.339 \, L \, \Omega \right)^{2} \right]^{5/6}} \, . \tag{38}$$

Certain properties of the von Karman spectrum, and the Dryden spectrum as well, are given in Appendix B of Reference 24 and Chapter 9 of Reference 52.

Comparison of the von Karman and Dryden Spectra

The most obvious difference between the von Karman and Dryden spectra is, of course, the asymptotic behavior at large values of frequency, the former behaving as $\Omega^{-5/3}$ and the latter as Ω^{-2}. The preponderance of recent experimental evidence favors the $\Omega^{-5/3}$ behavior, and this is in accordance with the accepted theory. Although the von Karman spectrum generally results in better correlation between direct gust data and VGH-type data (Chapters 2 and 10 of Reference 52), the differences between the von Karman and Dryden spectra are small and considered negligible when the spectra are used with peak count or exceedance data.

In addition, the Dryden spectrum facilitates analytical computations because of its rational form (i. e. , the numerator and denominator are simply polynomials in $L\Omega$). Analytical integrations may therefore be performed
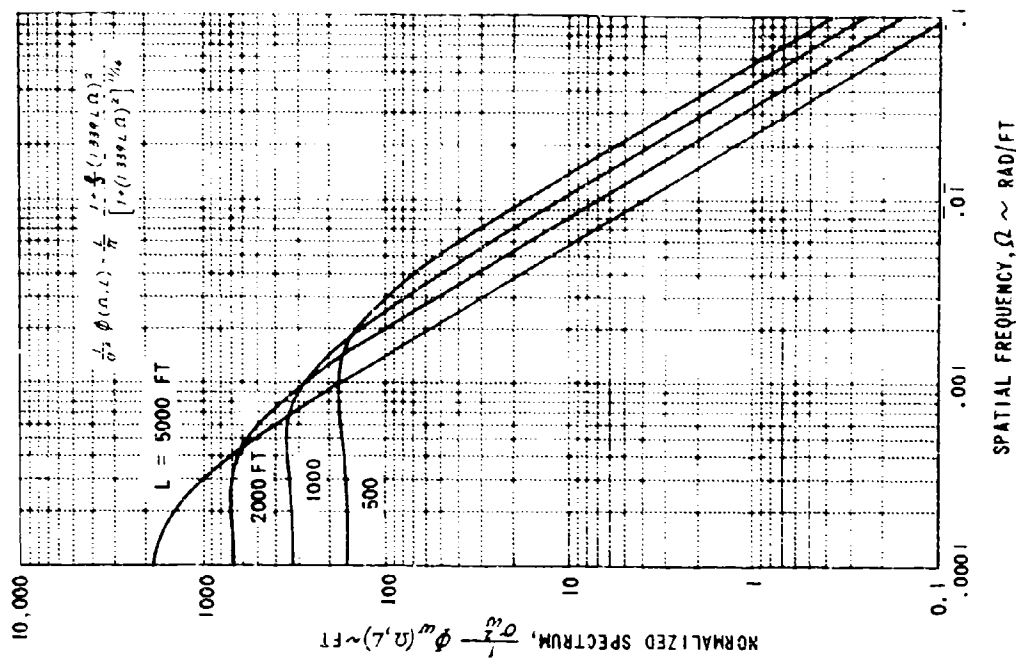
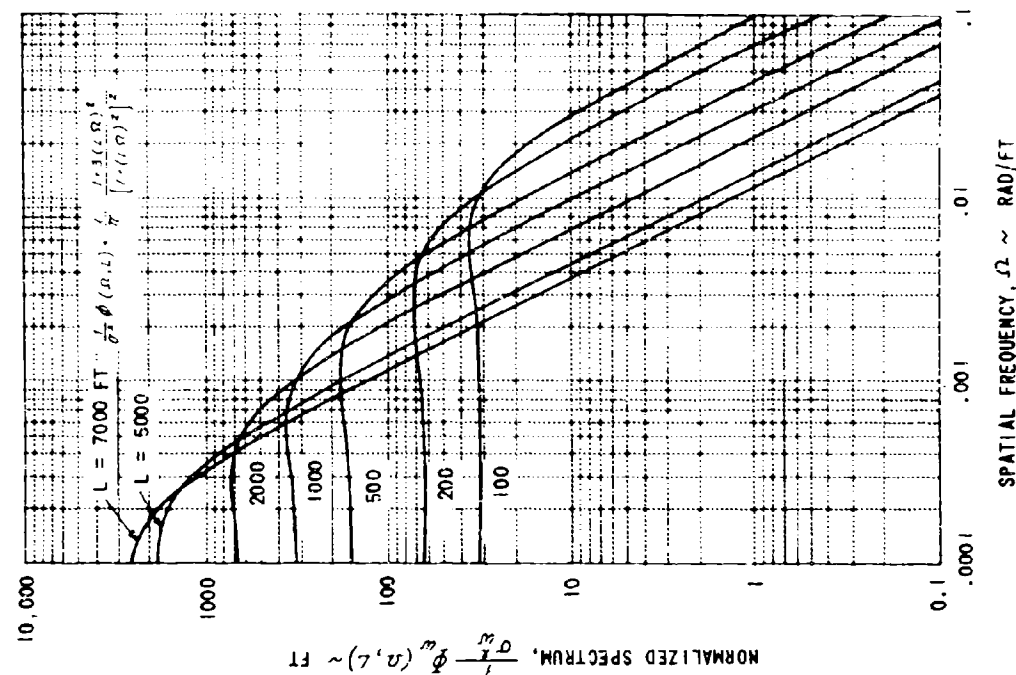Figure 16. The von Karman Spectral Form for the Vertical Turbulence Velocity

Figure 15. The Dryden Spectral Form for the Vertical Turbulence Velocity

if desired, and the spectrum may easily be factored to determine a transfer function that can be used to shape (filter) white noise to obtain a time history representation of atmospheric turbulence for simulations. Thus, the rationality of the Dryden spectrum is a strong argument in its favor.

Both the von Karman and the Dryden spectra have the disadvantage of having too much curvature near the knee of the spectra. The two spectra have been shown to fit experimental data reasonably well in the high frequency asymptotic region, but the data shows generally much less curvature near the knee than do the spectral forms. In fact, this is one of the reasons that led to the selection of the simpler spectrum of Equation 8 in Section 3.

The Spectrum Chosen for the Present Exceedance Model

In order to apply an exceedance probability model of atmospheric turbulence, a spectrum must be selected and corresponding scales specified. This is required, first, so that values of $N_{0,x}$ and A_x can be calculated in order to determine the exceedance model. Second, the same spectrum and scales used for obtaining the model should also be used when applying the model. However, because of the similarity of results obtained for exceedance calculations mentioned previously, and because the turbulence environment is not even now well enough known, either spectrum may be used when applying the turbulence model.

The Dryden spectrum, Equation 34, has been chosen for use in developing the exceedance model, and corresponding values of L are given in Table 4. Wherever data were available, the scales of turbulence were chosen as rounded averages of the scales determined from the spectral data in References 1, 4, 5, 7, 8, 9, 10, 44, 45 and 46.

TABLE 4

SCALE OF TURBULENCE L USED FOR DEVELOPMENT OF THE EXCEEDANCE MODEL OF TURBULENCE

Type of Turbulence	Altitude Above Terrain, Z, ft	Scale of Turbulence, L, ft
Primary	$0 < Z \leq 200$	500
	$200 < Z < 1000$	750
	$1000 \leq Z \leq 100,000$	1000
Secondary	$0 < Z \leq 1000$	500
	$1000 < Z \leq 10,000$	1000
	$10,000 < Z \leq 100,000$	2000
Tertiary	$0 < Z < 1000$	600

Reduction and Analysis of the Data

Equation 32 is the common basis for all techniques for evaluating the P and b parameters. For convenience, the equation is repeated here but without the term for tertiary turbulence which will be treated separately in a subsequent section:

$$\frac{M(x)}{N_{0,x}} = P_1\, exp\left(-\frac{1}{b_1}\frac{|x|}{A_x}\right) + P_2\, exp\left(-\frac{1}{b_2}\frac{|x|}{A_x}\right) \tag{32 repeat}$$

The basic data on turbulence are almost never given in this form, the usual forms being the cumulative frequency distributions of derived gust velocity U_{de} or incremental normal acceleration n_z. These data are obtained by counting normal acceleration, n_z, peaks from records and presenting the data as a number of peak counts or exceedances per acceleration category in a given altitude band. In place of, or in addition to, the n_z data, U_{de} peak counts may be given and the cumulative frequency plots shown. As written above, Equation 32 may be considered valid for the cumulative frequency distribution of any airplane response variable (e. g. n_z, U_{de}) or, in fact, for the gust velocity w itself. With each different variable, however, the appropriate values of $N_{0,x}$ and A_x must be used.

Many reports that deal with VGH gust data present results in the form of cumulative frequency of U_{de} per mile. In the U. S. A., a standard procedure has been used to convert acceleration peak counts into U_{de} peak counts. Reference 47 describes the conversion procedure in detail. Equations 39, 40 and 41 outline the calculation:

$$U_{de} = \frac{2W}{\rho_0 C_{L\alpha} S V_e K_g} \qquad n_z = \frac{n_z}{C} \tag{39}$$

where the gust alleviation factor K_g is given in terms of the mass ratio μ_g:

$$K_g = \frac{0.88\,\mu_g}{5.3 + \mu_g} \tag{40}$$

$$\mu_g = \frac{2W}{\rho_0 C_{L\alpha} \bar{c} g S} \tag{41}$$

Usually the weight W is either estimated as some constant fraction of the airplane design gross weight or it is calculated on the basis of fuel usage. The values of V_e in Equation 39 are obtained from the VGH-type records for the same time at which the n_z peak is read.

The normal acceleration peak count data, when available, have been used in preference to U_{de} data in the present work simply because of the more basic nature of the acceleration data.

In a few reports. notably References 5, 9, 10, 44, 45, 46 and 48, various kinds of direct vertical gust velocity data are available. These direct data are considered preferable to the VGH-type data for determining the k parameters, but the P parameters usually cannot be determined from the direct data.

The Major Source of Error in the Reduction of VGH Data

The acceleration recorded near the center of mass of an airplane would be the ideal source for the statistical data on turbulence if the accelerations were caused only by the atmospheric turbulence. In reality, of course, the accelerations recorded represent the response due to maneuvers as well as turbulence. The problem then is to separate, some-how, the gust acclerations from the maneuver accelerations.

The approach has been to separate the gust acceleration peaks from those due to maneuvers according to the length of time between crossings of the reference +1 g level by the acceleration trace on the VGH record. Several of the data sources (e. g. , References 29, 30, 35) use a two-second interval to separate maneuvers and gusts. The peak is called a gust peak if the acceleration trace crosses the reference level, peaks, and then returns to the reference level within two seconds. NASA (NACA) has used, in the past, four seconds as the rule for the separation (Reference 49, page 4). However, the present NASA approach, if different from the four-second rule, is not described clearly or with enough detail in their reports.

Certain English and Canadian studies (References 31, 33, 41, 43) have employed various counting accelerometers which record, on counters, the number of accelerations greater than any of a series of preselected levels. Periodically the counters are photographed or otherwise recorded versus time. These counting accelerometers make even the crudest attempt to separate maneuvers and gusts very difficult; in fact, in some cases, it is totally impossible to effect a separation of any kind.

In some reports in which it has been admitted that separation of maneuver and gust accelerations was impossible (Reference 50), the total acceleration environment has been presented in combined form.

Figure 17 has been prepared to compare VGH-type data, as repre-sented by rms-derived equivalent gust velocity, with the directly measured gust data, σ_w . The results of all the B-66B low-level gust data runs (References 48 and 51) for which both rms values are given are plotted. The rms values for each variable were calculated by integrating measured spectra. It can be seen, first, that the points are not centered about the line (slope 1. 0) of perfect correlation; instead, the points appear to be better centered about a line of slope 1. 1 that corresponds to the value of the inverse of

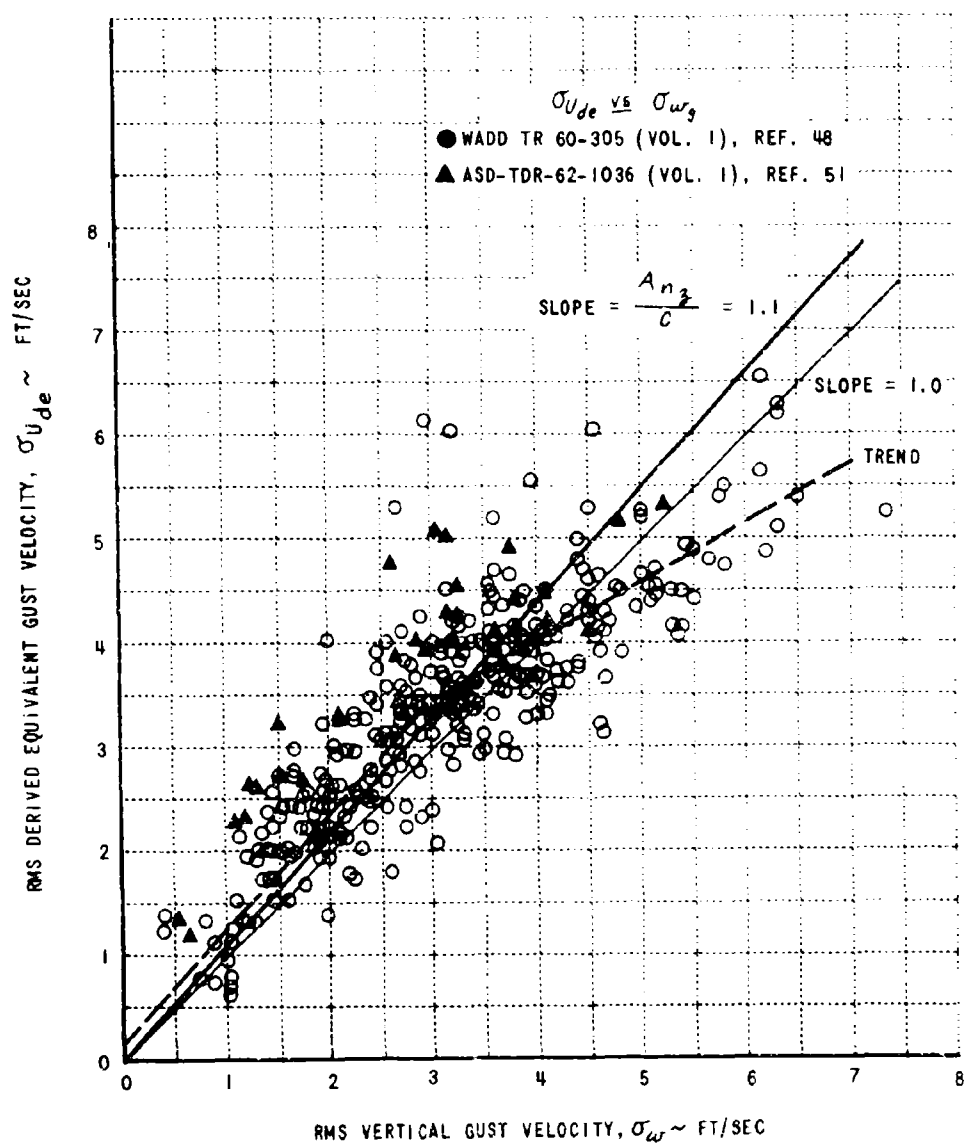$$\frac{C}{A_{n_y}} = \sqrt{\frac{P_c}{P}} \; \frac{K_q}{K_\phi} \; ,$$

Figure 17. Comparison of rms Values of the Derived Gust Velocity and the
True Vertical Gust Velocity

where the constant C/A_{n_q} is the conversion factor relating σ_{w} to $\sigma_{U_{de}}$ at a given flight condition, with no pilot input, and K_ϕ is defined as

$$K_\phi \triangleq \frac{2\frac{W}{S}}{\sigma_{w} \rho V C_{L\alpha}} \left[\int_o^\infty \left| \frac{n_y}{w}(i\omega) \right|^2 \phi_{w}(\omega)\,d\omega \right]^{1/2} \tag{42}$$

The line labeled "trend" in Figure 17 represents just that, a trend in the data, occurring for all values of σ_{w} but especially for the larger values where nonlinearity exists. Although they are not presented in this report, similar data from the B-66 thunderstorm penetrations (Reference 9) show the non-linear trend continuing through substantially larger values of σ_{w} .

Figure 17 shows, therefore, that even without separating gusts from maneuvers, the normal acceleration, or equivalently, the derived gust velocity, may be used to determine the parameters for primary turbulence where the intensity is small. This means, for example, th   dues of P and b_1 determined in Reference 50 may be used to he'   ie these parameters for the exceedance model in this report.

Finally, results presented later in Table 6 and Figure   the data of Reference 29 (two-second rule) and, for example, for the data of References 28 and 40 (presumably the four-second rule) show a large discrepancy which may be caused mostly by the different crossing times for separating gusts from maneuvers. It is significant that the average crossing interval of the $+1.0$ g reference level for normal acceleration due to turbulence is on the order of one second.

Some Examples of the Determination of the P and b Parameters

Because many methods, differing only in detail, were required to analyze the VGH and spectral data which were combined into the exceedance model, the basic approaches are described in a series of representative examples which follow.

The VGH Data of Reference 28

Figure 8 of Reference 28 (NASA TN D-29), which is reproduced as Figure 18 of this report, is a plot of the cumulative frequency per mile of derived gust velocity, U_{de} , peaks. These data have been obtained by combining the VGH data summarized in Reference 28 into a single distribution for each of several 5000-foot intervals of pressure altitude. The data represent 4.8×10^6 miles of flight of several transport airplanes in several different airline operations. Because of the size of the combined sample, great care was taken in attempting to determine the P and b parameters. However, the results of the analyses made to determine P and b are judged to be relatively poor.
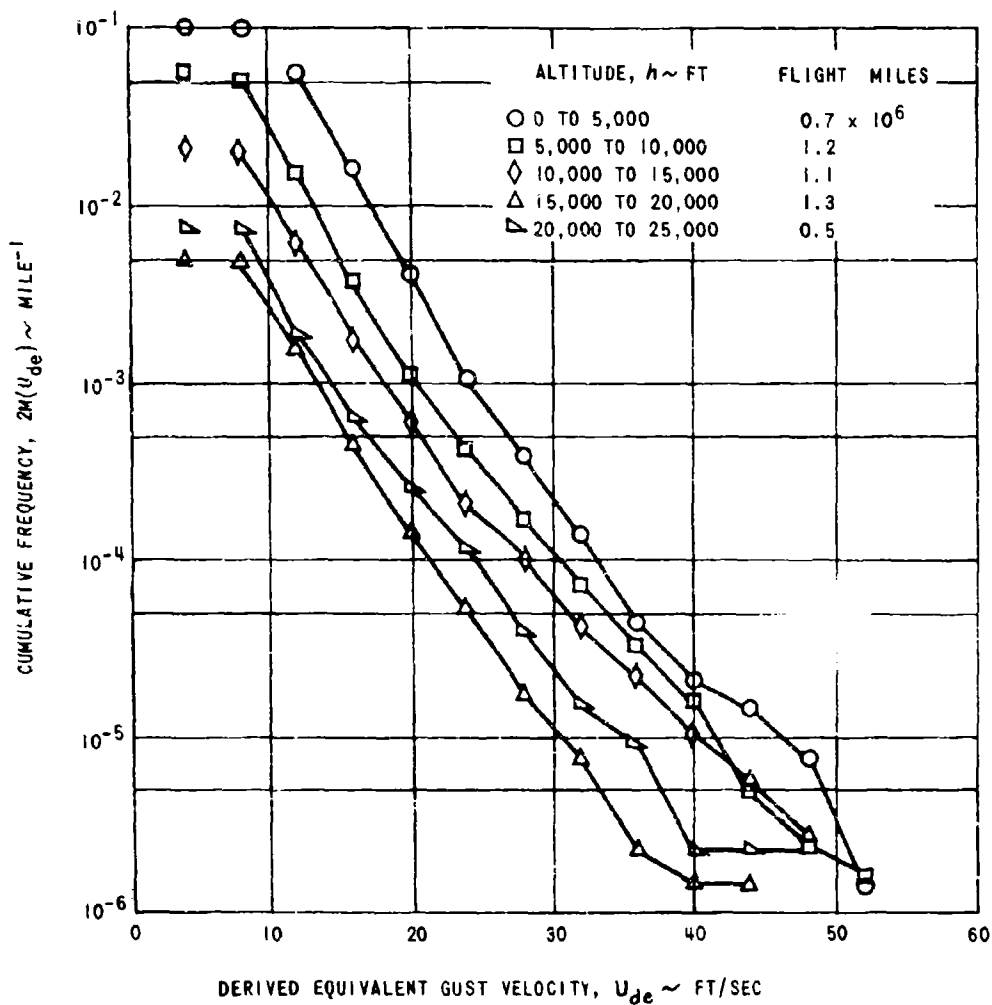
Figure 18. Frequency of Exceeding Given Values of Derived Gust Velocity per Mile of Flight with Pressure Altitude (from Ref. 28)

52

Specifically, the numerical steps for determining ℓ_1 and P_1 are described here. Following the basic approach given in Reference 27, ℓ_1 is calculated according to the relation

$$\ell_1 = \frac{C}{A_{n_3}} \, a_1$$

where

$$\frac{C}{A_{n_3}} = \sqrt{\frac{\rho_0}{\rho}} \, \frac{K_g}{K_\phi}$$

and a_1 is the inverse slope of the U_{de} cumulative frequency distribution. The calculations of K_g a K_ϕ are based on the following assumed average data:

$$C_{L_\alpha} = 4.95 \text{ rad}^{-1}$$

$$W = 70,000 \text{ lb}$$

$$S = 1200 \text{ ft}^2$$

$$\bar{c} = 11.5 \text{ ft}$$

The estimated average true velocity, V_T, is given in Table 5. Since the calculation of K_ϕ requires spectral data, the Dryden spectrum was chosen with a scale L of 1000 feet as specified in a previous section. The transfer factor C was calculated using the procedure of Reference 47. Moreover, since the average data assumed above do not warrant detailed calculations, K_ϕ was calculated using only the vertical translation degree of freedom and was then multiplied by 1.2 to account for the pitching and flexibility degrees of freedom. The resulting ℓ_1 values are given in Table 5.

The P_1 values in Table 5 were calculated by solving the relation

$$2M(U_{de}) = 2N_{0, U_{de}} \, P_1 \, exp\left(-\frac{|U_{de}|}{a_1}\right) \tag{43}$$

for P_1 using the values of a_1 also given in the table. Because of the close similarity of the gust data in Reference 28 with that used in Reference 27, $2N_{0, U_{de}}$ was taken as 20 gust peaks (or equivalently, zero crossings) per mile (page 9, Reference 27). The P_1 values, which are considered poor at the higher altitudes, depend greatly on the values of a_1 which, as stated previously, are also considered poor.

The resulting data, P_1 and ℓ_1, are plotted in Figures 19 and 20 respectively. It is observed that at the lower altitudes, 2500 and 7500 feet. the P_1 and ℓ_1 values given in Table 5 agree well with the final curves of Figures 19 and 20. At higher altitudes, the agreement is considerably poorer.

TABLE 5

CALCULATION OF ρ_1 AND ℓ_1 FOR VGH DATA OF REFERENCE 28

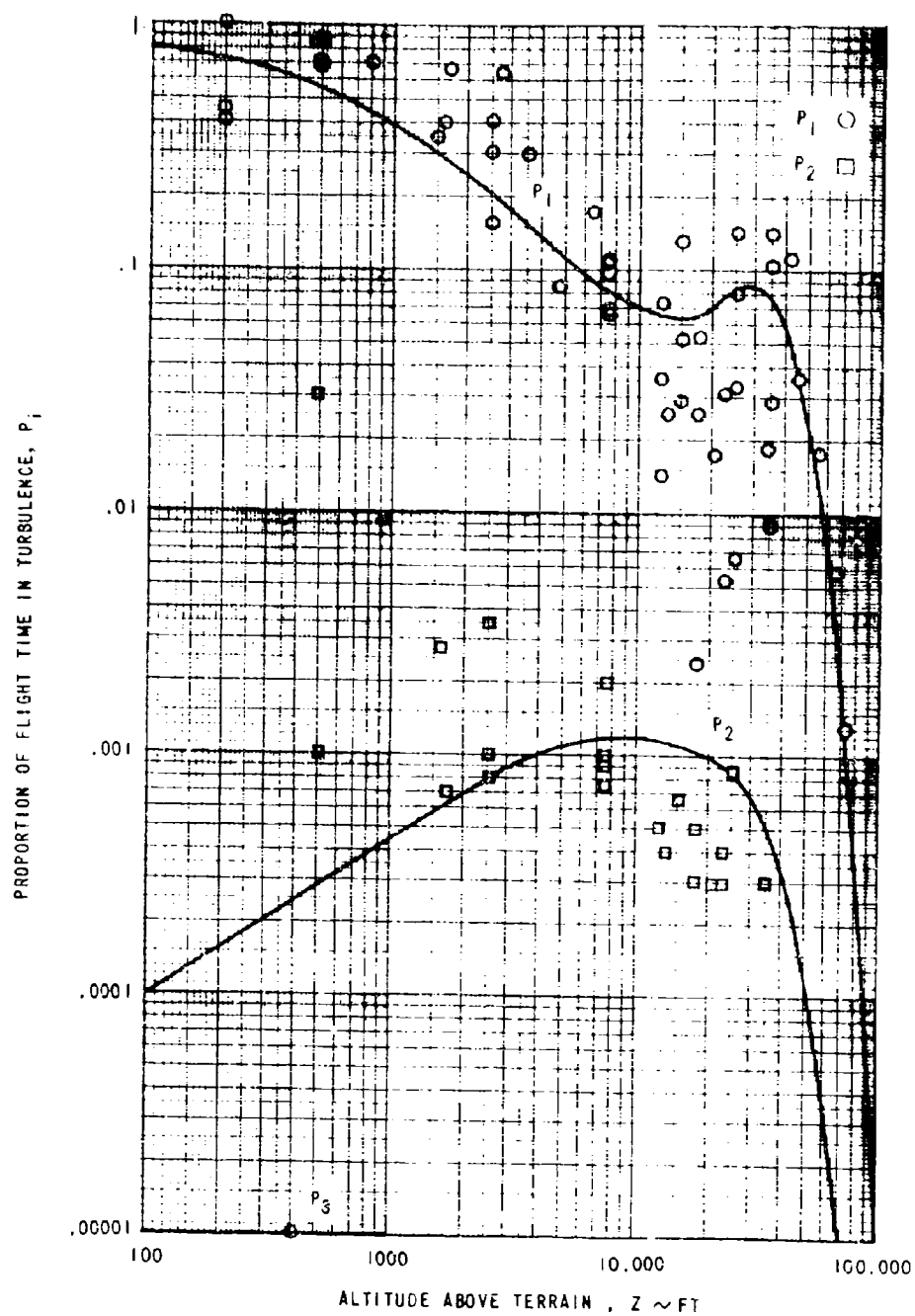| z	a_1	$\sqrt{\rho_1/\rho}$	V_T	μ_g	K_g	$1.2\,K_\phi$	$\dfrac{C}{A}$	ℓ_1	U_{de} at $M(U_{de})=5\times10^{-1}$	ρ_1
kilofeet	ft/sec EAS	—	ft/sec	—	—	—	—	ft/sec	ft/sec EAS	—
2.5	2.96	1.038	270	28.8	.745	.594	1.30	3.85	19	.153
7.5	2.68	1.119	280	31.5	.76	.618	1.37	3.67	15	.0675
12.5	3.10	1.211	290	39.3	.78	.669	1.41	4.37	12.5	.0141
17.5	3.33	1.313	300	46.1	.80	.710	1.48	4.93	7.5	.0328
22.5	2.96	1.429	310	54.8	.815	.745	1.56	4.52	9	.00526

Figure 19.   The Proportion of Flight Distance in Atmospheric Turbulence
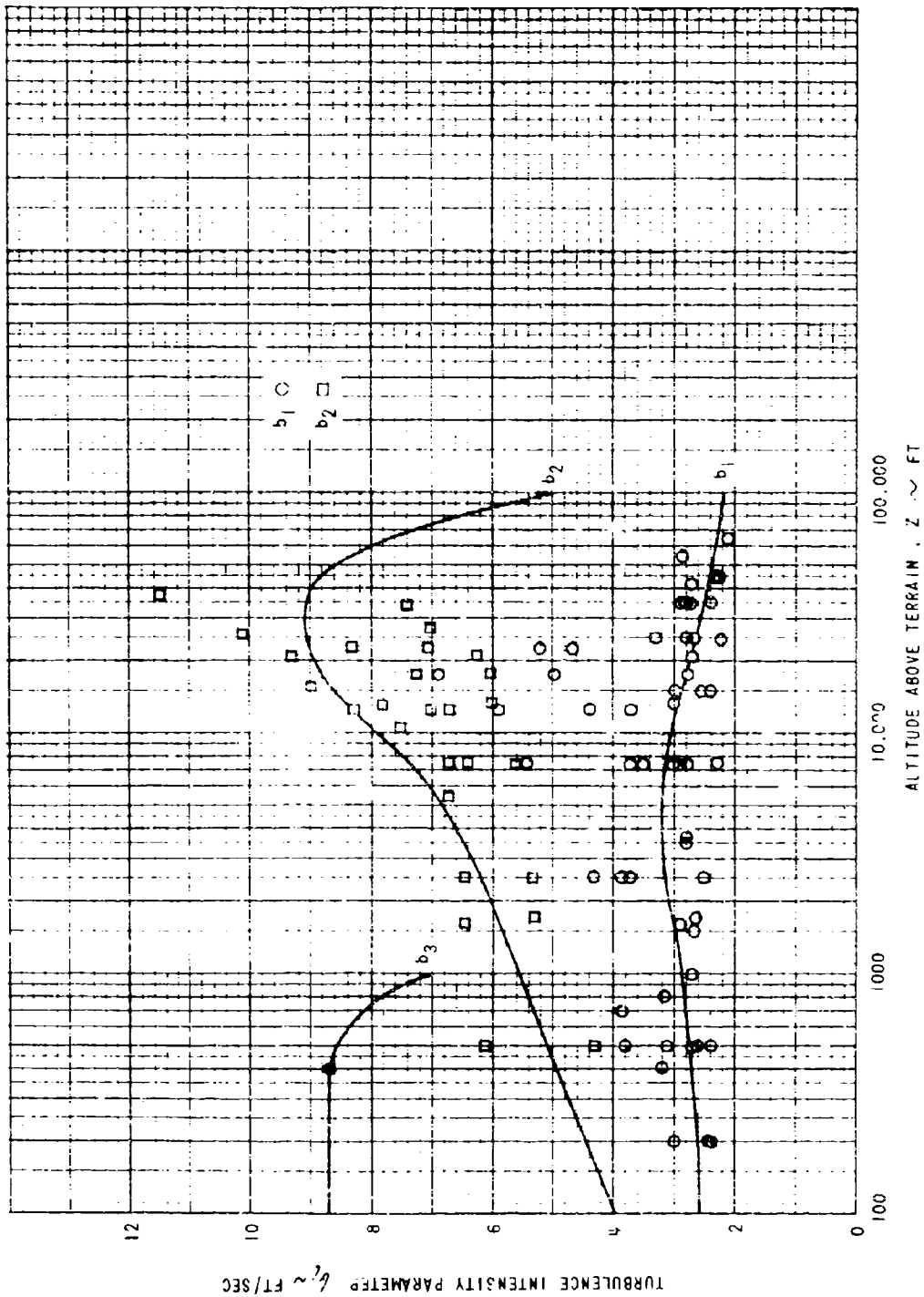as Functions of Altitude - Data Points

Figure 20. The Intensity Parameters of Atmospheric Turbulence as Functions of Altitude-Data Points

Although it is likely that there is a large number of factors contributing to these discrepancies, such as the assumption of average physical data for the airplanes involved and the average altitudes and airspeeds, it appears that the major contributor is the basic nature of the U_{de} distribution itself. The distributions shown in Figure 18 appear to contain decreasing amounts of the primary turbulence as altitude increases (as determined by the slopes). This is caused by the apparent drop-off in the cumulative frequency of U_{de} at the small values of U_{de}, which in turn is caused by the distributions of airspeed and altitude used to calculate the U_{de} distributions from the n_z peak counts. Hence the small values of U_{de}, from which b_1 should be determined, are unreliable and clearly cannot be used. These are the points in Figure 18 which are not connected by lines to the corresponding distributions. Curve-fitting the reliable points results in b_1 values which are considerably larger than what is believed to be correct.

There are two obvious ways to improve the determination of b_1 and P_1.

1. The simplest is to work directly from the n_z distribution, if available, and ignore the U_{de}, and

2. In the original data reduction of VGH records, use a much lower reading threshold for n_z to provide a reliable estimate of the cumulative frequency of U_{de} at smaller values of U_{de}.

The former could not be done because the data were not available, and the latter is more in the form of a suggestion for future improvement that obviously could not be effected during the present study. A third way to improve the value of P_1 is described below.

The VGH Data from U-2 Operations (References 36 and 37)

The VGH data for clear air turbulence at high altitudes (Reference 36) reported and supplied (Reference 37) by NASA, gives the total miles of flight in each altitude band and also gives the miles of flight spent in turbulence. If the turbulence is assumed to be entirely primary turbulence, then P_1 can be obtained simply by dividing the miles of flight in turbulence by the total miles of flight. Thus, P_1 can be determined simply by inspecting the VGH records.

The b_1 parameters were evaluated as in the previous example except that A_{n_z} was calculated using a digital computer program with an estimated two-degree-of-freedom, short period, representation of the airplane.

The U_{de} distributions showed no recognizable signs of any secondary turbulence, a result that is not unexpected, since in Reference 36 (page 4) it is stated that the operations were almost entirely in clear air.

B-66 Low-Level Data (References 48 and 54)

Reference 4ᴥ presents turbulence data in many forms that would be useful for the development of the exceedance model, for example:

1. Peak counts of the vertical gust velocity, w

2. Peak counts of the derived equivalent gust velocity, U_{de}, and

3. Tabulated spectral variances of the gust velocity, σ_w^2,

but only peak count data were considered here.

Exceedance analyses of the B-66 results have been made by several workers, but the results of Saunders (Reference 54) and Jensen and Hoblit (Reference 55) are more representative of the general approach used here. They have achieved similar results for the parameter $\mathcal{L}_1$ using very dissimilar approaches. Saunders obtained $\mathcal{L}_1 = 2.72$ ft/sec, and Jensen and Hoblit obtained $\mathcal{L}_1 = 2.94$ ft/sec.

Since the results of Saunders (Reference 54), based on 42 representative data runs, are considered directly applicable in the exceedance model developed here, a more detailed discussion is in order. Saunders obtains $\mathcal{L}_1$ directly from the peak count distribution of the vertical gust velocity. He determines $\mathcal{L}_2$ by analyzing the distribution of the extremes of peaks from the 42 data runs. Finally, Saunders presents the constants (P_1 $2N_0$) and (P_2 $2N_0$) (peaks/mile) in an unseparated form. A value of $2N_0$ was therefore digitally calculated to determine P_1 and P_2. The P and $\mathcal{L}$ parameters are given in Table 6 for both primary and secondary turbulence.

Spectral Data from References 5, 44 and 45

The probability density of σ_w given by Equation contains the $\mathcal{L}$ parameter. It is easily shown that the second moment the distribution yields[2]

$$\int_0^\infty \sigma_w^2 \sqrt{\frac{2}{\pi}} \frac{1}{b} \, exp\left(-\frac{\sigma_w^2}{2b^2}\right) d\sigma_w = b^2$$

(44)

The $\mathcal{L}$ parameter may therefore be considered approximately equal to the rms value of σ_w. When a sufficiently large number of spectral samples is obtained for one flight condition, it is possible to evaluate b by simply taking the square root of the sum of the spectral variances, σ_w^2. The discrete probability P cannot be determined from spectral data.

---

[2] This integral is of the form $\int_0^\infty x^2 e^{-x^2} dx = \frac{\sqrt{\pi}}{4}$,

which is commonly found in tables of definite integrals. Here $x = \frac{\sigma_w}{\sqrt{2} \, b}$.

TABLE 6

P AND b PARAMETERS FOR PRIMARY AND SECONDARY TURBULENCE

Reference	Aircraft	Altitude $Z \sim$ Kft.	P_1	ℓ_1	P_2	ℓ_2	Flight Time~ hours
30	KC-135	0.5	.85	2.61	.001	6.1	47
		1.7	.65	2.63	.00068	5.3	63
		3.7	.083	2.82	--	--	39
		7.5	.097	3.01	--	--	47
		15	.051	2.65	--	--	101
		25	.032	2.77	--	--	265
		35	.028	2.87	--	--	539
		45	.035	2.32	--	--	67
29	B-52	0.5	.87	3.07	--	--	933
		0.5	.67	2.40	--	--	6
		1.5	.34	2.63	--	--	108
		3.5	.29	2.75	--	--	268
		7.5	.17	2.75	--	--	489
		15	.13	2.41	.00065	6.9	695
		25	.14	2.21	.00087	5.4	1830
		35	.14	2.37	--	--	7071
		42	.11	2.70	--	--	299
31	Sabre Mk. V	.5	.703	3.77	--	--	14.1
32	DC-4M	13	--	--	--	7.8	48.3
5	Canberra B.6	.41	--	3.22	--	--	1.04
33	Canberra B.6	.2	0.40	2.97	--	--	12.34
		.2	0.45	2.44	--	--	5.19
44	FH-1	1	--	2.72	--	--	0.4
45	FH-1	.71	--	3.83	--	--	1.1

TABLE 6 (CONT'D)

Reference	Aircraft	Altitude $z \sim$ Kft.	P_1	l_1	P_2	l_2	Flight Time $\sim$ hours
34	A3D	.47	.84	2.75	--	--	39.1
		.2	1.0	2.41	--	--	21.5
		.8	.686	3.16	--	--	17.6
48, 54	B-66B	.493	.7	2.72	.03	4.31	26.1
35	YRB-58A	2.5	.300	2.48	.0008	5.32	14.0
		7.5	.104	2.31	--	--	5.05
		15	.0284	2.98	--	--	13.8
		25	.0065	3.27	--	--	88.6
		35	.0087	2.76	--	--	67.2
36, 37	U-2	25	.0794	2.65	--	--	47.8
		35	.1015	2.77	--	--	62.8
		45	.0252	2.26	--	--	112
		55	.0174	2.86	--	--	313
		65	.0057	2.12	--	--	1250
		72	.00128	--	--	--	15.0
9	NB-66B	27.3	--	--	--	7.06	1.2
38	P-61	5.5	--	--	--	6.73	7.0
		10.5	--	--	--	7.52	9.3
		15.5	--	--	--	8.95	10.2
		20.5	--	--	--	9.29	7.7
		25.5	--	--	--	10.1	5.8
10	T-33	37	--	--	--	11.46	0.57
	F-86	12.5	--	--	--	6.86	0.11
39	F-27	2.5	.40	4.27	.001	15.4	1162
		7.5	.065	5.40	.001	14.5	807
		12.5	.035	5.91	--	--	123
		17.5	.025	6.88	--	--	8.2

TABLE 6 (CONT'D)

Reference	Aircraft	Altitude $z \sim$ Kft.	P_1	ℓ_1	P_2	ℓ_2	Flight Time $\sim$ hours
40	Viscount	2.5	.63	3.70	--	--	298
		7.5	.11	3.54	.00075	6.43	373
		12.5	.073	3.71	.00049	7.03	682
		17.5	.052	2.76	.00051	5.98	438
		22.5	.030	5.18	.00030	7.05	48
28	Transports	2.5	.153	3.85	.0035	6.43	1770
		7.5	.0675	3.67	.002	6.71	2920
		12.5	.0141	4.37	.0005	8.26	2590
		17.5	.00238	4.93	.0003	7.22	2950
		22.5	.00526	4.62	.0004	8.29	1100
43	Transports	1.6	.403	2.87	.00275	6.44	1001
		7.4	.108	2.93	.00087	5.61	3350
		13.4	.025	3.03	.000398	6.01	9310
		20.1	.0173	2.67	.000287	6.23	3550
		33.8	.0180	2.76	.000293	7.38	2320

The Parameter P_2

The parameter P_2 represents the discrete probability of encountering the turbulence of above normal intensity usually associated with violent thunderstorms. In essence, therefore, determination of P_2 involves the probability of encountering a thunderstorm. What appears to be a crude attempt at defining P_2 was undertaken in Reference 27. At this time, there is still no method that will assure reliable estimation of P_2 as a function of height. All VGH data obtained from airplane operations, both civil and military, are biased to an unknown degree by storm avoidance procedures. Furthermore, there are no readily available statistics on the likelihood of encountering thunderstorms as a function of height. As a result, the P_2 curve in Figure 19 has been determined by multiplying the P_2 values obtained from the data of Table 6 by an appropriate factor, and then by curve fitting the modified P_2 values. This factor, approximately equal to 5, was based on a discussion of the problem by Notess in Appendix B of Reference 57, and on data in References 58 and 59. The latter two references show that storm avoidance procedures affect essentially only the value of P_2, and not ℓ_2.

Evaluation of P_3 and ℓ_3 for the Low-Level Environment

The tertiary turbulence represents an effort to incorporate into the exceedance model a way of accounting for the severe turbulence of mechanical origin which is sometimes found when high winds blow over rough terrain. The estimate $\ell_3 = 8.7$ ft/sec is based straightforwardly on the F-106A High Intensity Gust Investigation (Reference 46) peak count data. The value of $P_3 = 10^{-5}$ was estimated by Austin (Reference 56) using data on the actual experience of B-52 fleet airplanes that have been used in low-level flight missions. Austin chose this value so that the F-106A lateral gust velocity distribution would pass through the values of $M(x)/N_0$ vs. $|x|/A$ that were carefully estimated for certain turbulence encounters in which B-52 vertical stabilizers failed. His basic assumption is that P_3 is the same for vertical turbulence as for lateral.

The parameters P_3 and ℓ_3 are determined, therefore, for some average height above the terrain which should be less than 1000 feet. The value $z = 400$ ft was selected as representative. In Figure 19, P_3 is plotted as a constant since there is no information to support other possibilities. Because terrain-induced turbulence is known to decrease in intensity with height above the terrain, a reasonable but completely arbitrary variation of ℓ_3 with height is suggested in Figure 20. Note that no information is given for either P_3 or ℓ_3 at heights above 1000 feet. Use of the concept of tertiary turbulence above $z = 1000$ feet is not recommended simply because of the complete lack of supporting data.

Compilation of the Data

The parameters P_1, $\mathcal{L}_1$, P_2 and $\mathcal{L}_2$ are presented in Table 6 for the data sources listed in Table 3. For tertiary turbulence the following data were obtained.

$$P_3 = 10^{-5}$$

$$\mathcal{L}_3 = 8.7 \text{ ft/sec}$$

All the data are plotted in Figures 19 and 20 along with the final fitted curves. The curves for primary and secondary turbulence were fitted by weighting the data points according to the following:

1. The type of data, VGH or direct gust velocity

2. The sample size in hours of flight

3. An estimate of the statistical bias.

The curves for P_3 and $\mathcal{L}_3$ are rough estimates and should be considered accordingly.

6.3 THE BASIC EXCEEDANCE MODEL AND ITS USE

The basic exceedance model is given by Equation 32 which is repeated here for convenience:

$$\frac{M(x)}{N_{0,x}} = P_1 \exp\left(-\frac{1}{\mathcal{L}_1}\frac{|x|}{A_x}\right) + P_2 \exp\left(-\frac{1}{\mathcal{L}_2}\frac{|x|}{A_x}\right) + P_3 \exp\left(-\frac{1}{\mathcal{L}_3}\frac{|x|}{A_x}\right) \qquad (32) \text{ repeat}$$

in which the P and $\mathcal{L}$ parameters vary with altitude as shown in Figures 21 and 22, respectively. For twelve selected altitudes covering the range from 200 to 100,000 feet above the terrain, the P and $\mathcal{L}$ parameters are listed in Table 7 and the corresponding exceedance curves are plotted in Figure 23. The exceedance curves are also called "generalized prediction curves" in " Reference 24.

When the P and $\mathcal{L}$ parameters are specified, it is possible to evaluate the probability density $p(\sigma_w)$ by using Equation 27 along with an equation for the three types of turbulence that is analogous to Equation 29. Then, further, an integration of $p(\sigma_w)$ results in the cumulative probability distribution $P(\sigma_w)$.

In order to apply the exceedance model, for example, in structural design calculations, a spectrum function must be used. The Dryden spectrum
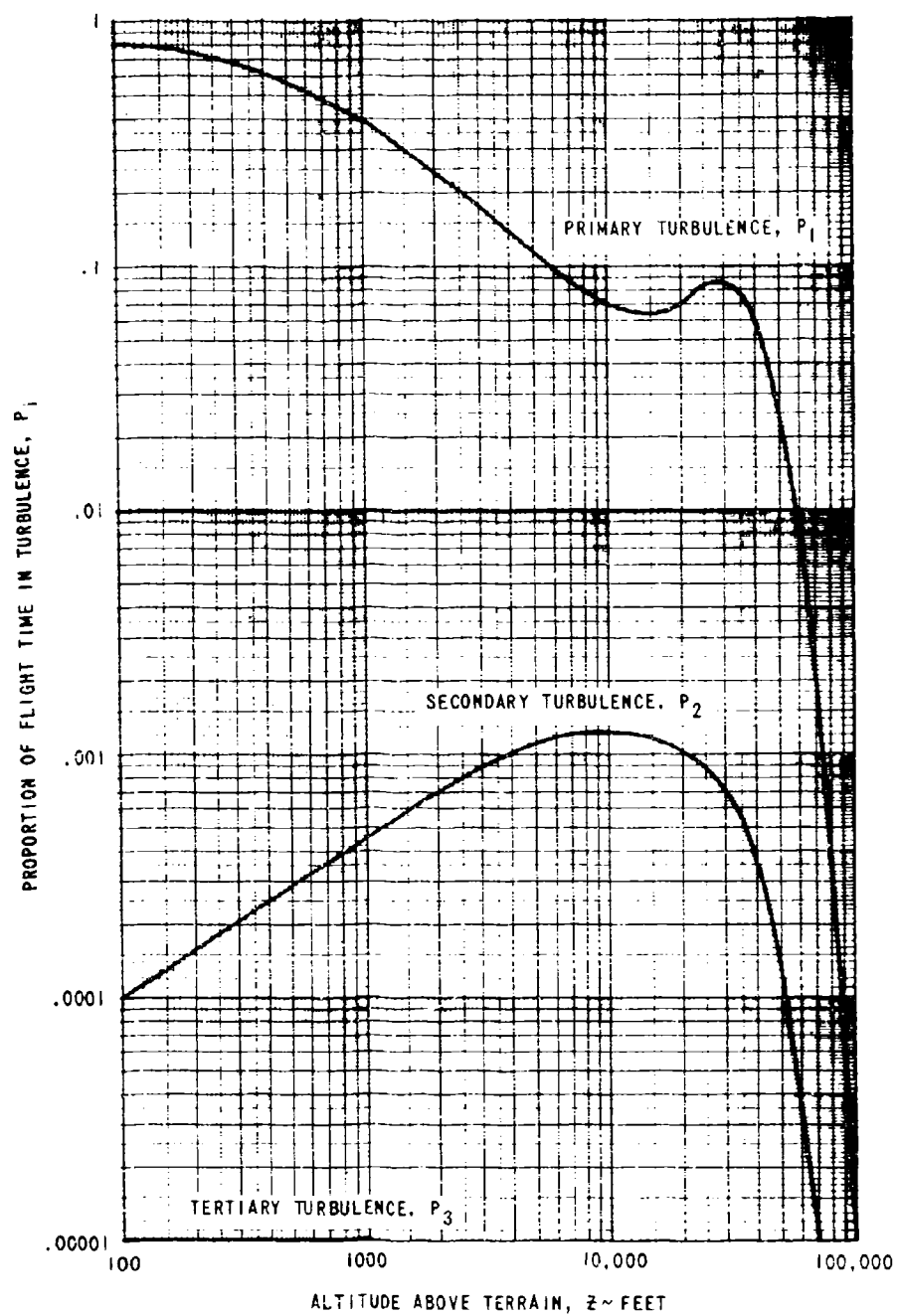
Figure 21. The Proportion of Flight Distance in Atmospheric Turbulence
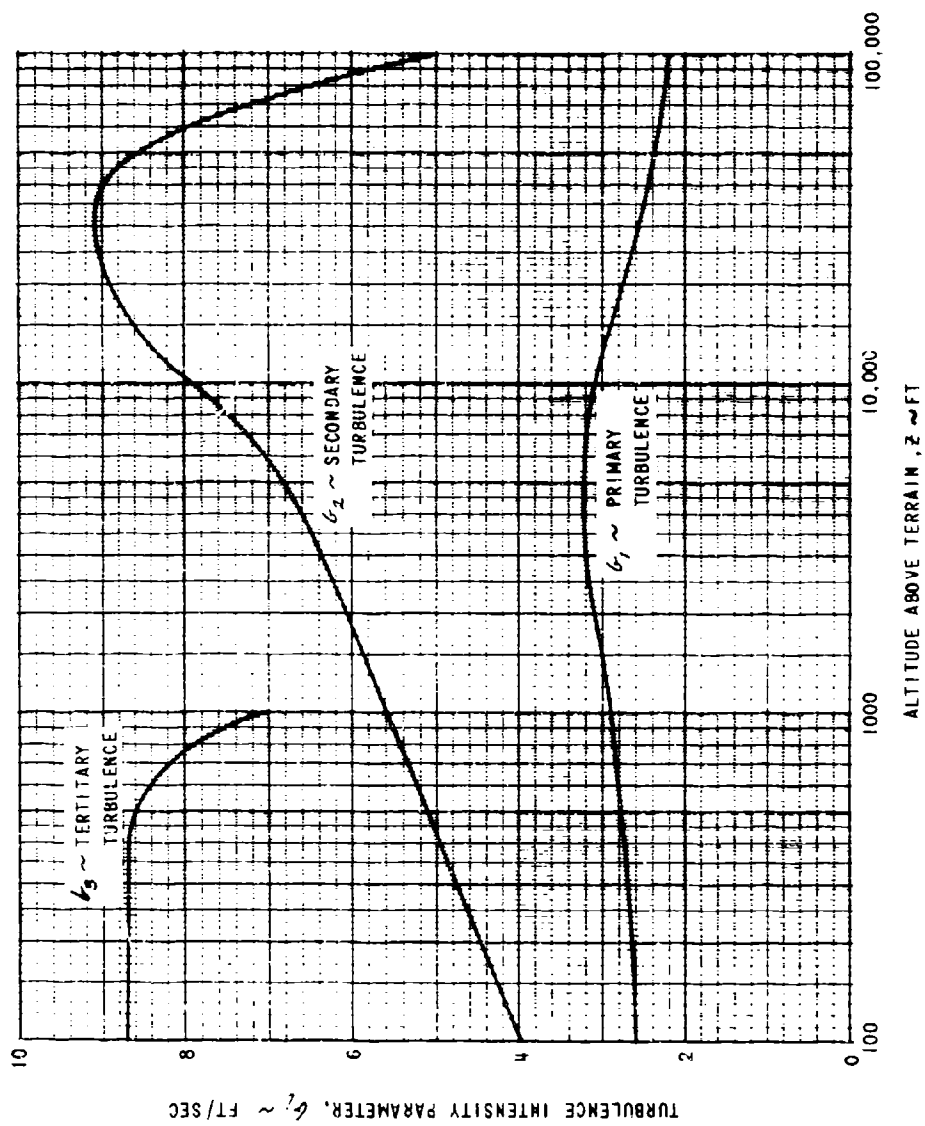as Functions of Altitude - Final Model

64

Figure 22. The Intensity Parameters of Atmospheric Turbulence as Functions of Altitude – Final Model
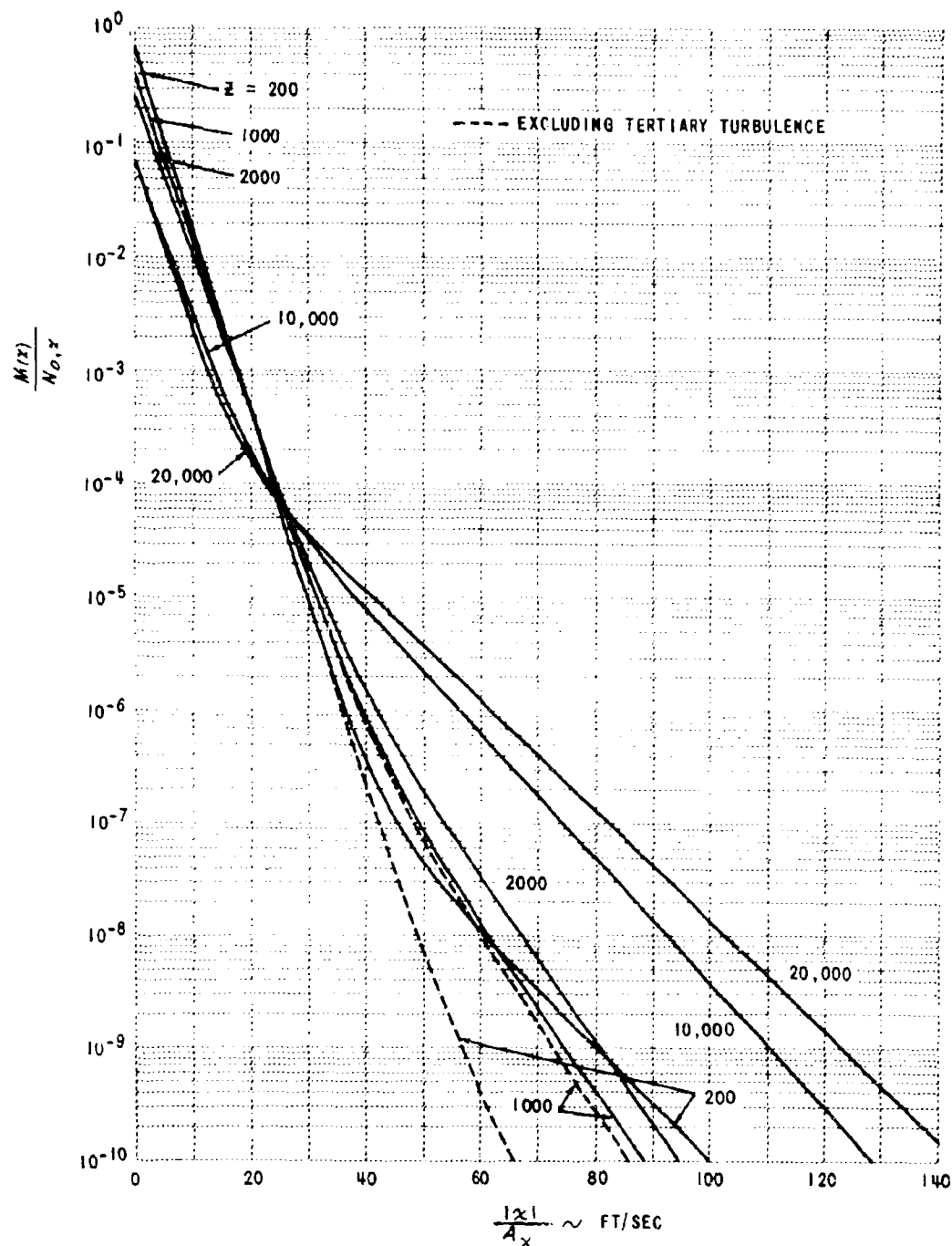
Figure 23.   Exceedance Curves for Selected Altitudes Above Terrain
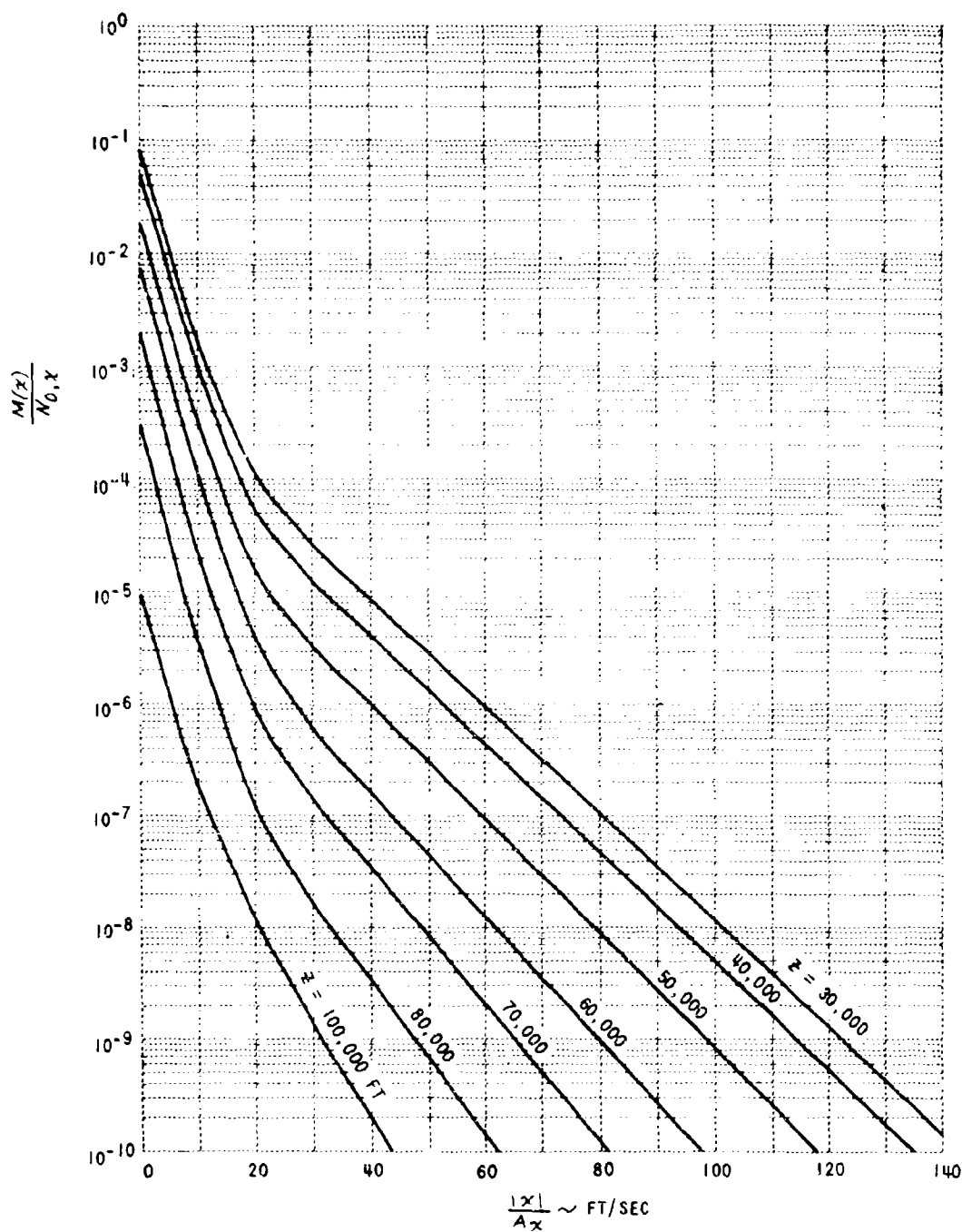(a)   Altitudes from 200 to 20,000 Feet

Figure 23.   Exceedance Curves for Selected Altitudes Above Terrain

(b) Altitudes from 30,000 to 100,000 Feet

67

TABLE 7

EXCEEDANCE MODEL PARAMETERS AT SELECTED ALTITUDES

Altitude Above Terrain, Z ft.	Primary Turbulence P_1 -	ℓ_1 ft/sec	Secondary Turbulence P_2 -	ℓ_2 ft/sec	Tertiary Turbulence P_3 -	ℓ_3 ft/sec
200	.72	2.65	.00016	4.5	10^{-5}	8.7
1000	.38	2.90	.00045	5.6	10^{-5}	7.0
2000	.24	3.10	.0007	6.0	-	-
10,000	.07	3.10	.0012	7.9	-	-
20,000	.07	2.75	.001	8.9	-	-
30,000	.085	2.60	.0007	9.1	-	-
40,000	.06	2.50	.00035	9.0	-	-
50,000	.02	2.40	.00011	8.5	-	-
60,000	.008	2.35	$2.7(10)^{-5}$	7.8	-	-
70,000	.002	2.30	10^{-5}	7.1	-	-
80,000	.0003	2.25	$2(10)^{-6}$	6.4	-	-
100,000	.00001	2.20	$6(10)^{-7}$	5.0	-	-

is recommended for use with the exceedance model, because of its relative simplicity when compared with the von Karman spectrum, and because it fits measured data nearly as well. However, the von Karman spectrum may be used if desired; and furthermore, the Lappe spectrum discussed in Section 3 may also be used.

The calculation of $N_{o,x}$ depends on the scale of turbulence L , and therefore use of the values of L given in Table 4 will result in three separate values of $N_{o,x}$ for a single altitude. To realize the convenience and simplicity afforded by a single value of $N_{o,x}$ that is valid for all types of turbulence at one altitude, a single value of L must be used. Table 8 presents the recommended single values of L .

TABLE 8

SCALE OF TURBULENCE FOR THE EXCEEDANCE MODEL

Altitude Above Terrain, $Z \sim$ ft	Scale of Turbulence, $L \sim$ ft
$0 \leq Z \leq 500$	500
$500 < Z < 1000$	750
$1000 \leq Z < 5000$	1000
$5000 \leq Z \leq 100,000$	2000

The effect of neglecting the tertiary turbulence is shown in Figure 23a for two pertinent altitudes, 200 and 1000 feet above the terrain. The tertiary turbulence is seen to be important to the description of the environment at heights less than 1000 ft. Because of its definition, however, the tertiary turbulence should be employed only when airplane operations involve flight over rough terrain. Therefore, tertiary turbulence would most likely be considered in conjunction with terrain following operations.

6.4   CORRECTION FACTORS FOR THE EXCEEDANCE MODEL

Since the basic exceedance model for atmospheric turbulence as developed to this point varies only with altitude due to the nature of the available data, an effort has been made to define "correction facto. :", m, to be used to account for the variation of the exceedance probabiliti s with the following quantities:

1.   season of year,

2.   time of day,

3.   nature of terrain (surface cover),

4.   geographical location, and

5.   terrain roughness.

Whereas most of the parameters considered for the spectral model are of a direct meteorological nature, those listed abc e are more of an operational nature and, therefore, may be related to proposed mission profiles for airplanes.

First, assume that the basic exceedance model having altitude as a parameter represents an average model, that is, the appropriate average of the five parameters in the list. This model is represented as

$$\frac{M(x)}{N_{o,x}} = P_1(z)\,exp\left(-\frac{1}{\ell_1(z)}\frac{|x|}{A_x}\right) + P_2(z)\,exp\left(-\frac{1}{\ell_2(z)A_x}\frac{|x|}{}\right)$$

where, as indicated, P_1, P_2, ℓ_1 and ℓ_2 are functions of the altitude above the terrain. For other than average conditions of the five quantities, any or all of P_1, P_2, ℓ_1 and ℓ_2 may vary. Thus a given plotted distribution (e. g. as in Figure 23) may change in both slope and in its value at $|x|/A_x = 0$. As an example, over rough terrain an airplane is more likely to encounter turbulence and the turbulence is likely to be more intense; therefore, both P_1 and ℓ_1 should be larger.

Second, since correction factors are being presented here, it is logical that they be used as in the following example.

$$(P)_{\substack{rough \\ terrain}} = m_p\,(P)_{\substack{average \\ terrain}}$$

or

$$(\ell)_{\substack{rough \\ terrain}} = m_\ell\,(\ell)_{\substack{average \\ terrain}}$$

Furthermore, if corrections are needed for, say, three of the five quantities, the following product rule should be used:

$$(P)_{\substack{rough\ terrain \\ winter\ season \\ early\ morning}} = (m_p)_{terrain}\,(m_p)_{season}\,(m_p)_{time}\,(P)_{\substack{average \\ terrain, \\ season, \\ and\ time}}$$

Obviously, there are restrictions inherent in the use of a multiplication rule with the P values. Even if all the m_p's are greater than unity simultaneously, P cannot be greater than unity.

Third, only gross categories have been set up for evaluation of the factors. The data available at this time do not allow any finely scaled breakdown. For example, season may be broken down into either two or four categories. The two categories might be winter and summer, while the four categories might logically be winter, spring, summer and fall. Terrain might be categorized as in Section 3 (5 basic categories) or simply as smooth and rough. The time of day may be broken into maybe four six-hour periods.

70

Fourth, some of the correction factors vary with altitude as the parameters P_1, P_2, l_1 and l_2 do. For example, the effects of terrain generally decrease with height above the terrain.

Finally, along a different line, correction factors may be needed to account properly for the fact that the basic exceedance model described previously is given as a function of the <u>altitude above the terrain (z)</u> rather than <u>pressure altitude (h)</u>. Unfortunately no data exist that will permit estimation of these correction factors.

The Correction Factors

Correction factors have been developed only for low altitudes above the terrain because it is only for these altitudes that reliable data exist. Correction factors are given for season and time of day through the relation of these quantities with the incident solar radiation which is one of the primary factors in convective turbulence. The pertinent data may be found in References 44, 51, 52, 48 and 45. The effects of season and time of day are accounted for primarily through the parameter l_1.

TABLE 9

INTENSITY CORRECTION FACTORS — TIME OF DAY

Time of Day - Hours	$^m l_{1,\tau}$
10 pm to 4 am	.90
4 am to 10 am	.75
10 am to 4 pm	1.25
4 pm to 10 pm	1.10

TABLE 10

INTENSITY CORRECTION FACTORS — SEASON

Season (for north temperate zone) Months	$^m l_{1,s}$
Oct, Nov, Dec	.80
Jan, Feb, Mar	.95
Apr, May, June	1.07
July, Aug, Sept	1.18

Terrain roughness and the small effect of the nature of the terrain may be accounted for as done in Section 3 where the terrain factor R_T is defined from data in References 48 and 51. Here the symbol R_T is replaced by $m_{b_{1,R}}$ but the data are the same.

TABLE 11

INTENSITY CORRECTION FACTORS — TERRAIN CATEGORY

Terrain Category	$m_{b_{1,R}}$
Ocean, Water-Land, and Desert	1
Farm	1.1
Virgin Land (forested)	1.15
Low Mountains	1.3
High Mountains	1.4

These correction factors are the ones for which consistent trends are shown in the data. However, since the data come mostly from the northern hemisphere, and particularly the temperate zones, care must be used, and possibly adjustments made, to use these correction factors for other locations.

There are little or no available data showing consistent trends that might be used to determine correction factors for the P values.

72

SECTION 7

CONCLUSIONS AND RECOMMENDATIONS

7.1 CONCLUSIONS

The Low-Level Spectral Model of Turbulence

The preceding analysis of the low-level spectrum has shown that the rms vertical gust velocity is a function of wind speed, lapse rate, and height above the terrain for a given surface roughness. This functional dependence has been outlined, within a limited accuracy, for heights up to 1000 feet. The scale of turbulence is also shown to be mainly a function of height and lapse rate in the lower levels. These fairly simple relationships between the spectrum and the meteorological parameters are not likely to hold for heights much above 1000 feet.

Similarity theory points to the Richardson number as the important meteorological factor governing turbulence. At upper levels beyond the friction layer, there is no longer a simple relationship between wind shear and stability, height or surface roughness. Thus, any future work aimed at extending this type of analysis to higher levels would very likely require knowledge of the Richardson number, rather than just lapse rate.

A similar argument can be made for the scale of turbulence. Figure 4 shows that the scale factor A becomes less and less dependent on stability and height beyond about 1500 feet. Again, the parameter which is likely to be the most useful at greater heights, where the wind shear plays an important role, is the Richardson number.

The Convective Storm Spectral Model

For convective storm penetrations, it has been shown that a certain correlation exists between σ_w and the scale length. This relationship may be fairly complex for thunderstorm penetration, but it could exist in a simpler form for turbulence in clear air and possibly in cloud layers other than cumulus and cumulonimbus.

The Exceedance Model of Turbulence

The exceedance model has been developed following the basic approach first suggested by Press and Steiner (Reference 27) and updated by Houbolt et al (Reference 24). This approach has gained wide acceptance because of its simple, yet reasonable, analytical form. Within the confines of this approach, the exceedance model developed herein represents an improvement over previous models in the sense that a considerably greater sample of data has been used, and represents an extension, since the model is explicitly defined for both lower and higher altitudes than previous models.

73

The model is presented in the form of curves of the parameters P_i and ℓ_i in Equation 32 plotted versus altitude above the terrain. Parameter P_i is the discrete probability of encountering the ith type of turbulence, and ℓ_i is the intensity parameter for this type of turbulence. For altitudes above 1000 feet, two types of turbulence, representing different intensity distributions, define the exceedance model. The two types, called primary and seconday turbulence, may be associated with the nonstorm and storm types described by Press and Steiner (Reference 27) and by others. For altitudes of 1000 feet and below, a third intensity distribution, called tertiary turbulence, is added to account for the severe turbulence generated by high winds near rough terrain.

The parameters P_i and ℓ_i have been determined for all heights above the terrain up to 100,000 ft. Since applicable basic data do not exist for altitudes above approximately 70,000 ft, extrapolations were made. For all other altitudes, however, there were sufficient data available to determine the parameters with what is considered adequate statistical reliability. Unfortunately, because of the nature of the data used in the exceedance model, it was considered impossible to determine quantitative statistical confidence limits.

The basic exceedance model varies with altitude only. Correction factors have been developed, where data were available, to account for the change in turbulence statistics with the season, the time of day and with the nature (especially roughness) of the terrain. The correction factors developed herein relate only to changes of the turbulence intensity parameters, ℓ_i, since no consistent data exist to develop correction factors for the P_i parameters.

The exceedance model is the result of what is essentially an open-ended process, that is, the model has not been tested against the flight experience of an actual airplane to determine whether realistic structural design predictions can be made. Successful completion of tests of this nature is an essential measure of the reliability of the exceedance model, as well as the spectral models of turbulence described in Sections 3 and 4.

7.2 RECOMMENDATIONS

All of the work covered in Sections 3 and 4 of this report has dealt with the vertical component of turbulence only. There are definite indications, however, that the lateral and possibly the longitudinal spectra may be described in a similar fashion. Fortunately, most of the data sources used for the turbulence models in Sections 3 and 4 also contain similar data for the lateral and longitudinal turbulence. Primary among these sources is the B-66B low-level turbulence program, but tower data and other airplane data are also available. Therefore, since lateral turbulence has been known to cause disastrous failure of airplane structures at low levels and in thunderstorms, it is recommended particularly that a model of the lateral gust velocity component be developed. The model should be developed so that it is compatible with the vertical turbulence model in Sections 3 and 4 of this

report. This would permit use of the model of lateral gust velocity in conjunction with the vertical gust model.

Separation of pilot-induced normal accelerations from gust-induced normal accelerations is by far the greatest problem connected with the use of VGH-type data. Because the total current sample of directly measured gust data is relatively very small, the VGH data remains a necessary and useful supplement to the direct data for developing turbulence models. The current practice is to separate maneuvers from gusts on the basis of the time interval between crossings of the acceleration reference level. A simpler and more precise technique for effecting the separation can be obtained by working with the statistics, rather than the time series itself. Such a technique requires, however, some theoretical and experimental research to determine for given flight operations the pilot's contribution to the measured acceleration environment. It is recommended that this research be undertaken, not only to improve the quality of gust information obtained from VGH data, but also to determine how the interaction between the gust and the pilot affects airplane structural loads in turbulence.

Further improvement of turbulence models can be made through the universal adherence to basic standard procedures for measuring and reducing turbulence data and for reporting of the data. In view of current and future large-scale programs for measuring turbulence statistics in the U.S.A. and elsewhere, efforts toward standardization are especially significant and should be undertaken as soon as possible. It is recommended that primary emphasis should be placed on standards for direct gust data, but that standards for VGH data should also be covered.

Future work on thunderstorm penetrations should include traverses at many different altitudes, in order to get some measure of the height dependence of the spectra. Measurements of velocities in convective storms currently being made at CAL by Doppler radar indicate that the most intense updrafts are found in the upper levels of the storm and that, generally, there are two regions of upward acceleration, one in the lower levels from 5000 to 10,000 feet and the other at mid levels in the range of 15,000 to 20,000 feet. This would indicate that the turbulence intensity may increase upward in a similar fashion.

Intensity contoured radar data showing the flight track relative to the distribution of precipitation in thunderstorms would be very useful data to accompany storm spectra. Analysis of data available at present tends to show variations in scale and intensity which may well be related to the position of the flight track relative to the horizontal structure of the storm.

REFERENCES

1. Lappe, U.O., and B. Davidson: The Power Spectral Analysis of Concurrent Airplane and Tower Measurements of Atmospheric Turbulence. N.Y.U. Final Report under Navy Contract NOas 58-517-d, 1960.

2. Cramer, E., A. Record, and E. Tillman: Studies of the Spectra of the Vertical Fluxes of Momentum, Heat, and Moisture in the Atmosphere. Final Report under Contract No. DA-36-039-SC-80209, M.I.T. Department of Meteorology, Round Hill Field Station, April 1962.

3. Van der Hoven, I., H. A. Panofsky: Statistical Properties of the Vertical Flux and Kinetic Energy at 100 Meters. Final Report prepared for Air Force Cambridge Research Center under Contract No. AF19 (604)-166 by Pennsylvania State University, Department of Meteorology, June 1954.

4. B-66B Low Level Gust Study, WADD Technical Report 60-305 Volume II, Part I, Plots of Vertical Gust Velocity. Wright Air Development Division, Wright-Patterson Air Force Base, Ohio, March 1961.

5. Burns, A.: Power Spectra of Low Level Atmospheric Turbulence Measured from an Aircraft. Royal Aircraft Establishment, Technical Note Structures 329, April 1963.

6. Monin, A.S.: "On the Similarity of Turbulence in the Presence of a Mean Vertical Temperature Gradient." J. Geophysical Res., Vol. 64 No. 12 Dec. 1959, p. 2196.

7. Panofsky, H.A. and R. A. McCormick: "The Spectrum of Vertical Velocity Near the Surface." Quarterly Journal of the Royal Meteorological Society, Vol. 86, No. 320, October 1960, p. 495

8. Crane, H. L. and R.G. Chilton: Measurements of Atmospheric Turbulence Over a Wide Range of Wavelength for one Meteorological Condition. NACA Technical Note 3702, June 1956.

9. Strom, J.A. and T.G. Weatherman: B-66B High Altitude Gust Survey. Technical Documentary Report ASD-TDR-63-145, Volume I, April 1963. Aeronautical Systems Division, Wright-Patterson Air Force Base, Ohio.

10. Rhyne, R. H. and R. Steiner: Power Spectral Measurement of Atmospheric Turbulence in Severe Storms and Cumulus Clouds. NASA Technical Note TN D-2469, October 1964.

11. Press, H., M. T. Meadows, and I. Hadlock: A Reevaluation of Data on Atmospheric Turbulence and Gust Loads for Application in Spectral Calculations. NACA Report 1272, 1956.

12. Rice, S.O.: "Mathematical Analysis of Random Noise." Bell System Technical Journal. Vol. XXIV No. 1, January 1945, pp. 46-156.

13. Shur, G.N.: "Experimental Investigations of the Energy Spectrum of Atmospheric Turbulence." Trans. Cent. Aerol. Obs., U.S.S.R. Trudy, No. 43, 1962, p. 79.

14. Lumley, J. L.: "The Spectrum of Nearly Inertial Turbulence in a Stably Stratified Fluid." J. Atm. Sci., Vol 21 No. 1, January 1964 p. 99.

15. Kao, S. -K. and H. D. Woods: "Energy Spectra of Meso-Scale Turbulence Along and Across the Jet Stream." J. Atm. Sci, Vol 21 No. 5, September 1964, p.513.

16. Danielsen, E.F.: "The Laminar Structure of the Atmosphere and its Relation to the Concept of a Tropopause." Arch. Meteor. Geophys. Biokl. A, Vol. 11 (1959), p. 293.

17. Hildreth, W.W.: An Investigation of the Mesoscale Waves of Small Amplitude in the Westerlies. Ph. D. Dissertation, Texas A & M University, 1964.

18. Mantis, H.T.: "The Structure of Winds of the Upper Troposphere at Mesoscale." J. Atm. Sci., Vol. 20 No. 2, March 1963, p. 94.

19. Pohle, J.F., A. K. Blackadar, and H. A. Panofsky: "Characteristics of Quasi-Horizontal Mesoscale Eddies." J. Atm. Sci., Vol. 22 No. 2 March 1965, p. 219.

20. Peace, R. L., 1962: A Thermodynamic Explanation of Tornado Cyclones. Paper presented at 201st National Meeting of American Meteorological Society, Norman, Okla., February 15, 1962.

21. Papoulis, A.: Probability, Random Variables, and Stochastic Processes. McGraw-Hill Book Company, 1965.

22. Bendat, J.S.: Principles and Applications of Random Noise Theory. John Wiley and Sons, Inc. 1958.

23. Press, H.: Atmospheric Turbulence Environment with Special Reference to Continuous Turbulence. Advisory Group for Aeronautical Research and Development, Report 115, April-May 1957.

24. Houbolt, J. C., R. Steiner and K. G. Pratt: Dynamic Response of Airplanes to Atmospheric Turbulence Including Flight Data on Input and Response. NASA TR R-199, June 1964.

25. MacCready, P.B., Jr.: "The Inertial Subrange of Atmospheric Turbulence." Geophysical Res. Vol. 67, No. 3, March 1962, p. 1051.

26. McDougal, R.L., T. L. Coleman and P. L. Smith: The Variation of Atmospheric Turbulence with Altitude and its Effect on Airplane Gust Loads. NACA RM L53G15a, November 1953.

27. Press, H. and R. Steiner: An Approach to the Problem of Estimating Severe and Repeated Gust Loads for Missile Operations. NACA TN 4332, September 1958.

28. Walker, W. G. and Mr. R. Copp: Summary of VGH and V-G Data Obtained from Piston Engine Transport Airplanes from 1947 to 1958. NASA TN D-29, September 1959.

29. Final Summary of B-52B-F Service Load Recording Program. Document No. D3-6496-1. The Boeing Company, Wichita, Kansas, 24 October, 1964

30. Perry, Elmer, M. and Rievley, John F: Structural Flight Loads Data from Jet-Tanker Operations. WADD Technical Note 61-39. Wright Air Development Division, Wright-Patterson Air Force Base, Ohio, January 1961.

31. McGregor, D.M.: Investigation of Low Level Turbulence Encountered by a Sabre Mk. V Aircraft Over Eastern Canada. Aeronautical Report LR-298, National Research Council of Canada, January 16, 1961.

32. Sewell, R. T. and K. G. Pettit: Analysis of V-G-H Records from a DC-4M Aircraft in the Vicinity of Frontal Systems and Troughs. Aeronautical Report LR-402, National Research Council of Canada, July 1964.

33. Wells, E.W.: Low Altitude Gust Measurements over Three Routes in the U.K. Technical Note No. Structures 320, Royal Aircraft Establishment, October 1962.

34. Roeser, Erwin P.: Low Altitude Gust Data Obtained in Fleet Aircraft. Report No. NAMATCHEN-ASL-1041, Aeronautical Structures Laboratory, U.S. Naval Air Material Center, Philadelphia, Pennsylvania 21 July 1961.

35. Phillips, Lawrence: Structural Flight Loads Data from YRB-58A Aircraft (Title Unclassified). ASD Technical Note 61-162, Aeronautical Systems Division, Wright-Patterson Air Force Base, Ohio December 1961 Report CONFIDENTIAL.

36. Coleman, Thomas L. and Roy Steiner: Atmospheric Turbulence Measurements Obtained from Airplane Operations at Altitudes Between 20,000 and 75,000 Feet for Several Areas in the Northern Hemisphere. NASA TN D-548, October 1960.

37. Transmittal Letter from Floyd L. Thompson to Francis E. Pritchard, dated January 20, 1965. For use with: A Review of NASA High-Altitude Clear Air Turbulence Sampling Programs, by Roy Steiner, NASA. AIAA Paper No. 65-13, 1965.

38. Tolefson, H. B.: Summary of Derived Gust Velocities Obtained from Measurements Within Thunderstorms. NACA Report 1285, 1956.

39. Hunter, Paul A. and Walker, Walter G.: An Analysis of VG and VGH Operational Data from a Twin-Engine Turboprop Transport Airplane. NASA TN D-1925, July 1963.

40. Copp, Martin R. and Mary W. Fetner: Analysis of Acceleration, Airspeed, and Gust-Velocity Data from a Four-Engine Turboprop Transport Operating Over the Eastern United States. NASA TN D-36, September 1959.

41. Sewell, R. T.: Atmospheric Turbulence Encountered by a Britannia Aircraft on Polar and North Pacific Routes. Aeronautical Report LR-301, National Research Council of Canada, March 1961.

42. Transmittal Letter from John Samos, Langley Research Center (NASA) to Francis E. Pritchard, dated 15 January 1965. With: Preliminary Statistical Turbulence Data Obtained During Flights of Three Types of Commercial Transport Airplanes - AF33(615)-1883.

43. Bullen, N. I.: "Gust Loads on Aircraft." Paper No. 9 - Proceedings on a Symposium Held at the Royal Aircraft Establishment, Farnborough England on 16 November 1961 on Atmospheric Turbulence and its Relation to Aircraft.

44. Notess, Charles B.: A Study of the Nature of Atmospheric Turbulence Based Upon Flight Measurement of the Gust Velocity Components. WADC TR 57-259 (CAL Report No. VC-991-F-1), Wright Air Development Center, Wright-Patterson Air Force Base, Ohio 23 April 1957.

45. Notess, C. B.: Analysis of Turbulence Data Measured in Flight at Altitudes up to 1600 Feet Above Three Different Types of Terrain. CAL Report No. TE-1215-F-1, Cornell Aeronautical Laboratory, 10 April 1959.

46. Jones, Jerry W.: High Intensity Gust Investigation (WFT 1217 R_3). Document No. D-13273-333A, The Boeing Company. 24 October 1964.

47. Pratt, K. G. and W. G. Walker: A Revised Gust-Load Formula and a Reevaluation of V-G Data Taken on Civil Transport Airplanes from 1933 to 1950. NACA Report 1206, 1954.

48. Saunders, K.D.: B-66B Low Level Gust Study, Volume I Technical Analysis. WADD Technical Report 60-305, Wright Air Development Division, Wright-Patterson Air Force Base, Ohio March 1961.

49. Copp, M.R. and T L. Coleman: An Analysis of Acceleration, Airspeed, and Gust-Velocity Data from One Type of Four-Engine Transport Airplane Operated over Two Domestic Routes. NACA Technical Note 3475, October 1955.

50. Dempster, J.B. and C.A. Bell: Summary of Flight Load Environmental Data Taken on B-52 Fleet Aircraft. AIAA Paper No. 64-165, May 1964. Revisions transmitted to F.E. Pritchard from Mr. G.M. Jincz of the Boeing Airplane Company, Military Airplane Division, Wichita, Kansas along with letter dated 9 March 1965.

51. Gerlach, D.O.: B-66B Summer Low Level Gust Study, Vol. I Technical Analysis. ASD Technical Documentary Report 62-1036, Aeronautical Systems Division, Wright-Patterson Air Force Base, Ohio January 1963.

52. Taylor, J.: Manual on Aircraft Loads. AGARD ograph 83, Pergamon Press Ltd. 1965.

53. Military Specification: Airplane Strength and Rigidity Reliability Requirements, Repeated Loads, and Fatigue. MIL-A-8866 (ASG) 18 May 1960.

54. Saunders, K.D.: "Sample Estimates of B-66B Low Level, Clear-Air Gust Field Parameters." Journal of Aircraft, Vol. 1, No. 4, July-August 1964, p.218.

55. Jensen, R.V. and F.M. Hoblit: The Low Altitude Rough-Air Environment. Lockheed-California Company Report No. 18119, 18 December 1964.

56. Austin, W.H., Jr.: Environmental Conditions to be Considered in the Structural Design of Aircraft Required to Operate at Low Levels. USAF SEG-TR-65-4, January 1965.

57. Notess, C.B. and P.A. Reynolds: Application of Self-Adaptive Control Techniques to the Flexible Supersonic Transport. First Quarterly Technical Report. CAL Report No. IH-1696-F-1, Cornell Aeronautical Laboratory, October 1962.

58. Copp, M.R and W.G. Walker: Analysis of Operational Airline Data to Show the Effects of Airborne Radar on the Gust Loads and Operating Practices of Twin-Engine Short-Haul Transport Airplanes. NACA TN 4129, November 1957.

59. Aplin, J.E. : Atmospheric Turbulence Encountered by Comet 2 Aircraft Carrying Cloud Collision Warning Radar. R.A.E. Technical Note Structures 335, June 1963.

DOCUMENT CONTROL DATA - R&D

(Security classification of title, body of abstract and indexing annotation must be entered when the overall report is classified)

1 ORIGINATING ACTIVITY *(Corporate author)*	2a REPORT SECURITY CLASSIFICATION
Cornell Aeronautical Laboratory, Inc. 4455 Genesee Street Buffalo 21, New York	Unclassified 2b GROUP

3 REPORT TITLE

Spectral and Exceedance Probability Models of Atmospheric Turbulence for Use in Aircraft Design and Operation.

4 DESCRIPTIVE NOTES *(Type of report and inclusive dates)*

Final Report   June 1964-May 1965

5 AUTHOR(S) *(Last name, first name, initial)*

Pritchard, Francis E.
Easterbrook, Calvin C.
McVehil, George E.

6 REPORT DATE	7a TOTAL NO. OF PAGES	7b NO. OF REFS
November 1965	80	59

8a CONTRACT OR GRANT NO. AF33(615)-1883 b PROJECT NO. 1367 c Task No. 136702 d	9a ORIGINATOR'S REPORT NUMBER(S) CAL Report No. VC-1954-F-1 9b OTHER REPORT NO(S) *(Any other numbers that may be assigned this report)* AFFDL-TR-65-122

10 AVAILABILITY/LIMITATION NOTICES Qualified requestors may obtain copies of this report from DDC. Distribution is limited because report contains technology identifiable with the DOD Strategic Embargo List.

11 SUPPLEMENTARY NOTES	12 SPONSORING MILITARY ACTIVITY Air Force Flight Dynamics Laboratory Wright-Patterson AFB, Ohio 45433

13 ABSTRACT

Atmospheric turbulence data in many forms, from many sources, have been combined in both spectral and exceedance probability models of the vertical component of atmospheric turbulence. These models will be useful in aircraft structural design procedures as well as in other analytical procedures involving aircraft operation.

For the spectral probability model, a simple analytical form for the spectrum is chosen which fits well the available measured spectra. The parameters of the spectrum are related to physical and meteorological factors in tabular and graphical form, and probability distributions of the pertinent meteorological parameters have been obtained from climatological data. The resulting probability distributions of the spectral parameters have been computed.

A normalized exceedance model is developed that represents the overall cumulative probability distribution of the vertical turbulence velocity for the special probability density function of the rms vertical gust velocity recommended in NACA TN 4332. The basic model involves one parameter, altitude, but may be modified, by using correction factors that are also developed, to account for varying terrain roughness, nature of the terrain, season, time of day and geographical location.

These models of the vertical component of atmospheric turbulence represent what should be an improvement over previous models because of the significant amount of data which has become available in recent years. Nevertheless, the lack of sufficiently reliable data remains a substantial problem.

DD ᶠᵒʳᵐ 1473

| 14 | LINK A | | LINK B | | LINK C | |
KEY WORDS	ROLE	WT	ROLE	WT	ROLE	WT

INSTRUCTIONS

1. ORIGINATING ACTIVITY: Enter the name and address of the contractor, subcontractor, grantee, Department of Defense activity or other organization (*corporate author*) issuing the report.

2a. REPORT SECURITY CLASSIFICATION: Enter the overall security classification of the report. Indicate whether "Restricted Data" is included. Marking is to be in accordance with appropriate security regulations.

2b. GROUP: Automatic downgrading is specified in DoD Directive 5200.10 and Armed Forces Industrial Manual. Enter the group number. Also, when applicable, show that optional markings have been used for Group 3 and Group 4 as authorized.

3. REPORT TITLE: Enter the complete report title in all capital letters. Titles in all cases should be unclassified. If a meaningful title cannot be selected without classification, show title classification in all capitals in parenthesis immediately following the title.

4. DESCRIPTIVE NOTES: If appropriate, enter the type of report, e.g., interim, progress, summary, annual, or final. Give the inclusive dates when a specific reporting period is covered.

5. AUTHOR(S): Enter the name(s) of author(s) as shown on or in the report. Enter last name, first name, middle initial. If military, show rank and branch of service. The name of the principal author is an absolute minimum requirement.

6. REPORT DATE: Enter the date of the report as day, month, year, or month, year. If more than one date appears on the report, use date of publication.

7a. TOTAL NUMBER OF PAGES: The total page count should follow normal pagination procedures, i.e., enter the number of pages containing information.

7b. NUMBER OF REFERENCES: Enter the total number of references cited in the report.

8a. CONTRACT OR GRANT NUMBER: If appropriate, enter the applicable number of the contract or grant under which the report was written.

8b, 8c, & 8d. PROJECT NUMBER: Enter the appropriate military department identification, such as project number, subproject number, system numbers, task number, etc.

9a. ORIGINATOR'S REPORT NUMBER(S): Enter the official report number by which the document will be identified and controlled by the originating activity. This number must be unique to this report.

9b. OTHER REPORT NUMBER(S): If the report has been assigned any other report numbers (*either by the originator or by the sponsor*), also enter this number(s).

10. AVAILABILITY/LIMITATION NOTICES: Enter any limitations on further dissemination of the report, other than those imposed by security classification, using standard statements such as:

(1) "Qualified requesters may obtain copies of this report from DDC."

(2) "Foreign announcement and dissemination of this report by DDC is not authorized."

(3) "U. S. Government agencies may obtain copies of this report directly from DDC. Other qualified DDC users shall request through

_____ ."

(4) "U. S. military agencies may obtain copies of this report directly from DDC. Other qualified users shall request through

_____ ."

(5) "All distribution of this report is controlled. Qualified DDC users shall request through

_____ ."

If the report has been furnished to the Office of Technical Services, Department of Commerce, for sale to the public, indicate this fact and enter the price, if known.

11. SUPPLEMENTARY NOTES: Use for additional explanatory notes.

12. SPONSORING MILITARY ACTIVITY: Enter the name of the departmental project office or laboratory sponsoring (*paying for*) the research and development. Include address.

13. ABSTRACT: Enter an abstract giving a brief and factual summary of the document indicative of the report, even though it may also appear elsewhere in the body of the technical report. If additional space is required, a continuation sheet shall be attached.

It is highly desirable that the abstract of classified reports be unclassified. Each paragraph of the abstract shall end with an indication of the military security classification of the information in the paragraph, represented as (TS) (S) (C) or (U)

There is no limitation on the length of the abstract. However, the suggested length is from 150 to 225 words.

14. KEY WORDS: Key words are technically meaningful terms or short phrases that characterize a report and may be used as index entries for cataloging the report. Key words must be selected so that no security classification is required. Identifiers, such as equipment model designation, trade name, military project code name, geographic location, may be used as key words but will be followed by an indication of technical context. The assignment of links, rules, and weights is optional.